BORON NEUTRON CAPTURE THERAPY FOR HER2+ BREAST CANCERS: A FEASIBILITY STUDY EVALUATING BNCT FOR POTENTIAL ROLE IN BREAST CONSERVATION THERAPIES

by

Peter Anthony Jenkins

A dissertation submitted to the faculty of
The University of Utah
in partial fulfillment of the requirements for the degree of

Doctor of Philosophy

in

Nuclear Engineering

Department of Civil and Environmental Engineering

The University of Utah

December 2012

The University of Utah Graduate School

STATEMENT OF DISSERTATION APPROVAL

The dissertation of **Peter Anthony Jenkins**

has been approved by the following supervisory committee members:

Tatjana Jevremovic	, Chair	**10/25/2012** Date Approved
Edwin Stevens	, Member	**10/25/2012** Date Approved
Brian Wang	, Member	**10/25/2012** Date Approved
Scott Miller	, Member	**10/25/2012** Date Approved
Dong-Ok Choe	, Member	**10/25/2012** Date Approved
Jules John Magda	, Member	**10/25/2012** Date Approved
Christopher Watchman	, Member	**10/25/2012**

and by **Chris Pantelides** , Chair of the Department of **Civil and Environmental Engineering**

and by Charles A. Wight, Dean of The Graduate School.

ABSTRACT

A novel Boron Neutron Capture Therapy (BNCT) regimen for the treatment of HER2+ breast cancers has been proposed as an alternative to whole breast irradiation for breast conservation therapy patients. The proposed therapy regimen is based on the assumed production of boron delivery agents that would be synthesized from compounds of Trastuzumab (Herceptin ®) and oligomeric phosphate diesters (OPDs). The combination of the anti-HER2 monoclonal antibody and the high boron loading capability of OPDs has led to the assumption that boron could be delivered to the HER2+ cancer cells at Tumor to Healthy Tissue ratios (T:H) of up to 35:1 and boron concentrations above 50 μg/g. This significantly increased boron delivery efficiency has opened new BNCT possibilities.

This proof of concept study examined treatment parameters derived as the results in previous efforts in the context of patient-specific geometry and compared calculated dose results to those observed during actual patient therapy. These results were based on dose calculations performed with a set of calculated Kerma coefficients derived from tissues specific to the regions of interest for breast cancer. A comparison was made of the dose to the tumor region, the patient's skin, and the peripheral organs.

The results of this study demonstrated that, given the performance of the proposed boron delivery agent, the BNCT treatment regimen is feasible. The feasibility is based on the findings that the equivalent dose could be delivered to the treatment volume with less dose to the skin and peripheral organs. This is anticipated to improve the treatment outcomes by maintaining local control of tumor cells while reducing dose to healthy tissues.

This work is dedicated to my wife and family.

TABLE OF CONTENTS

LIST OF TABLES

LIST OF FIGURES

ACKNOWLEDGEMENTS

I'd like to thank all those who have made this work possible. Without the support of family, friends, and colleagues the completion of this work would not have been possible. Special thanks go to my wife, Heather, for her incredible patience and love. Special thanks go to David Tripp for his mentorship, his support, and friendship; to my co-workers for their patience in working with my schedule and for their overall support in this endeavor; and to the countless individuals who provided encouragement, words of wisdom, and help along the way. I'd like to thank my committee members for their willingness to always be available to help. Especially, I'd like to thank my advisor, Tatjana Jevremovic, for her confidence in me and her constant encouragement through this entire journey.

CHAPTER 1

INTRODUCTION, PREVIOUS WORK, AND SCOPE OF STUDY

Introduction

Boron Neutron Capture Therapy (BNCT) for the treatment of breast cancers positive for the human epidermal growth factor type 2 receptor (HER2+) has been suggested[1,2,3,4,5,6] as a new radiation therapy treatment method for patients with certain forms of breast cancer. Much of the previous work has focused on treatment parameters such as boron delivery agents, neutron sources, and preliminary, localized tumor dose estimates. Work continues to be performed in these areas; however, to this date, little or no effort has been made to examine the proposed treatment process in the context of current treatment options. Thus, motivation for this dissertation research is a feasibility study intended to provide a preliminary proof of concept of the proposed BNCT therapy for certain HER2+ breast cancers. As a proof of concept study, the following work relies heavily on the conclusions of previous work. These conclusions include such treatment parameters as neutron source characteristics and target tumor doses but also include projections of anticipated boron delivery agent performance. In fact, as described below, the projection of the performance of these boron delivery agents is the primary concept behind this newly proposed treatment regimen. This study examines these projections and treatment parameters previously proposed in the initial stages of development of the treatment process and compare them to parameters used in current photon radiation therapy for certain breast cancers.

By the nature of the current study, many parameters used in the following calculations and to base comparisons are based on those parameters and limits determined in previous works. Because many of these parameters have been justified through peer-review journal articles and MS and PhD dissertation defenses, no attempt is made in this study to review their validity or to argue their feasibility. With a few exceptions, these parameters are used by reference. Several parameters are expanded on in this dissertation, but almost always start with the conclusions of those made in previous works as the basis for their further development. The portions of these previous works that are used in this effort are summarized below.

It is recognized that many of the assumptions made in this study and previous works rely primarily on the expectation that the proposed boron delivery agents are not only feasible but likely to be produced. However, at of the time of this study, work has just begun to produce new delivery agents that possess the characteristics of the agents have been theorized and proposed in the previous work. This is an exciting work that holds much possibility and is thought to be progressing toward the expected goal. But, because the agents are not yet complete and their performance has not been positively demonstrated, the assumptions of their performance used in this study are hypothetical. The work of developing these agents is beyond the scope of the current study; accordingly, no effort is made to defend the assumptions of the proposed delivery agents' performance nor is any effort made to propose new agents or limitations on potential agents. The performance of the delivery agents is assumed to be reasonable for the purposes of this dissertation. It is therefore left to other researchers and future reviewers to determine the validity of these assumptions.

The original contribution of this study is the calculation of dose to the tumor in actual patient anatomy and comparison of the larger field radiation dose to the more common photon radiation therapy treatment regimens. Doses to the organs outside the breast in the thorax are

also calculated, specifically the lungs, heart, and skin, in order to compare radiation effects outside the intended treatment areas as compared to conventional photon radiation therapy. Additional contribution to the calculation of neutron dose is also completed here by reporting updated Kerma coefficient values based on more recent cross-section files than what has been made available in previously published works. Finally, calculations are performed and discussion is given describing the feasibility of using the proposed treatment protocols for nonlocal HER2+ breast cancer tumors in the lung, brain, liver, and skeleton.

Previous Work

Previous work was carried out under the direction of Professor Tatjana Jevermovic[*] who first noted the possibility of applying new advancements in monoclonal antibody research to BNCT therapies. It was postulated that these advancements would improve the prospect of successful BNCT treatments of HER2+ breast cancers by utilizing these new compounds for targeting and delivering boron to specific receptor sites on the cancer cells. This work began before 2005 and is marked by the publication of several key documents:

- "Monte Carlo Assessment of Boron Neutron Capture Therapy for the Treatment of Breast Cancer"[1]
- "Radiation binary targeted therapy for HER-2 positive breast cancers: assumptions, theoretical assessment and future directions"[2]
- "Numerical Assessment of Radiation Binary Targeted Therapy for Her-2 Positive Breast Cancers: Advanced Calculations and Radiation Dosimetry"[3]
- "MCNP5 Voxelized Dose Model for BNCT Applied to Breast Cancers"[4]
- "Advanced Applications of BNCT in Advanced Cancers"[5]

---

[*] Prof. Tatjana Jevremovic is currently the Energy*Solutions* Presidential Endowed Chair Professor in Nuclear Engineering and the Director of the University of Utah Nuclear Engineering Program.

- "Boron Neutron Capture Therapy Applied to Advanced Breast Cancers: Engineering Simulation and Feasibility Study of the Radiation Treatment Protocol"[6]

As previously stated, it is recognized that many of the parameters used in this study have been proposed and successfully defended both in front of MS and PhD committees as well as peer-reviewed journals. The current work relies heavily on the conclusions of these efforts rather than completely developing these same concepts independently for the current work. By the very nature of expanding on these previous results and performing a proof of concept study, a certain level of acceptance of the data is made without too much scrutiny or independent verification of the parameters used. It is recognized that many of the parameters used in the current dissertation have not been empirically demonstrated and, accordingly, there is a high degree of uncertainty in the results based on the use of these parameters. However, efforts into demonstrating these assumptions are currently underway and there is a high level of expectation that the concepts can be demonstrated. Additionally, much of the background information and the assumptions used in order test feasibility of the proposed BNCT therapy are based on assumptions that are well beyond the scope of the current dissertation. Parameters that are considered to be outside the scope of this dissertation are discussed and, where used, are based on the values that have been established in prior works. The parameters and assumptions from previous works that are used in the current dissertation are summarized below.

Boron Delivery Agents

Clearly one of the most vital components of Boron Neutron Capture Therapy is the successful delivery of boron to the correct site for irradiation by neutrons. One of the biggest assumptions made in this and previous work is that of the performance of a hypothetical boron

delivery agent. It has been proposed[6,7] that Trastuzumab (Herceptin ®), which is an anti-HER2 monoclonal antibody compound and has been shown to be effective in targeting HER2 receptors, could be modified in such a way to deliver boron in a highly efficient manner. Recent work with oligomeric phosphate diesters (OPDs) has demonstrated a highly preferential tumor uptake in animal studies. OPDs have also been demonstrated to have a relatively easy boron loading capability.[8] Because of these characteristics, tumor-to-healthy tissue boron concentration ratios (T:H) have been demonstrated to be as high as 35:1 in healthy animal tissues. When compared to other boron delivery agents that have been used in past studies, which produce typical T:H ratios on the order of 2:1 to 3:1 and in certain cases as high as 8:1, this is a marked improvement and leads to the assumption that there exits the possibility to create a new boron delivery agent that will greatly improve the boron concentrations in the HER2+ breast cancer tumors. All these improvements lead to the assumption that their application in BNCT therapies will greatly improve the viability of therapies that include their use.

Previous work[1,3,5,6] suggested that a new delivery agent could be created by combining boron-rich OPDs (^{10}B-OPDs) and Trastuzumab that could be the basis for treating HER2+ cancers, but specifically breast cancers, with greater success than what has been observed in other BNCT therapies. The assumption behind the suggestion was that Trastuzumab would seek out and bind to the HER2 receptors. Once bound to the cancer cell, the ^{10}B-OPD would then be taken up by the cell and accumulate in the nucleus. The action of both these processes would lead to very high boron concentrations in the tumor, T:H ratios up to 35:1 with boron concentrations up to 100 μg/g boron to tissue mass.

Previous calculations[6] that were performed in order to help establish treatment parameters and desirable characteristics of the boron delivery agents looked at varying boron

concentrations ranging from 0 μg/g up to 1,000 μg/g. It was noted that with current boron delivery agents, typical boron concentration levels of 0 to 50 μg/g are obtainable. Thus, it was assumed that the lowest performance characteristic of the boron delivery agent would still be able to perform at least as well as current delivery agents. The work also examined maximum boron concentration levels. It was noted that there appears to be a maximum boron concentration level above which additional boron does not contribute positively to increased dose. The maximum concentration level was found to be 316 μg/g. For the current study, it was assumed that the maximum reasonably achievable concentration level was 100 μg/g, a level twice that currently achieved with conventional boron delivery agents.

These assumptions are adopted for study here without further justification. The need to demonstrate these properties is vital and a significant effort is underway to produce these agents and to demonstrate their performance characteristics. However, the current work is also vital to the potential role of any such class of delivery agent. The actual treatment options that would be available if such agents are eventually created need to be thoroughly established in order to define design parameters, demonstrate potential uses, and to assist in the design of current laboratory and potential future clinical studies. This is the primary reason for the current study. Simply put, both the performance of the delivery agents and the feasibility of the proposed treatment are both relatively unknown. This study addresses the feasibility of the proposed BNCT treatment for HER2+ cancers by examining the dose to other tissue and organs. Feasibility is here assumed to be based on the ability to deliver the prescribed dose to the tumor volume while maintaining dose to peripheral organs to levels less than current treatment options provide. The performance of the delivery agent is currently the effort of other research groups.

Target Tumor Dose

The target tumor dose proposed in previous studies was 50 Gy. As described in Chapter 2, this is a typical tumor dose used in breast conservation therapy for whole breast irradiation. One of the intents of the previous work was to develop a treatment regimen that would deliver the same dose to the tumor cells, but minimize the dose to other surrounding tissues and organs. The selection of the target dose of 50 Gy immediately establishes the proposed BNCT regimen as a potential alternate for conventional breast irradiation therapies. The validity of the 50 GY target dose is demonstrated In one study[9] which looked at the use of radiotherapy in breast-conserving efforts for patients with lobular carcinoma *in situ*(LCIS)followed a group of 25 patients who were treated from 1980 to 1992 (ages 47 to 74 years). Each patient first underwent surgery: 20 for lumpectomy or wide excision and 5 for quadrantectomy. All patients then underwent whole breast irradiation (WBI) with a median dose of 52 Gy (45 to 56 Gy) in fractions of 2 Gy per day. An additional boost by direct electron field was given to 20 patients with a median dose of 10 Gy (6 to 15 Gy). The study noted that after a mean follow-up of 153 months, only one invasive local recurrence was recorded.

It is assumed that the treatment method and results of this study are typical for most WBI breast treatments for the cancers that the proposed BNCT therapy would be relevant. Accordingly, the same target dose of 50 Gy is used in this work. The possibility of the increased relative biological effectiveness (RBE) of the neutron beam in the irradiated tissue raises the question of whether or not a boost dose would be necessary for patients undergoing BNCT therapy. Also, the improved boron delivery and increased T:H ratios assumed for this study also raise the very exciting possibility that fewer surgeries (lumpectomies, etc.) may be necessary as a result of the assumed ability for the delivery agents to better seek out cancerous cells, etc. This notion is also discussed in Chapter 5.

Skin Dose

In previous work[6] it was proposed that a target skin dose of 18 Gy was reasonable. It was assumed that the radiation-induced effects associated with this maximum skin dose were acceptable. Even though 18 Gy to the skin is likely to produce moist dequamation, it was well below the maximum tolerance dose of skin of 22 to 30 Gy that would produce dermal necrosis.[10] Therapy parameter design demonstrated is was desirable to have a tumor dose of 50 Gy and a skin dose of 18 Gy or less. This resulted in the definition treatment parameter of Tumor-to-Skin dose ratio (TS) of at least 2.7. That is, the total effect of the neutron beam, tumor uptake ratios, and boron concentrations would result in a tumor dose of 50 Gy while the dose to the skin would remain below 18 Gy. However, because one of the goals of the proposed BNCT treatment is to improve upon the results of current practices, lower skin doses were also considered in the tumor to skin dose ratios for evaluation of the feasibility of the proposed study.

The effects to human skin are well known and documented.[11,12] The thresholds for different radiation-induced skin injuries are examined in the context of tumor to skin dose. Special attention is given to the fact that significant, permanent skin injuries may occur at doses lower than 18 Gy. Some injuries that may impact a patient's satisfaction and cosmetic effects to the skin of the breast and surrounding areas include telangiectasia, induration, dermal atrophy, and pigmentation changes. The threshold for these effects varies from about 10 Gy to about 15 Gy with times of onset of symptoms varying from about 6 weeks up to a year post irradiation.[11,12] In light of these effects, the lower tumor to skin dose ratios of 10 Gy and 15 Gy are also examined in addition to the 18 Gy skin dose proposed in previous work.

The Massachusetts Institute of Technology Reactor—
Fission Convertor Beam (MITR-FCB)

Without a proper neutron source, BNCT would not be possible. An effort has been made in previous work[6] to identify the most useful neutron beam for breast cancer therapy amongst the major existing facilities. The previous studies looked at issues such as likely tumor depths in the tissue, dose ratios of tumor to skin, neutron energies, and other factors in order to determine the most appropriate beam. Of the different beams that were examined, the MIT-FCB[13] was determined to be the best for the parameters used in the proposed breast cancer BNCT therapy. The MIT-FCB beam is widely used and has been part of many research studies in BNCT of different therapy proposals. It is one of the easiest sources to find information necessary to calculate dose and has been the focus of many research studies and even clinical trials.

The MIT-FCB was determined to be the most appropriate for the proposed breast cancer BNCT.[6] This conclusion was reached by making certain assumptions regarding tumor depth, boron uptake, etc. If any of these assumptions were shown to not be feasible, it is possible that a different source would be more appropriate for the proposed use. Additionally, one area of therapy that the current work examines is the use of the proposed agent in treating distant tumor sites. In this new role, most of the assumptions about tumor depth and surrounding anatomy will be much different from those relevant to the whole breast. It is noted that different neutron sources may be more appropriate for these other treatment sites. However, no additional effort is made to try and determine the best neutron source for each proposed tumor site. The same source for all treatment sites is the MIT-FCB source. The conclusions drawn are all based on the assumption of the use of this single source.

Dose Conversion Factors: Biological Weighting Factors

The calculation of dose in this work is described in Chapter 3. Some of the factors used in the calculation are based on assumptions derived in previous works. As described in fuller detail later and mentioned above, the dose from the neutron beam and boron capture reaction is based on several modifying factors. Most important are the relative biological effectiveness factor (RBE) of the neutrons themselves and the compound biological effectiveness factor (CBE), which is the multiplication factor due to the boron capture reaction. The RBE and CBE will vary from tissue to tissue and the actual performance of the boron delivery agents. Some effort has been made to identify these factors for different tissue types but not specifically for the agents and concentrations proposed in the current work. This is a focus of future work and is not explored in detail in the current dissertation.

The RBE and CBE factors used in previous work[6] are used again here by reference. The RBE for the skin used was 3 for neutrons. The RBE in other tissues was assumed to be the same as the skin. The CBE was estimated to be 3.8. Again, this value is accepted as referenced in previous work.[6] However, it should be kept in mind that many uncertainties exist about the CBEs and RBEs and whether they are the most appropriate for the proposed treatment with the given parameters. Additional work is needed in measuring these values for the concentration proposed and the neutron energies that likely will be used in the proposed therapy.

Kerma Approximation and Kerma Coefficients

Absorbed dose in previous work was estimated using the Kerma approximation. This same approach is again applied in the current study. However, the Kerma coefficients used in previous work were based on published values that included large sections of extrapolated date in the neutron energy spectrum. Some effort was made in this current work to expand upon

these published values. The results, described in Chapter 4 and the data partially reported in Appendix A, are a neutron beam and tissue specific set of Kerma coefficients that are directly applicable to the BNCT treatment being proposed and for the anticipated T:H and boron concentration levels for the tissues found in the female thorax. These derived coefficients are used throughout this dissertation to estimate absorbed dose.

Detailed discussions for both absorbed dose (estimated) and weighted dose (equation 1-5) as they are applied in this study are presented in Chapter 3. Generally, however, the absorbed dose for neutrons, gamma rays, and the boron-effect within cells is calculated. Any additional biological weighting factor is applied after the absorbed dose calculation; i.e., biological weighing factors are not inherent in the dose calculation steps employed in this study. This is in part due to the uncertainty of the biological weighting factors applied in previous works, but also facilitates modification of the current data to newly proposed biological weighting factors that likely will be determined in the future.

Study Design

In order to demonstrate proof of concept, a hypothetical study was devised that would allow comparison of the propped BNCT treatment regimen to conventional radiation therapy. This proof of concept study relied on the treatment parameters described above to develop a virtual treatment plan. The virtual treatment plan was then used to compare the hypothetical patient treatment using the proposed BNCT regimen to an actual patient treated with conventional photon therapy. The results of this hypothetical plan were then used to compare key factors such as tumor dose, skin dose, and dose to other organs. Additional comparisons points are discussed in Chapter 2 as part of the description of conventional radiation therapy. Additional calculations and definitions are summarized in Chapter 3. The following discussion

summarizes the elements of the proposed treatment design that were derived in previous works that are specifically applied in the current hypothetical treatment plan:

For all calculations, boron concentrations are examined at 0 μg/g, 10 μg/g, 50 μg/g, and 100 μg/g. These values have been demonstrated to bracket the reasonable performance expectations of the proposed boron delivery agents. These boron concentrations are examined in the context of Tumor-to-Healthy Tissue ratios (T:H) of 8:1 and 35:1. These values are also thought to bracket the expected performance of the agents as was briefly described above. T:H of 8:1 is assumed to be the maximum achievable ratio for present BNCT delivery agents and represents the lower limit of the desired design performance of the proposed agent. T:H of 35:1 represents the maximum observed ratio in animal tissues from previous works. This ratio is assumed to represent the upper limit of the performance of the proposed boron delivery agent.

A tumor target dose of 50 Gy was assumed for the hypothetical treatment. This is the target dose that was assumed in the previous work and is also the standard treatment dose that is expected during conventional breast conservation therapy. Using this target dose, it is indirectly implied that the proposed BNCT regimen is meant to improve upon radiation therapy used in those treatment situations where breast conservation therapy is appropriate. These patient populations will be examined in Chapter 2. In short, 50 Gy is the target tumor dose for this study because it is the standard for breast conservation therapy, the procedure that the proposed BNCT regimen is compared to.

An additional dose target of 18 Gy or less is used for the skin. Again, this value is set in this study by reference for its use in conventional photon therapy and for practical limits on the tolerance of the skin to radiation-induced effects. Although this 18 Gy level is used as a standard for setting practical limits during radiation therapy, lower skin doses are discussed in subsequent chapters in order to address issues related to skin injuries other than necrosis.

These issues are most relevant in the context of patient satisfaction, with appearance, and avoidance of cosmesis. These issues are further discussed in Chapter 2.

As was stated previously, the only neutron source considered in this study is the MIT-FCB beam. The justification for the use of this source is accepted by reference from the previous efforts of different research groups.[1,6] No other source is considered nor is the idea of improving treatment options with beam optimization considered. The radiation dose is calculated for the defined source. All other comments and work along these lines are expected in future efforts. A full description of the MIT-FCB is given in Chapter 3.

Absorbed dose is used throughout this work as is estimated by the Kerma approximation. Weighted dose is defined in this study as the absorbed dose multiplied by the appropriate biological weighting factor. These factors are recognized to have been defined generally in previous work and not specifically; however, no additional effort is made here to further define these values. The RBE and CBE factors used in previous work[6] are used again here by reference. The RBE for neutrons in the skin was defined to be 3; this RBE was applied to all other tissues for neutrons. The CBE for the boron effect was estimated to be 3.8. This value was used for all T:H combinations and all boron concentrations.

The above summarized values represent the framework of this proof of process study. While these values are used in order to make comparisons to conventional radiation therapy techniques and to examine the feasibility of the proposed regimen, it is recognized that some parameters are better established than others. It is envisioned that this study will further illustrate these items so that improvements can be made in future efforts.

Organization of the Dissertation

Chapter 2 contains background information on breast cancer and BNCT therapy. A description of how radiation therapy is applied for certain patient populations and breast cancer stages is given. The characteristics of radiation therapy application for different treatment scenarios are summarized. An overview of those applicable aspects of BNCT is also given. These subjects combined lead to an overview of how the characteristics of BNCT may compliment current therapy techniques. This chapter forms the basis for evaluation for the proof of concept and ultimately the conclusions of this study.

Chapter 3 describes the method used to determine dose, compare therapy doses, and evaluate fluence requirements. A description of the method used to import patient-specific data into MCNP as well as dose comparison values is also given. Also included in this chapter is a section on the calculation of updated Kerma coefficients that are used in the MCNP input files.

Chapter 4 contains the results of the study calculation and the comparison of the hypothetical patient treatment with the actual photon-therapy treated patient. This is largely accomplished by comparing the dose calculation results from the MCNP input file and actual patient data.

Chapter 5 summarizes the results and discusses the feasibility of the study in the context of the findings. Future work recommendations are also included here.

Appendix A contains tables of calculated Kerma coefficients calculated in Chapter 3.

Appendix B contains MATLAB script and function files used to handle MCNP mesh tallies and loading into CERR.

CHAPTER 2

BACKGROUND

Introduction

This proof of concept study examines the proposed BNCT regimen and the conclusions made in the previous efforts to evaluate the feasibility of the proposed treatment parameters. In order to evaluate these proposals, some background information on the subject is necessary in order to form the evaluation questions and criteria. In this section, brief background information is given on the topics of radiation therapy for breast cancer, BNCT dosimetry, and effects of radiation to the skin. These general subjects make up the main evaluation criteria used later in the study. Previous efforts' conclusions have implied that the characteristics of the proposed BNCT regimen should result in more effective radiation therapy outcomes than what is currently observed with photon based therapy. Thus, it is the overall goal of this study to evaluate this implication in the context of realistic treatment parameters.

In order to make comparisons and evaluate the parameters of the proposed therapy regimen, some information on the therapeutic goal of current radiation therapy is given. Also, the characteristics of BNCT, as they are applicable in the current context, are also briefly described. Finally, the effects of radiation on the skin and to the peripheral organs are summarized. These subjects are not meant here to be exhaustive or to provide a comprehensive discussion on each topic. Rather, the information given here is meant to provide

context to statements of comparison and provide points on which to evaluate feasibility of the proposed regimen.

Essentially the proof of concept study asks a few key questions that can be summarized simply:

1. Why is radiation therapy performed as part of breast conservation therapy?
2. How is the effectiveness of radiation therapy judged?
3. What are the potential side effects of radiation therapy?
4. What characteristics of the proposed BNCT therapy would improve the effectiveness?
5. What characteristics of the proposed BNCT therapy would improve the side effects?

This section is meant to provide background information so that these questions can be answered. Again, the information in this section is not meant as a complete evaluation and description of these topics, but rather provides the context for the evaluation discussion.

Radiation Therapy in Breast Conservation Therapy

Radiation has long been used in cancer treatment because of its ability to kill cells. At its most basic essence, the goal of radiation therapy is to kill as many cancer cells while minimizing the number of healthy cells that are irradiated. Much effort is made to reduce the amount of radiation to healthy tissue through the use of beam limiting devices that shape the beam and other efforts to minimize patient movement. However, because most radiation therapy utilizes high energy photons, much of the radiation intended for the cancer cells also irradiates healthy tissue, leading to increased side effects for the patient. From this, we begin to see the answer to our first question: radiation therapy is desirable because of its ability to kill cancer cells and one way to weigh effectiveness is to examine the seriousness of the side effects.

Radiation therapy has been established as an important tool in breast conservation therapy (breast-conserving surgery plus radiation therapy) for the treatment of ductal carcinoma in situ (DCIS) or early stage invasive cancer. It has also been shown to be a valuable tool in the treatment of patients with locally advanced disease who respond sufficiently to neoadjuvant chemotherapy. Typically, complete excision of the cancerous cells is performed followed by radiation therapy. Typical radiation therapy includes fractionated radiation dose delivered to the whole breast with a target dose of 50 Gy to the tumor bed in 2 Gy fractions. For patients with extensive areas of cancerous cells, mastectomy is typically the only treatment option. The primary function of radiation therapy in these cases is to treat cancer cells that potentially were not excised during surgery. Any cancer cell that is left may lead to recurrence in the patient. Irradiation of the entire breast is intended as a method to try and inactivate any cancer cells that may have been left from surgery.

External beam partial breast irradiation (PBI) has been examined in different patient populations with varying degrees of success, the recurrence rate here serving as the metric for success. Typically, in order to be eligible for external beam PBI, patients must meet certain criteria regarding their specific cancer; factors such as excised tumor size and cancer-free margins, weighed heaviest on eligibility for PBI. For example, selection of patients for PBI at one facility was offered only to patients with unifocal DCIS less than 3 cm with histologically negative margins.[14] Whereas recurrence rates have been reported for WBI of 0 to 5% at 5 years, PBI studies have reported recurrence rates at two to three times this rate.[14] For this reason, PBI is typically not offered as a treatment option to therapy patients with large DCIS tumors. However, PBI for early-stage invasive cancers does show some promise and there is currently several large clinical studies to test the efficacy for these cancers.[14] Because 70-80% of recurrent breast cancers occur in the immediate adjacent areas to the tumor bed, it is believed

that the entire breast does not need to be irradiated. A few options are currently available for PBI in this role: multiplane multicatheter brachytherapy, point source brachytherapy, or shaped external beam. Current large-scale clinical trials are still underway testing the efficacy of these methods and complete results are likely to be available until 2016.[14]

In cases where the patient may not meet all the criteria for PBI, or when there is doubt as to the efficacy of PBI for the patient, WBI is the standard treatment. The few PBI methods listed above rely on photons to deliver the dose to the tumor bed. These photons are low-LET so the attenuation in tissue is still similar to that of photons from external beam. Thus, the dose to peripheral organs can still be relatively high. The proposed BNCT treatment would not only use high-LET particles to irradiated the tumor bed, which have a much smaller effective range than photons, but the BNCT method would be dependent upon delivery agents that target the tumor cells and would have a high concentration of boron in those tumor cells to deliver direct dose to the cells that are being controlled. It is not yet well understood how effective the boron delivery agent will be at targeting the tumor cells. However, if the level of success that is anticipated is obtained, the ability to irradiate cells left after surgery will greatly improve, possibly to the point that conditions such as those described above for eligibility for PBI could be exceeded.

From this brief description of the use of radiation therapy as part of breast conservation therapy, we have an outline of the use, measurement of effectiveness, and potential areas where improvements can be made. In the context of breast conservation therapy, radiation is mainly used for those cases in which the cancer cells are relatively localized. The primary purpose is to inactivate cells that may be left from surgery. Probably because some of the cancer cells were not localized, WBI has a lower rate of recurrence than PBI. Thus, the preferred

method is to irradiate the entire breast tissue. Because WBI is preferred, dose to adjacent tissue can lead to unwanted side effects.

One other aspect of radiation therapy considers cosmetic appearance. For instance, some surgical decisions are sometime made on the likelihood of being able to adequately reconstruct the breast postsurgery. Of course cosmetic appearance goes a long way to contributing to a patient's overall perception of treatment success and well-being.

Radiation Side Effects

When considering treatment options with radiation therapy, one concern is always the additional risk to the patient from the irradiation of healthy tissue. Much effort is given to reduce as much as possible the dose to healthy tissue in order to minimize these effects. However, in many cases irradiation to adjacent organs is unavoidable. In fact, in some cases, the dose to adjacent organs is unavoidable in order to provide the maximum benefit to the patient. In order to better to estimate the effects on the adjacent organs, dose to these healthy tissues is calculated and planning of therapy is such that these doses are controlled as much as possible. The current preferred method of estimating the dose to adjacent organs is estimating effects are with Normal Tissue Complication Probability (NTCP) models.[15] Typically, Dose Volume Histograms (DVH) are used to measure dose to the tissue or organ. The DVH displays the fraction of the organ and amount of dose that fraction has received. There are several stated issues with this method, such as the DVH not being sensitive to sensitive structures within the organ, but they do provide a simple means for comparison of effects from the different treatment modalities. In this study, DVHs are used to compare the effect to the adjacent organs from the photon-based regimen to the BNCT regimen.

Much effort has been undertaken to improve understanding of the effects of radiation therapy on the healthy tissues.[16] As a result of these efforts, more data are available regarding the effects of radiation on healthy tissues. These efforts have also produced dose treatment planning recommendations to minimize these effects. For this current study, the effects to three organs were examined: the lungs, the heart, and the skin. The recommended dose/volume limits to these organs varies based on the number of fractionations, the total dose, and several other key factors. However, in the current study it is noted that the proposed study is capable of delivering the desired dose to the tumor volume in a single fraction. Most tolerance dose limits are based on standard fractionation for the organ in question. Additionally, for this study, a comparison is made between the doses to the tumor bed from the standard 50 Gy (25 x 2 Gy) fraction schedule to the proposed single BNCT fraction. Thus, two sets of tolerance limits were found.

For the skin, it is noted that several thresholds exist for different radiation-induced injuries. Different sources list different tolerance levels depending on the context of the study. For instance, it has already been mentioned in Chapter 1 that tolerance levels can be found for the skin varying from 18 to 30 Gy,[10] which covers effects ranging from moist desquamation to necrosis. Other endpoints such as ulceration exist at around 16 Gy for a single dose.[17] Other limits for multifraction doses range from 20 Gy[18] to over 50 Gy.[19] The difference being how the endpoint is measured and the actual effect studied. As mentioned previously, the maximum dose to the skin for this study was 18 Gy. But as can be seen from these data, doses lower than 16 Gy should be considered in the context of cosmetic effects and other patient care issues when feasible.

For the heart, different dose/volume limits were indicated in the organ of interest. Specification of dose to the whole heart resulted in different dose/volume limits than for the

pericardium. The standard dose/volume limit typically given is 25 Gy (or more) to less than 10% of the whole heart. This limit is associated with less than 1% risk of cardiac mortality. Another limit is for a dose of 30 Gy to less than 46% of the pericardium of a mean organ dose of less than 26 Gy to limit the risk of pericarditus to less than 15%.[20] These limits are based on the standard dose fraction treatment plans. Single fractions to the heart have observed to contribute to myocardial vascular changes with mean doses of 20 Gy and necrosis at 40 Gy[17] in animal studies. Also, a significant risk of pericarditus exists with single doses of 20 Gy to less than 15 cc of the pericardium.[17] The tolerance dose for this study will be assumed to be similar to the V25 <10% for comparison to the photon-based, fractionated study. However, because of the treatment geometry this dose limit is not expected to be met.

In the case of a tolerance limit to the lungs, it has been point out that the dose to both lungs should be considered because of the effects of the overall function of the lungs. Additionally, because of the different functional parts of the lung different volume sizes are often listed in order to better account for dose to different parts of the lung. The typical dose/volume limit given is 20 Gy or more to less than 30% of the whole lung to limit symptomatic pneumonitus to less than 20%. Other limits suggest less than 7 Gy to 1,500 ml in order to preserve basic lung function and not more than 7.4 Gy to 1,000 ml in order to avoid pneumonitus.[17] For single fractions, recommendations to limit 10% of the organ to a dose less than 20 Gy[21] and 50% of the organ to less than 2.5 Gy.[22] It is noted that there is not a threshold for which effects to the lung may be observed. Thus, it is recommended that the dose always be minimized as much as practicable.[21]

Because this is a proof of study, these values are used for reference for comparing the photon-based therapy to the proposed BNCT regimen. More specifically, the doses to adjacent organs from the BNCT regimen are evaluated with respect to these recommended

doses/volume limits. However, more specific discussion on the dose to the skin is given below due to its importance in treatment regimen parameters described in Chapter 1.

Skin Effects

A large part of the feasibility of certain aspects of the proposed radiation therapy treatment is concerned with the idea of dose to the skin. The skin plays a vital role in the evaluation process not only from the perspective of radiation-induced damage to the skin but also from the standpoint that patients' quality of life and treatment satisfaction is tied to things such as physical appearance and function of the irradiated skin. Simply put, if the proposed treatment regimen can lead to the same local control of the tumor but with lower skin damage, this would obviously be a huge advantage to any potential patient who may receive the proposed treatment. Accordingly, some description of how the proposed treatment would interact with the skin is warranted. The following overview of the skin and radiation effects to the skin provides a summary of radiation-induced injury to the skin, framework for comparisons to conventional photon therapy, and also provides the context for calculation of dose in the skin the subsequent sections.

Skin anatomy and thickness varies over the body both among different individuals as well as within the individual. Average skin thickness on the breast has been found to vary from 0.7 to 2.3 mm over the superior quadrant; 0.7 to 2.7 mm over the inferior quadrant; 0.6 to 2.4 mm over the medial quadrant; and 0.5 to 2.1 mm over the lateral quadrant.[23] This is an important observation since it helps provide context to the depth at which radiation dose to the skin should be calculated. A well-known phenomenon of neutron interactions with tissue, and one that is noted in the results given in Chapter 4, is that the dose from the incident beam of neutrons will increase gradually with depth in tissue until it reaches a maximum and then will

decrease exponentially with depth. If the dose in skin were calculated for the epidermis, a slight underestimate of skin dose may result. Conversely, if the dose were calculated at a point too deep in the tissue, a slight overestimate may result.

When considering the dose to the skin and the overall effect the dose will have, it is important to consider the anatomy of the skin. The different layers of the skin all have a unique purpose, but their purposes are interrelated and co-dependent. For instance, if the epidermis is unharmed by a dose of radiation that is delivered to the lower layers of the skin, the function of that layer may be impaired and not observed directly until the epidermis has finished its life cycle. Thus, the dose to the skin should be viewed as a functional unit.[12] A functional unit would be a group of cells that are interrelated and co-dependent such that the effect to one layer would have an effect on the others, whether the effect is immediate or delayed. From this standpoint, the dose to the skin should be considered at the level for which the maximum dose would be observed.

As described above, the skin thickness over the breast of healthy individuals can vary from 0.5 to about 2.7 mm. Also, because of the nature of neutron interaction mechanisms, the dose to tissue increases in the first few centimeters of tissue (see discussion in Chapter 3). The question becomes then, at what depth to calculate dose in skin. The Nuclear Regulatory Commission has defined the term,[24] shallow dose, as the dose to skin at a depth of 7 mg/cm^2, which is about 0.1 mm. However, the discussion above has shown a need to consider the dose to the entire skin functional unit, which may extend the entire depth of the epidermis and papillary dermis. Because the neutron and photon doses increase over the depth range of the skin and underlying tissue layers, it is convenient to describe the skin dose at a depth of the functional skin unit. In the case of the model described above, this may extend to 3 mm (Figure 2-1). In order to provide a conservative estimate of skin dose, the dose to skin in this study will

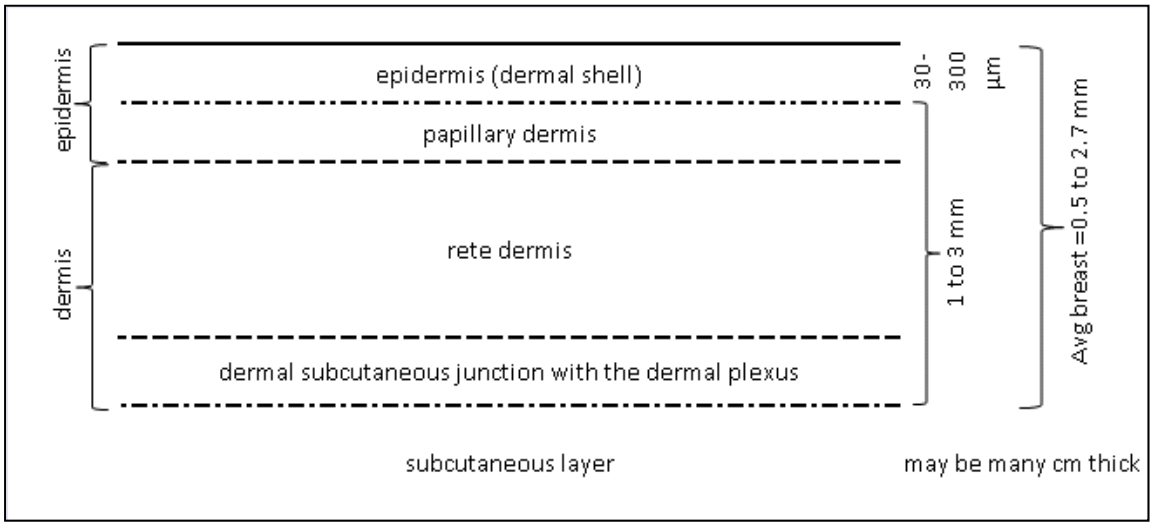

Figure 2-1. Diagram of breast skin layers and thicknesses

be stated at the skin depth of 3 mm. A more complete discussion of skin dose calculation is given in Chapter 3. The results of these calculations discussed in Chapter 4 show good comparison to skin dose estimates in previous work.

However, as noted in the introduction, the RBE for neutrons used in this study is 3, whereas as the RBE and DRF for photons is assumed in this study to be 1. That is to say, that for the same amount of absorbed dose in the skin, the dose from the neutron beam is expected to triple the biological damage to the skin. In order for the proposed BNCT therapy to a viable option to conventional photon therapy, it should not cause any worse skin reaction that what is currently observed in conventional photon therapy.

Effects to the Skin from Conventional Therapy

The most obvious and likely side effect of radiation therapy is skin injuries. As has been identified in Chapter 1, the maximum skin dose for the proposed BNCT regimen is 18 Gy. Many factors affect the actual skin injury observed in a patient such as location on the skin, relative health of the skin, dose, etc. For typical breast cancer patients who have received radiation

therapy, the majority see no effect during the first 2 weeks postirradiation. Following this period, many patients begin to see signs of skin erythema, epilation, dry desquamation, and decreased sweating. Many patients (24 to 40%), around 5 weeks postirradiation, experience symptoms of moist desquamation and moderate edema; and, almost no patient who received radiation therapy for breast conservation therapy experiences ulceration, hemorrhage, or necrosis.[11] It should be pointed out that the dose level selected in previous work of 18 Gy is the threshold for dermal necrosis at about 10 weeks. Thus, if the skin dose from the BNCT regimen routinely is near the max skin dose, there is a high probability that some necrosis would be observed.

As was described above for the effects to other organs, when determining the feasibility of the proposed BNCT therapy, the specific goal was not to show the specific mechanism of interactions, but, assuming the equivalent doses (absorbed dose x biological weighting factors) would produce the same biological effects, rather to merely show that lower doses to peripheral organs was achievable while maintain the dose to the target volume.

BNCT Dosimetery

Boron Neutron Capture Therapies (BNCT) have been much discussed and examined both in peer-reviewed journals as well as laboratory and clinical trials. A simple literature search returns sufficient information on the background, technical aspects, and current uses that no effort to expand on any of these issues will be attempted in this dissertation. Additionally, the previous work, upon which this effort expands, has provided significant background and justification for the conclusions used in this dissertation. However, because this dissertation deals with the dosimetry of BNCT, some general information is given in order to provide some

context to subsequent discussion. Specifically, those aspects of BNCT that relate to the calculation of dose are summarized below.

BNCT relies on the large capture cross-section of Boron-10 of thermal neutrons, which results in a large, mixed-field radiation emission. The resulting radiation field is complex and significantly complicates the calculation of radiation dose. The primary boron capture reaction (equation 1-1) results in the emission of alpha particles and Li-7 ions. Gamma rays are induced by the capture of neutrons by hydrogen (equation 1-2). And fast neutron interactions and capture results in the emission of protons (equation 1-3).

$$^{10}_{5}B + ^{1}_{0}n \rightarrow ^{7}_{3}Li + ^{4}_{2}He + 2.79\ MeV \qquad 2\text{-}1$$

$$^{1}_{1}H + ^{1}_{0}n \rightarrow ^{2}_{1}H + \gamma + 2.2\ MeV \qquad 2\text{-}2$$

$$^{14}_{7}N + ^{1}_{0}n \rightarrow ^{14}_{6}C + ^{1}_{1}p + 580\ keV \qquad 2\text{-}3$$

All these components contribute to the overall absorbed dose to the target region. However, each component, because of the type of radiation interaction each will undergo, may contribute a greater biological effectiveness to the target. For instance, a gamma ray, which has no mass, interacts in a completely different manner than a charged particle which may undergo columbic or scattering interactions. Additionally, because of the nature of the boron delivery agents, some of the energy may be deposited internal to a cell's nucleus, which results in a much greater biological effectiveness than energy deposited external to the nucleus. For this reason, the concept of weighted dose equivalent is often used.

Equivalent dose (also sometimes referred to a weighted dose equivalent or in the context of BNCT, simply weighted dose) is simply the absorbed dose multiplied by some biological effectiveness factor (equation 1-4). Biological effectiveness factors are very complex and specifically defined for each situation and biological effect. In equation 1-4 below, D is the

absorbed dose associated with γ: gamma rays, n: fast neutron interactions, and N: protons from the nitrogen capture reaction. The absorbed dose associated with gamma rays is multiplied by a dose reduction factor, DRF, which varies with dose-rate. The absorbed dose for fast neutrons is weighted by the Relative Biological Effectiveness (RBE) for fast neutrons, which varies by neutron energy. The absorbed dose associated with the N-14 reaction is weighted by the Relative Biological Effectiveness factor for protons. Finally, the Chemical Biological Effectiveness factor for the main B-10 reaction is a combination of the RBE for alpha particles and accounts for the micro-distribution of boron throughout the cell.

$$D_w = \left(D_\gamma \cdot DRF_\gamma\right) + \left(D_n \cdot RBE_n\right) + \left(D_N \cdot RBE_N\right) + \left({}^{10}_{5}B \cdot CBE\right) \qquad 2\text{-}4$$

Typically, the DRF for gamma rays is considered to be 1 and the absorbed dose related to protons is considered negligible to the overall dose contribution from the boron interactions.[25] Thus, equation 1-4 is typically simplified to equation 1-5. As described in Chapter 3, the absorbed dose for the energy ranges in the ranges associated with the neutron interactions in the energy ranges studies in the current work, are dominated by the $^{10}B(n,\alpha)^{7}Li$ reactions below 10 MeV.[25]

$$D_w = \left(D_\gamma\right) + \left(D_n \cdot RBE_n\right) + \left({}^{10}_{5}B \cdot CBE\right) \qquad 2\text{-}5$$

The biological weighting factors RBE and CBE for this work have been assumed to be the same as those described in the most recent previous work.[6] As is described in the introduction to this study and the conclusion of this study, many of the conclusions are based on these values. In order to show future potential of the proposed BNCT regimen, positive demonstration of these values, and boron delivery agents, is vital.

Comparison Criteria

This brief description of these underlying principles of breast conservation therapy and radiation therapy provide adequate framework to form the basis of comparison for this proof of concept study:

1. Tumor volume dose equivalency
2. Effects to the skin due to dose
3. Effects to peripheral organs and tissues

For the purposes of comparisons, it is assumed that all weighted doses (absorbed dose multiplied by the appropriate biological weighting factor) would produce the same effect. Thus, for comparison to the dose to the tumor volume, an equivalent dose would assume to produce the same local control of the tumor cells. Dose to the skin and peripheral organs of equal or lesser dose would results in the same or reduced effects. These three general comparisons are the basis for the other comparisons made in Chapter 5.

CHAPTER 3

CALCULATION METHODS

Introduction

The primary basis for conclusions made from this proof of concept study is the comparison of a hypothetical patient treatment with the proposed BNCT regimen and an actual patient dose from a conventional photon treatment scenario. In order to make such a comparison, a method for calculating dose from such a hypothetical treatment regimen needs to be defined. In this chapter, such a process is described. In addition to a description of the overall process, specific definitions and descriptions of different parameters are given. The process described below allows for not only the calculation of dose at any point in a patient or organ, but also allows for the comparison of dose between treatment regimens. The results of this process and the conclusions that can be drawn from the results are described in the subsequent chapters.

There are three main processes described below: 1) calculation of Kerma coefficients, 2) calculation of skin dose and maximum tumor treatment depth, and 3) calculation of dose to a patient. All three processes are defined specifically for this proof of concept study to examine the assumptions summarized in Chapter 1 in the context of comparison to the conventional photon radiation therapy in breast conservation treatments. The calculation of Kerma coefficients serves to provide the means to estimate the absorbed dose in the specific tissues that are found in the female thorax. The determination of skin dose is vital to the proof of

concept as skin dose is one parameter in the proposed BNCT therapy that has been assigned a maximum threshold value. Skin dose is also an important point for evaluation in the context of therapy comparisons. Maximum tumor treatment depth is an important parameter as it helps to identify tumors that potentially would or would not be feasible to treat with the proposed BNCT therapy. Finally, the ability to calculate dose to a patient from the proposed BNCT method is vital in determining whether or not the method will be able to meet the assumed therapy parameters and how well it compares to other radiation therapy techniques for the same treatment types. The process to calculate dose to the patient also includes steps to calculate the dose to individual organs as well as derive dose volume histograms.

Software Utilization

Different software packages were used in the completion of this study. Because each of the packages is well-known and readily available, a full description of each is not provided. However, a brief description of the use and application of each is given below for reference:

1. MCNP, Monte Carlo N-Particle Transport Code, Version 5_1.6.[26] MCNP was primarily used to calculate fluence in different geometries. Primarily, these fluence values were modified by Kerma coefficients so that MCNP provided estimates of absorbed dose. MCNP was also used to determine fluence values at various points in tissue which is the primary dose estimation tool for T/S ratios and skin dose calculations.
2. Scan2MCNP version 1.08, 2010.[27] Scan2MCNP is a tool that transforms DICOM images into MCNP-compatible geometry. Scan2MCNP allows for the partition of Hounsfield units and library definition in order to pass material information to MCNP along with geometry. Primarily, Scan2MCNP was used to convert patient CT images to lattice structures with the defined materials.

3. Moritz.[28] Moritz is a graphical editing tool that reads and writes MCNP compatible geometry files. Moritz was used to visualize tumor volume placements, neutron beam orientation, and assist with geometrical transformations needed to convert from DICOM images coordinates and the coordinates used in MCNP to coordinates used in CERR for the patient studies.
4. MATLAB®, R2010a Student was used to handle script processing for handling MCNP output mesh tallies. 3D dose matrices were created using MATLAB scripts and multiplication factors for RBE, CBE, and irradiation time were applied during the script runs. Scripts also included definition rules and commands to load the 3D dose matrices in to CERR.
5. CERR, A Computation Environment for Radiotherapy Research, version Beta 4 9/27/2011[29] is an add-in package for MATLAB that allows for visualization and manipulation of patient images and dose information. CERR is a free tool that is licensed by the CERR development team under a general public license. The tool was designed specifically for radiation therapy research and provides many tools that clinical therapy tools provide such as organ dose metrics, etc. CERR was used to evaluate the anonymized patient treatment study and was used as the platform to perform dose metrics on both the photon therapy data set and the BNCT based datasets.

Kerma Approximation of Absorbed Dose

The primary unit calculated and used throughout the current work is the unit of absorbed dose. The absorbed dose is estimated by the KERMA-approximation. However, the KERMA coefficients used here were uniquely derived for the specific neutron energy spectrum of the source and the specific boron and tissue compositions used. These KERMA coefficients

were then used in computer simulations to estimate dose to the tumor and surrounding organs both in simplified models and in a patient-specific treatment scenario. Also, in order to address issues of feasibility in nonlocal sites, several calculations were made, also using computer simulations, to determine limits of the proposed treatment protocol. Specific information such as the tumor to skin dose ratios, the neutron fluence as a function of depth in tissue, and skin dose rate were part of these calculations.

Dose calculation in BNCT is complicated because of the many different reactions and mixed radiation fields that are present during irradiation. Dose in BNCT arises from four primary sources: 1) thermal neutron interactions, 2) Boron-10 capture reactions, 3) fast neutron interactions, and 4) photon interactions.

Equation 2-5 described generally the different elements needed in order to calculate dose from BNCT therapies. As explained below, the formula in its current form is of little use in the current study because the individual absorbed doses are values that must be measured and cannot be calculated directly. In order to estimate the absorbed doses, Kerma coefficients are applied to neutron fluence values. Both Kerma coefficients and fluence are values that can be reasonably calculated (these concepts are described in more detail below). By using the calculated values of Kerma and fluence, absorbed dose can be estimated:

$$D_w = \left(K_\gamma\right) + (K_n \cdot RBE_n) \; + \; (K_B \cdot CBE) \qquad 3\text{-}1$$

This version of the equation 2-4 is useable for the current proof of concept study because each element is either able to be calculated or derived from reference. It is the calculation of these elements that are first described below.

Absorbed dose, D, is defined by the ICRP[30] as the mean energy imparted, $d\bar{\varepsilon}$, to a mass, dm:

$$D = \frac{d\bar{\varepsilon}}{dm} \qquad 3\text{-}2$$

The unit of absorbed dose is the gray (Gy). It is the basic physical quantity used to measure dose in radiation biology, clinical radiology, and radiation protection and is defined for all types of radiation. Absorbed dose is a measureable quantity that is derived from the average value of energy imparted, ε, which is a stochastic quantity that also accounts for secondary charged particles which are released in surrounding mass. Absorbed dose can be defined at any point in matter because it is derived from the average energy deposited over dm; it does not account for any small random fluctuations but rather the average over many atoms.[20]

Kerma, K, or the *Kinetic Energy Released in Matter*, is defined by the ICRU[30] as, "the quotient of dE_{tr} by d*m*, where dE_{tr} is the expectation value of the sum of the initial kinetic energies of all the charged particles liberated by uncharged ionizing particles in a material of mass d*m,*

$$K = \frac{dE_{tr}}{dm} \qquad 3\text{-}3$$

The unit of K is J kg-1 and the special name for the unit is gray (Gy)." Note that the Gy is also used for absorbed dose as well.

As noted in the definitions of K, it is the value of the sum kinetic energy from the charged particles deposited in a mass. It can be shown the K = D in cases where the energy loss outside the mass of interest from charged particles is small. Absorbed dose accounts for both the primary and secondary charged particles, whereas Kerma only accounts for the initial charged particle. So, in situations where the loss of the initial charged particle energy is small, K and D would be numerically equal. This is referred to as "charged particle equilibrium" and is the assumption upon which the Kerma approximation is based. In the case of the interaction

results associated with boron capture (Chapter 2), the resulting charged particles will travel a very short distance before expending all their energy. In other words, the boron capture reaction is an almost ideal situation for using the unit of Kerma for estimating Absorbed Dose.

Another important unit that needs to be defined is the unit of "fluence." Fluence, ϕ, is defined by the ICRP[30] as the number of particles, dN, incident upon a small sphere of cross-sectional area, da

$$\phi = {}^{dN}/_{da} \qquad 3\text{-}4$$

Fluence has units of particles per unit area, e.g., n/cm^2, as is typically used in this study. The ICRP further describes fluence as an expectation value not subject to random small fluctuations. It is worth noting here the difference between the units of fluence and flux used in this study. Flux is understood to define the flow of particles per unit time, e.g., n/s. Oftentimes, the term flux is used interchangeably with the term "flux density," which is used to describe the flow of particles per unit time per unit area, e.g., $n/cm^2/s$. This latter use of the term is synonymous with the term "fluence rate," which describes the same phenomena. In order to avoid confusion, the terms fluence, flux, fluence rate, and flux density are used with these described meanings: the term "flux" used in this study is used to describe the flow of particles per unit time (n/s) and not in the manner that "flux density" is defined above ($n/cm^2/s$); fluence describes the flow of particles per unit area (n/cm^2); and fluence rate or flux density describes the flow of neutrons per unit area per unit time ($n/cm^2/s$).

Having defined absorbed dose, Kerma, and fluence in these terms, we arrive at the idea that if the fluence is known (or calculated) at a certain point and some understanding of the types of interactions that are occurring at the point exists, the amount of energy transferred, Kerma, to the mass can be calculated. Using MCNP, the neutron fluence can be easily calculated

for all the situations described in this study. All that remains is determining how much energy is transferred for the given particle energy in the type of mass (tissue). This is the idea of the Kerma coefficient. The Kerma coefficient is the ratio of Kerma at a given point to the fluence, K/ϕ. Thus, by multiplying the Kerma coefficient by the calculated fluence, the Kerma can be calculated and the absorbed dose estimated.

In practical application, the Kerma coefficient is essentially a multiplication factor that, when multiplied by the fluence for the correct energy and materials, will result in the amount of Kerma at the given point. And, as pointed out above, the Kerma at charged particle equilibrium is numerically equivalent to Absorbed Dose, which is actually the value we need. In rigorous efforts, Kerma coefficient determination involves very detailed calculations for which material compositions and exhaustive cross section files are required.[31] Cross section files are readily available from different repositories (e.g. http://www.nndc.bnl.gov/exfor/endf00.jsp) but in order to use them detailed calculations are required. For a given incident neutron energy, En, and target nuclide, the Kerma coefficient is given as:

$$K_{\phi}=N\sum_{i}\int E\int\frac{d^{2}\sigma_{i}(E_{n})}{d\Omega dE}d\Omega dE \qquad 3\text{-}5$$

where N is a coefficient equal to $9.64853/M_A$; M_A is the atomic mass of the target nuclide in atomic mass units; E is the energy of the ejected particle or photon, i, at incident neutron energy E_N; $d^2\sigma_i(E_N)/d\Omega/dE$ is the double-differential cross section of the ejected particle or photon (for energy and solid angle). As can be seen, in order to calculate the Kerma coefficient for each incident neutron energy with each different element in the material would require an exhaustive effort or the use of software to assist with the calculations. In fact, there are many

different software packages that will do just this; they are specifically designed to calculate Kerma coefficients from cross section files. Some examples of software that will perform these calculations include NJOY,[32] MAZE,[33] and MCNP.[34] Because MCNP was used for all other calculations in this study, MCNP was also used to calculate the Kerma coefficients used here. MCNP has been shown to be a valid method for calculating the Kerma coefficients.[33]

Several publications were searched for Kerma coefficients of elements and tissues present in this study. In many of these sources, it was argued, correctly, that the contribution of certain elements present in different tissues contributed negligibly to the total tissue Kerma coefficient, and, thus, often left many elements out of the Kerma coefficient. However, it was desired to demonstrate this fact for this study since the incident neutron energies were specifically defined for the neutron source and many different tissue types would be examined not typically looked at in other works. Historically, much of the research for BNCT has been performed for the brain or skin. In this work, organs of the female thorax were studied for dose from BNCT reactions. Thus, a more full description of the Kerma coefficients for these organs was desired. But, because these data were largely unpublished, the Kerma coefficients were calculated for the specific tissues that would be used in this study.

Kerma coefficients were calculated using a method roughly based on the definitions of fluence and Kerma. Specifically, recall that fluence describes particles incident on a small sphere per unit area. A calculation in MCNP was performed that modeled the interactions of a beam of neutrons incident upon a small sphere of material for which the Kerma coefficient was sought. The beam of neutrons was composed of the same energy flux that was used for all patient dose calculations. The beam was assumed to be a 20-cm radius circular beam located 50 cm from the 0.1 cm radius sphere of material. All areas outside the sphere of material were assumed to be a vacuum. The material within the sphere was varied first by element (at the normal atomic

density) and then by tissue composition, which is further defined below. Results were obtained using the MCNP tally types F2, F4, and F6.

Tally type F2 provides the fluence[†] averaged over a surface, per source particle, in units of particles per cm^2. The F4 tally provides the fluence averaged over a cell, per source particle, in units of particles per cm^2. And, the F6 tally provides the average amount of energy deposited in a cell per unit mass, reported by MCNP as MeV per gram. It was first thought that the proper estimation of Kerma coefficient would be to divide the F6 tally by the F2 tally. However, when the F6 tally was divided by the F4 tally, results were obtained that varied on average less than 2% of other published values when based on the same cross section data. The coefficient values obtained using the F6 and F4 tallies demonstrated much better agreement to published values and lower overall deviation the tallies using the F6 and F2 results. This better agreement obtained with the F4 tally is due in part to the calculation of fluence in the F2 tally that averages the entire surface of the cell, when only a portion of the source actually is being irradiated. When the F4 tally is used, the average over the small volume considers neutrons fluence in every direction. Additionally, the MCNP manual notes that for particles grazing the surface that there exists some uncertainty in the surface fluence estimator and that the F2 tally is not an exact estimate of surface fluence.[35] Because of these factors, the F4 tally is a better approximation of the fluence across the cell. Therefore, the F6 to F4 ratio is used throughout this work to estimate Kerma coefficients.

[†] The MCNP User Manual[35] used the term flux in the description of the tallies. However, as described earlier, the formalism used in this work to describe particles per unit area is the unit of fluence. As was mentioned in this earlier discussion, the term "flux" is often used to mean "flux density." In this context the term used in the MCNP manual is correct as the actual results are given as flux per source particle, which is typically reported as a flux (particle flow per time).

The Kerma coefficient was calculated from the MCNP results by:

$$k_{coef}(\text{Gy cm}^2) = \left(\frac{\text{F6 tally } \left(\frac{\text{MeV}}{\text{g}}\right)}{\text{F4 tally } \left(\frac{1}{\text{cm}^2}\right)} \right) \times \left(1.602 \times 10^{-13} \frac{\text{J}}{\text{MeV}}\right) \times \left(\frac{1000\ \text{g}}{\text{kg}}\right) \qquad 3\text{-}6$$

This equation provides the Kerma coefficient for the element or tissue in units of Gy-cm^2. By multiplying the results by the total neutron source fluence rate and the irradiation time, the dose at the desired location is estimated.

In order to demonstrate the feasibility of this method, the elemental Kerma coefficient of a few of the elemental coefficients published in ICRP 63[36] were compared to the results generated with MCNP. ICRP 63 states that the cross section files used for the calculation of the Kerma coefficients we contained in the ENDF/B-VI database.[37] Thus, the ENDF/B-VI cross sections contained in the MCNP cross section data base were used for comparison. Comparisons between the calculated values and published values were based on the elemental Kerma coefficients found in ICRU 63. ICRU was selected because of its wide use and reference in other Kerma related papers.[25,34] Figure 3-1 shows the ICRU 63 Kerma coefficients graphed alongside the MCNP calculated Kerma coefficients for four commonly used elements used for tissue composition calculations. As can be seen in these Figures, the agreement between the two sets of data is very good. With only a few exceptions, the data varied by less than about 2% on average. In the cases where good agreement was not observed, it was assumed that these areas were those where poor data extrapolation existed in the ICRU data. For instance, no data points exits in the ICRU data between neutron energies of 1 x 10^{-10} and 2.53 x 10^{-8} MeV. As can been seen in Figure 3-1 for the comparison for Hydrogen-1, there is some disagreement as the

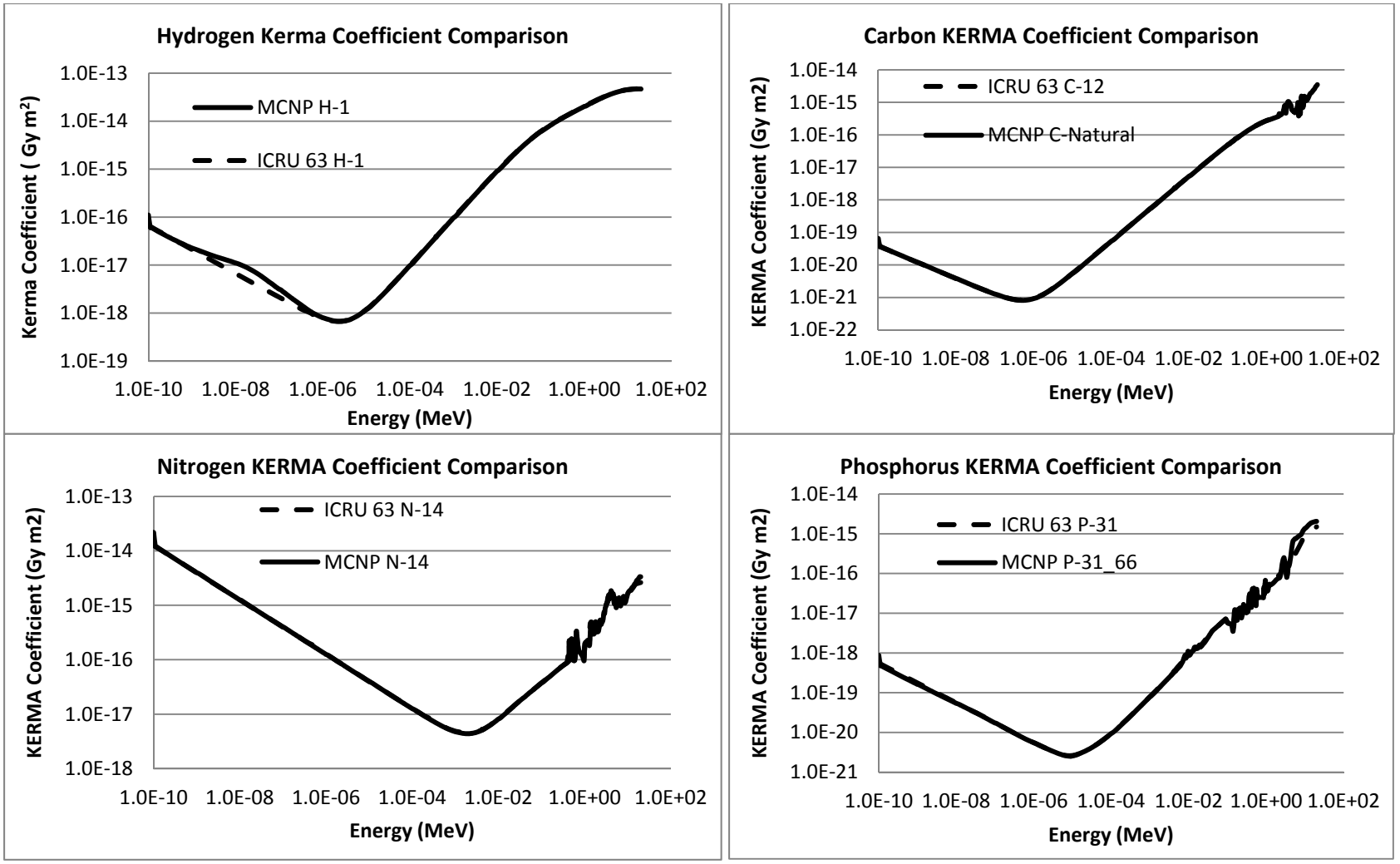

Figure 3-1. Comparison of calculated Kerma coefficients derived using MCNP calculation method and published values in ICRU 63[2]

calculated data shows some change in the slope of the curve in this region. The ICRU data are simply extrapolated between these energy points. Other such regions exist in other elements. One additional difference observed has to do with the distance between data points. Because the MCNP calculation method included 1,000 data point between a 10^{-6} MeV and 20 MeV, the appearance of resonance regions were more pronounced in some cases as compared to the ICRU 63 published data, which included only 110 data points between 2.58 x 10^{-8} and 20 MeV.

A closer examination of this discrepancy observed in the comparison chart for hydrogen-1 is shown in Figure 3-2. In Figure 3-2, a comparison is made between several calculation methods and the published values for hydrogen-1 in ICRU 63. Note the curve for the MCNP derived values using the ENDF/B-VII database seem to drop significantly greater than the other methods. Because the newer database were supposed to have updated thermal cross sections, this was curious. However, it has been suggested that thermal treatment of hydrogen be used for low energy neutrons.[25] When the thermal treatment is applied, the results from the calculation method are more in line with the expected values (i.e., the published values). Figure 3-2 also shows the relative fluctuations observed in the F6 to F2 ratio for Kerma estimation compared to the F6 to F4 values.

Based on these results, it was assumed that the MCNP calculation results could be considered to be accurate and were relied on in this study for the dose estimation used for comparisons with dose from photon therapy. At the time these calculations were performed, the ENDF/B-VI cross section database had been updated by the ENDF/B-VII[‡] cross section

---

[‡] Kerma coefficient calculations were performed in October 2011. At the time of writing it was noted that the ENDF/B-VII.1 database was published in December 2011. The Kerma coefficients in this work are based on the earlier published ENDF/B-VII.0.

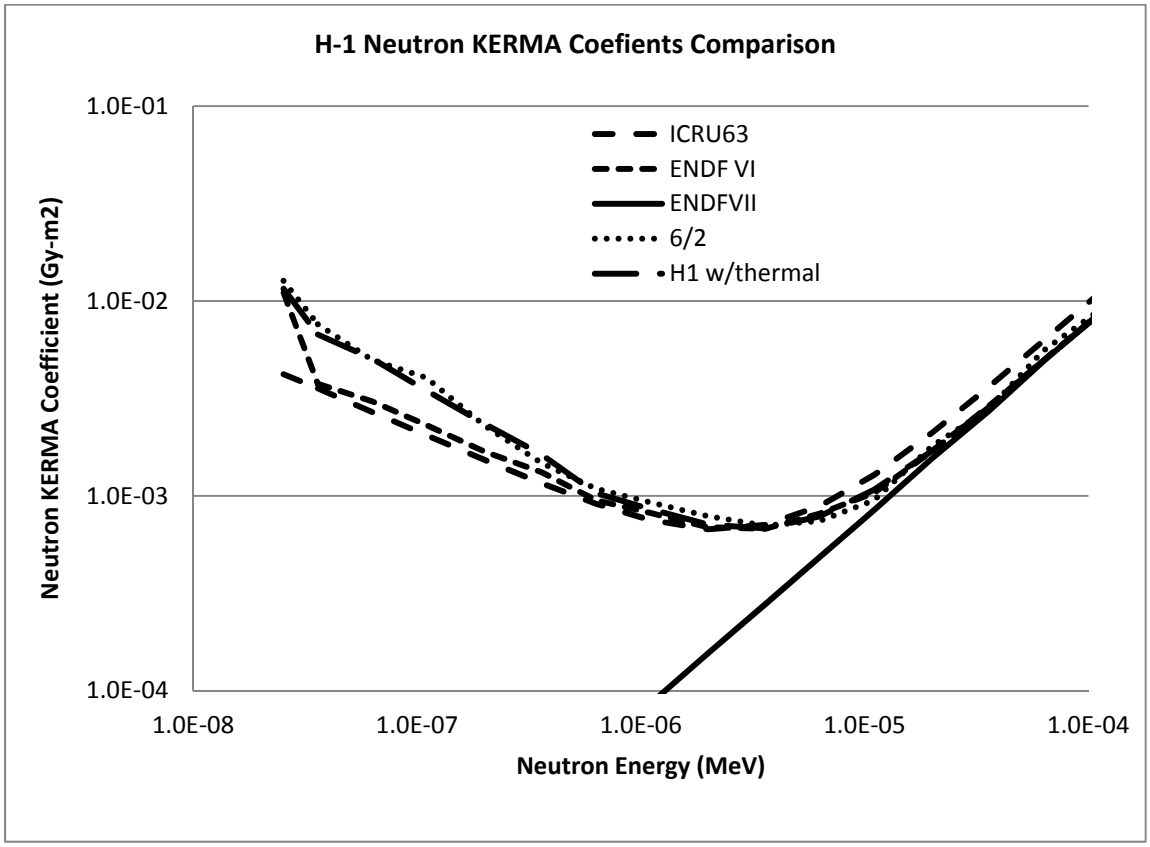

Figure 3-2. Comparison of results from different elemental Kerma coefficient calculations for hydrogen. Note improved results for ENDF/B-VII with H-1 thermal treatment. Also, note relative comparison of results with F6 to F2 tally ratios for Kerma coefficient calculations.

database. This database was available in the MCNP5 v. 1.6 used in this study, thus, the newer database was used. Several elements were calculated for use in the calculation of tissue Kerma coefficients. The results of these calculations were used to calculate the total tissue Kerma coefficients.

Elements were selected based upon the elemental compositions of the tissues for which doses were calculated in this work. The elements calculated included hydrogen, carbon, nitrogen, oxygen, sodium, phosphorus, sulfur, chlorine, potassium, calcium, iron, iodine, and boron. The tissue and organs were those present in the female thorax, specifically skin, adipose, muscle, heart, lung, mammary gland, breast 50% fat/50% tissue, and ribs. The elemental tissue

composition of these organs was taken from ICRU 46.[38] In addition to these organs, the Kerma coefficient for adenocarcinoma was also calculated based on the compositions found in literature.[39] The MCNP cross section files used for each element are shown in Table 3-1.

Once the MCNP Kerma coefficient calculations with the ENDF/B-VII cross sections were completed, these values were again compared to the ICRU 63 published values. Most of the results showed little or no variation. This was to be expected as many of the cross section files were not updated from the previous database or only updated in small aspects.[40] However, the comparison of calcium-40 showed a significant difference that is worth noting. The result of the Kerma coefficient calculation for calcium-40 is shown in Figure 3-3 alongside the ICRU 63 values.

Table 3-1. MCNP Cross section files used for element Kerma Coefficient estimation. C-0 indicates natural carbon abundances

Nuclide	MCNP Cross section
H-1	1001.70c
H-2	1002.70c
C-0	6000.70c
N-14	7014.70c
N-15	7015.70c
O-16	8016.70c
Na-23	11023.70c
P-31	15031.70c
S-32	16032.70c
S-33	16033.70c
S-34	16034.70c
S-36	16036.70c
Cl-35	17035.70c
Cl-37	17037.70c
K-39	19039.70c
K-40	19040.70c
K-41	19041.70c
B-10	5010.70c

The region between 10^{-2} MeV and 10^{-8} show a significant difference. However, this is an example of the ICRU 63 values being extrapolated between known points.

Tissue Compositions

Many of the calculations performed were performed for different tissue types, tumor-to-healthy tissue ratios (T:H), and boron concentrations. In order to ensure that consistent materials were used throughout the current work, materials and tissue compositions were defined for the use in all calculations. As stated above, ICRU 46[38] was the primary source used for the definition of tissue compositions. The brain and thyroid were also included for reference and for possible treatment sites. Table 3-2 summarizes the tissues defined for this dissertation, their elemental compositions, and relative tissue densities.

Material definitions based on female soft tissue and metastatic tumor tissues were defined for T:H ratios of 8:1 and 35:1 for boron concentrations of 0 μg/g, 10 μg/g, 50 μg/g, and 100 μg/g. The density and composition of metastatic breast cancer tissue was assumed to be adenocarcinoma. The elemental fractions used of the T:H and boron concentrations used in the MCNP simulations are shown in Table 3-3. The associated data for the MCNP materials definitions cards are shown in Table 3-1.

Tissue Kerma Coefficients

Having calculated elemental Kerma coefficients and defined tissue compositions, the task then turned to calculating total tissue Kerma coefficients. This process was approached in two ways. At first, the tissue compositions were entered into MCNP using the same geometry described for the elemental compositions. However, when the results were compared to the second method, the MCNP method for tissues was not selected due to the time required for the calculation runs. The second tissue Kerma coefficient calculation essentially created a weighted

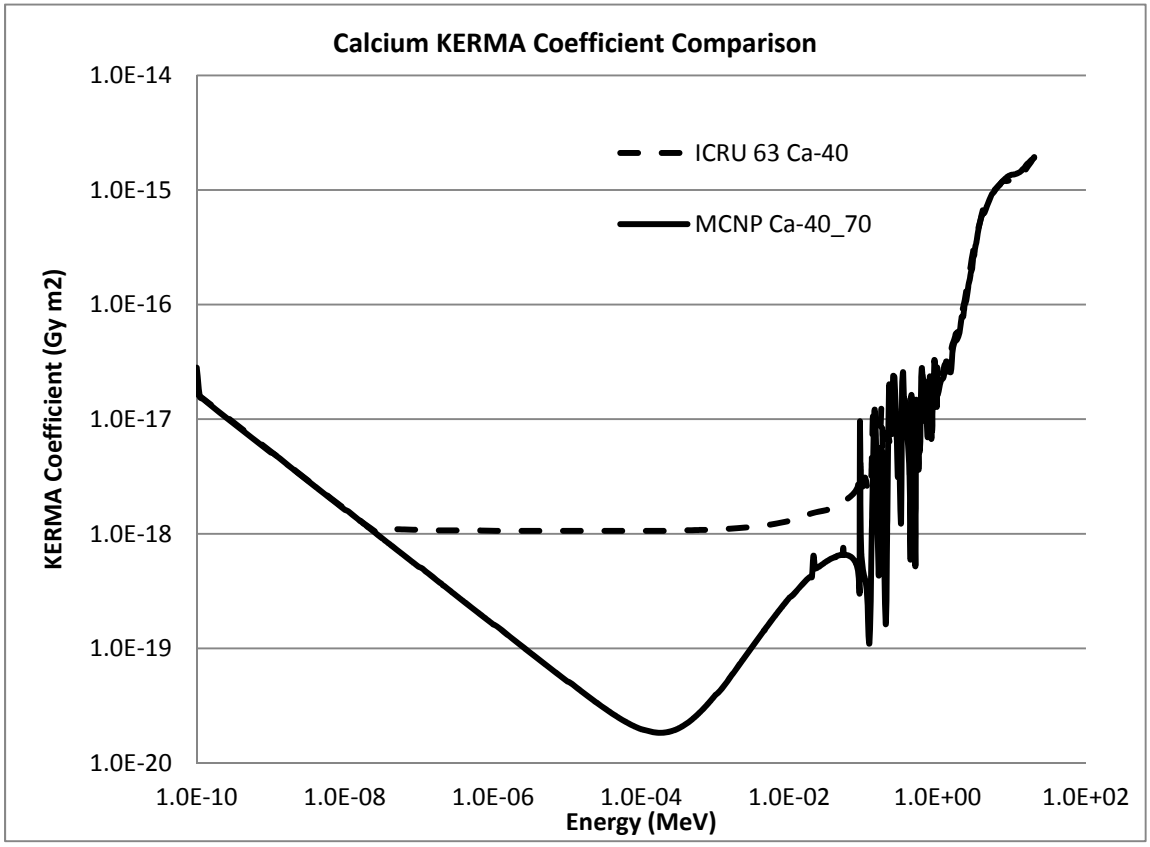

Figure 3-3. Comparison of oxygen Kerma coefficients illustrating the difference between ICRU 63 and MCNP calculated values.

Table 3-2. Table of elemental tissue composition for organs used in this study

	Adipose	Brain	Breast 50/50	Mammary	Heart	Lung	Muscle	Ribs	Skin	Soft Tissue	Thyroid	Adeno-carcinoma
ρ (kg m3)	950	1040	960	1020	1050	260	1050	1410	1090	1020	1050	1122
H	0.114	0.107	0.115	0.106	0.104	0.103	0.102	0.064	0.100	0.106	0.104	0.099
C	0.598	0.145	0.387	0.332	0.139	0.105	0.143	0.263	0.204	0.315	0.119	0.269
N	0.007	0.022		0.030	0.029	0.031	0.034	0.039	0.042	0.024	0.024	0.045
O	0.278	0.712	0.498	0.527	0.718	0.749	0.710	0.436	0.645	0.547	0.745	0.569
Na	0.001	0.002		0.001	0.001	0.002	0.001	0.001	0.002	0.001	0.002	0.002
P	0.001	0.004		0.001	0.002	0.002	0.002	0.060	0.001	0.002	0.001	0.004
S	0.001	0.002		0.002	0.002	0.003	0.003	0.003	0.002	0.002	0.001	0.005
Cl		0.003		0.001	0.002	0.003	0.001	0.001	0.003	0.001	0.002	0.003
K		0.003				0.002	0.004	0.001	0.001	0.002	0.001	0.004
Ca								0.132				
I											0.001	

Table 3-3. Composition description of T:H ratios and boron concentrations used for tumor definitions

T	8	8	8	8	35	35	35	35
H	1	1	1	1	1	1	1	1
B (ppm)	0	10	50	100	0	10	50	100
ρ (kg m3)	1109	1109	1109	1109	1119	1119	1119	1119
H	0.100	0.100	0.100	0.100	0.099	0.099	0.099	0.099
C	0.275	0.275	0.275	0.275	0.270	0.270	0.270	0.270
N	0.042	0.042	0.042	0.042	0.044	0.044	0.044	0.044
O	0.566	0.566	0.566	0.566	0.568	0.568	0.568	0.568
Na	0.002	0.002	0.002	0.002	0.002	0.002	0.002	0.002
P	0.004	0.004	0.004	0.004	0.004	0.004	0.004	0.004
S	0.005	0.005	0.005	0.005	0.005	0.005	0.005	0.005
Cl	0.003	0.003	0.003	0.003	0.003	0.003	0.003	0.003
K	0.004	0.004	0.004	0.004	0.004	0.004	0.004	0.004
B		8.75E-06	4.38E-05	8.75E-05		9.71E-06	4.86E-05	9.71E-05

sum of the elemental Kerma coefficients at each energy level. Table 3-4 shows the elemental weighing factor defined for each tissue. These weighted tissue Kerma coefficients disagreed by up to 80% greater from the MCNP generated tissue weighting factors at the higher (> 10^{-5} MeV). However, when compared to other published data using the same weighting technique[17] the values derived for the brain were almost identical (Figure 3-4).

It is therefore observed that the weighted calculation method resulted in a slightly higher tissue Kerma coefficient than what was determined using the MCNP calculation method. There may be many reasons for this that were not examined further in this work. Some possible reasons for the discrepancy include rounding errors, elemental weighting errors, and self-shielding that was not accounted for in the weighted calculation technique. However, for this study, the weighted tissue Kerma coefficients were used to estimate the dose to all tissues in the body, except the tumor volume. The Kerma coefficients in the tumor volume were derived using the MCNP calculation method. This is a conservative approach as it overestimates the dose to the surrounding tissues and underestimates the dose to the tumor volume. This would tend to lead to lower dose ratios at the higher energies. However, because most of the neutron energies tended toward the lower region, where no discrepancy was observed between the calculation methods, this effect was not thought to be significant.

Kerma Approximation

Ultimately, absorbed dose was estimated by first calculating neutron fluence at each point in the volume of interest and then applying the appropriate Kerma coefficient. The Kerma coefficients for each element were calculated using MCNP. These elemental Kerma coefficients were then used to calculate the tissue Kerma coefficients using a weighted sum calculation method. The Kerma coefficients for the tumor volumes and borated tissues were calculated

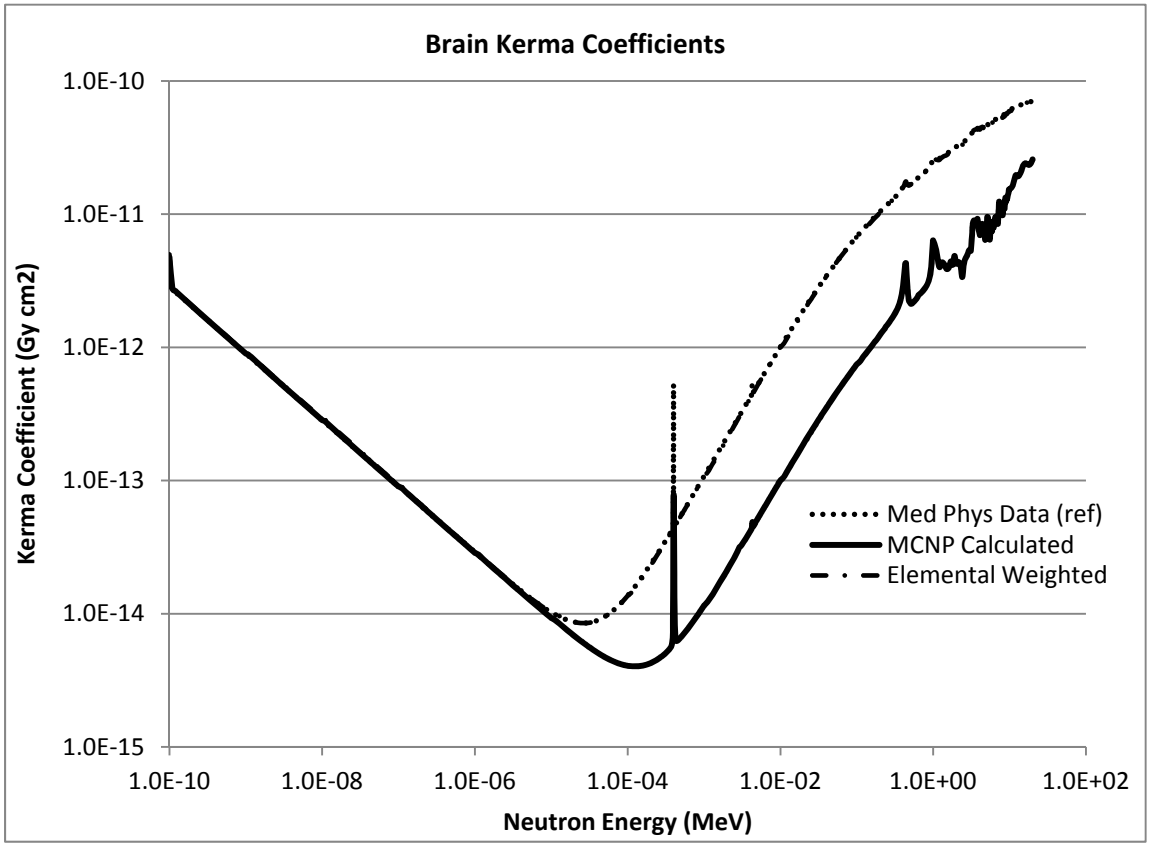

Figure 3-4. Comparison of published Brain tissue Kerma coefficients, MCNP calculated Kerma coefficients and elemental weighted Kerma coefficients. Note that published value and elemental weighted values are indistinguishable.

using the MCNP calculation method. Each method included calculations or evaluation at 1,000 incident neutron energy points in each of the defined tissues. A summary data set of these results is given in Appendix A. In the patient-specific geometry mesh tallies, only soft tissue Kerma coefficients were used outside the tumor volume. Chapter 4 discusses the calculations of the elemental Kerma coefficients. For many of the elements, the lower energy was dominated by the boron contribution and the higher energies were dominated by the hydrogen contribution. In fact, even when no boron was present, the Kerma coefficients in the lower energies were very close to the same values. The application of each elemental Kerma coefficient to each element in the MCNP calculation would be a very labor and computationally

difficult task. In order to simplify dose calculations, only soft tissue Kerma coefficients were used outside the tumor volume and T:H and boron concentration-specific Kerma coefficients were used inside the tumor volume.

Absorbed dose at each point was calculated by multiplying the MCNP mesh tally output by the Kerma coefficient so that the results given in were in units of Gy per source neutron. Once the mesh tally was parsed into more the more useable 3D dose matrix using MATLAB, the data at each point could be multiplied by the source flux and irradiation time to calculate the absorbed dose at the point of interest.

Dose-Depth Limitations

As has been explained previously, one evaluation point for this proof of concept study was the tumor to skin ratio (T/S). The maximum skin dose was set at 18 Gy-equivalent and the target tumor dose was set at 50 Gy-equivalent. This resulted in the T/S dose ratio limit being set to at least 2.7. Also, when considering the possibility of applying the proposed therapy to different areas within the breast or even to areas outside the immediate breast tissue (e.g., axilla, liver, etc), there is an obvious limit to how deep the tumor can reside in the surrounding tissue before the T/S ratio is unobtainable due to simple attenuation and neutron slowing.
In order to calculate the T/S ratio as a function of depth, MCNP was again used to calculate the fluence in a mass of soft tissue from the neutron beam source. A 20 cm3 mass of soft tissue, as was defined above, filled the volume. The first 3 mm of the cube was defined to be skin. The neutron beam was modeled as per the source definition summarized in Chapter 1. That is, an 8-cm diameter beam, with the neutron energy fluence defined for the MIT-FCB beam was directed directly into the surface of the skin of the volume. A tumor, modeled as a 1-cm radius sphere, was placed at varying depth in the volume of tissue. The tumor was modeled with the various

combinations of T:H and boron as described for all other tissue definitions. The appropriate Kerma coefficients were applied to the Fmesh4 tally to in order to provide an estimate of absorbed dose per source neutron. By multiplying this result by the total neutron fluence rate and the irradiation time, the dose at the point of interest from the mesh tally is found.

The T/S ratio was found for depths of 0 cm (surface of the sphere touching the lower edge of the skin), 1 cm, 2 cm, 4 cm, 6 cm, 8 cm, 10 cm, and 15 cm. The simulation was repeated for each T:H ratio and boron concentration. The results are given in Chapter 4 along with the calculated skin dose rate. The skin dose rate determined in this exercise was used to estimate skin dose in the patient specific scenario.

CT Image to MCNP Geometry

As has been described earlier, the software code Scan2MCNP was used to generate an MCNP compatible lattice geometry. Several parameters are defined once the DICOM images from the CT study are loaded into Scan2MCNP. The size of the voxel and limits of the image are defined for inclusion in the lattice generation. For this study, the entire image field present in the DICOM files was included to ease the geometric concerns with overlaying the image data with the dose datasets. The size of the voxels was selected to be 0.4 cm in each of the three directions. Voxel size selection considered image resolution considerations and computational time considerations. The smaller the voxel size, the better the image resolution and the better tissue and organ boundaries could be defined. On the other hand, small voxel sizes result in higher computation time. Thus, the voxel size selected was considered to be a good balance between image resolution concerns and computation times. The materials were selected as previously described and included the materials for female soft tissue, compact bone, air, lung, and metastatic tumor tissue. As was described, this simplification of materials resulted in a

better model for dose determination. Figure 3-5 is a 3D reconstruction of the DICOM images from the patient-specific case and the 3D lattice representation of the patient.

The agreement between the actual CT-acquired images and the lattice representation was very good. Some fine structure was lost in the lung, breast, and liver. Because the values of tissue and material densities (and, thus Kerma coefficients) of these organs were very close and because these regions were relatively small, this loss of fine structure was assumed to not have a significant effect of the calculation of dose. Interaction data were not assumed to be affected by averaging these materials because the elemental compositions and densities remained relatively similar.

After the patient-specific geometry was successfully defined in MCNP-compatible lattice geometry, Moritz was used to generate a tumor volume that represented the tumor volume defined in the patient dose plan. The MCNP cell type “arb” was used to represent the patient’s actual tumor volume. The actual tumor volume from the dose plan was a very complex volume that had multiple facets in each axial, sagittal, and coronal slice. The arb surface did a reasonably good job of capturing most of the tumor volume, but some portions of the volume fell outside the actual defined regions. As discussed below, this led to some error being introduced for the dose comparison section of this study. However, it was assumed that the concepts were well represented and the arb cell provided sufficient basis on which to make conclusions for this proof of concept study. The patient lattice geometry with the arb-based tumor volume is shown in Figure 3-6. The external skin and other soft tissue have been removed for visualization of the tumor volume.

Moritz was also used for visualization of the source neutron beam to ensure proper irradiation of the tumor volume. As has been described above, there exists a maximum tumor depth at with the proposed BNCT treatment regimen remains viable. In traditional photon

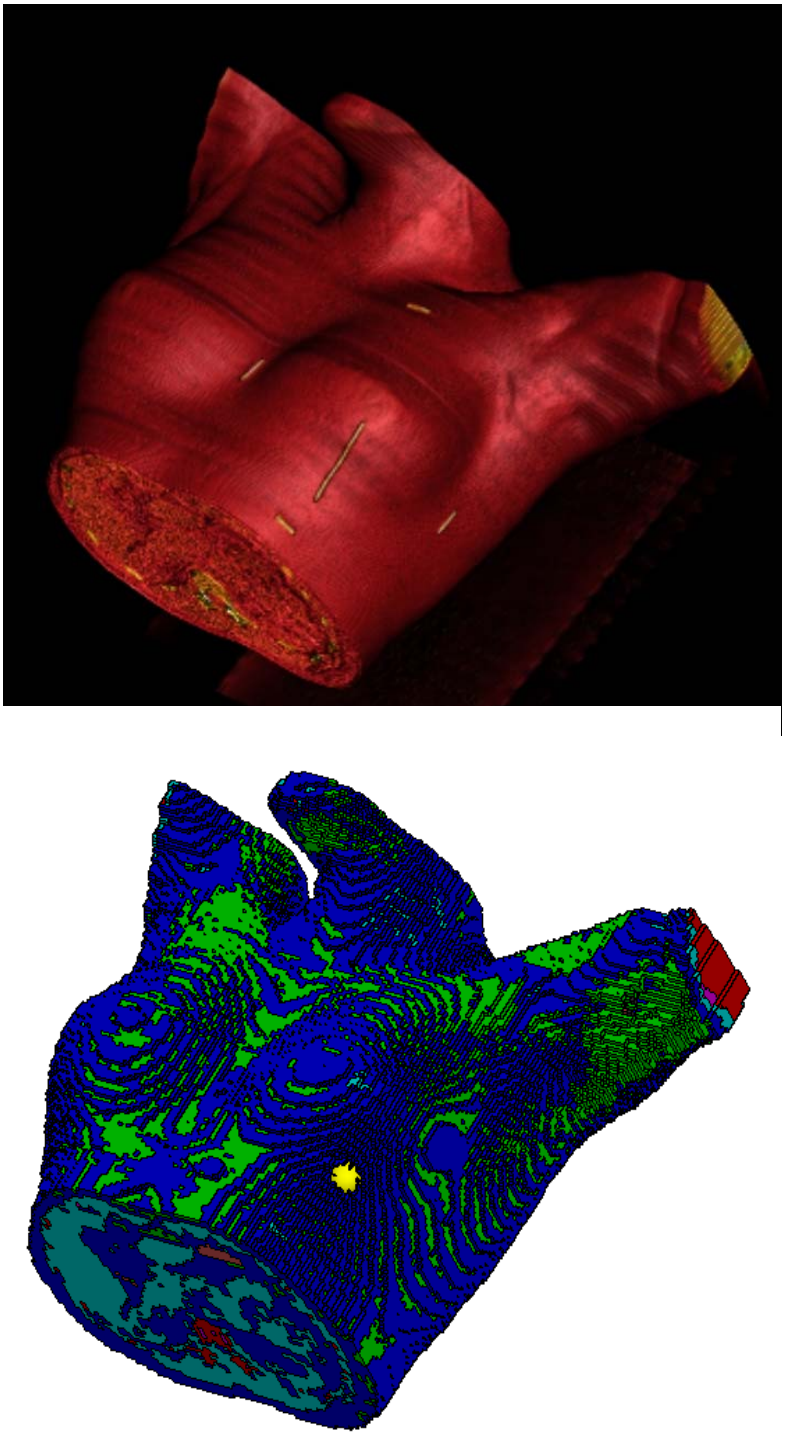

Figure 3-5. 3D reconstruction of patient-specific images used. Wire scares used for photon beam alignment observable (top). Lattice representation of patient geometry (bottom) used in MCNP calculations.

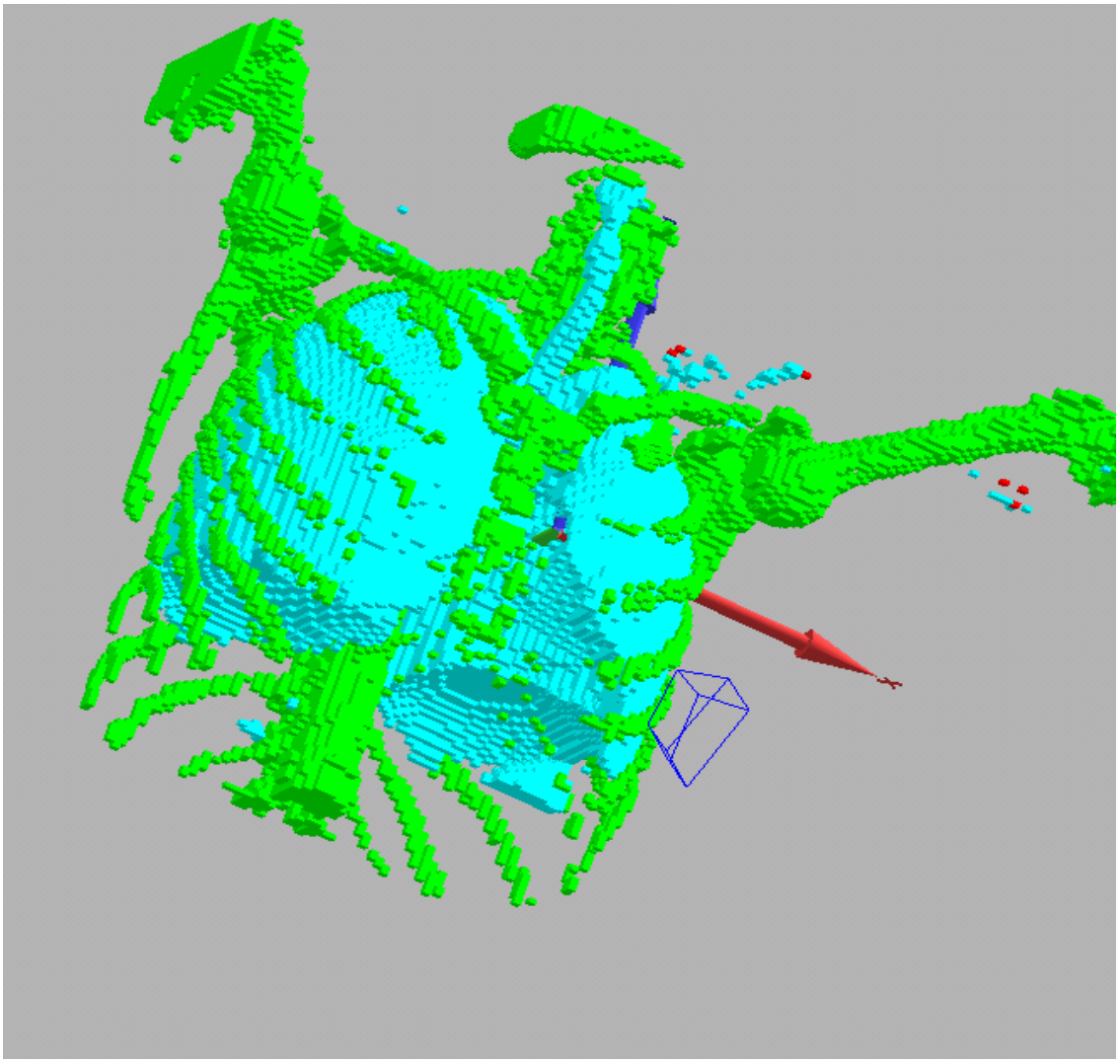

Figure 3-6. Moritz-generated image of patient lattice showing the MCNP “arb” cell type representing the tumor volume. The cell represents the tumor volume defined in patient dose plan. (Soft Tissue not shown)

therapy, multiple beam angles are used to reduce the exposure to the skin and to ensure better average dose throughout the treatment volume. However, once the placement of the beam effort began, it became obvious that the location of the tumor volume and its relative location within the patient's body, limited the number of views that would result in the T/S ratios that have been defined for this study. Ultimately, a direct beam, perpendicular to the surface of the skin was chosen as the representative treatment beam for this study. This placement resulted in an effective tumor volume depth of approximately 1 cm; other possible beam angles would have resulted in an effective tumor depth of 2 to 3 cm. This resulted in other complications that are described below, but it was assumed that the results were representative of the potential of the proposed therapy so no other beam angles were considered. An example illustration of the Moritz planning screen, with particles tracks is shown in Figure3-7.

MCNP Simulation and Dose Evaluation

The contents of the MCNP modeled tumor volume were filled with the different tissue and boron concentrations that were examined for this study. The tissue compositions, MCNP cross section files, and Kerma weighting factors for neutrons and photons were defined in each individual MCNP input file. Nine files were run, each with different T:H and boron concentrations, including one with normal soft tissue with no boron present. Each MCNP file was run for 10^7 histories. Mesh tallies with the appropriate Kerma weighting factors were obtained for both photons and neutrons throughout the entire volume of the DICOM dataset. The mesh tallies used voxels of 0.5 cm in each of the three directions. This provided dose at each point throughout the patient volume. Additional Kerma weighted tallies of the tumor volume were also obtained.

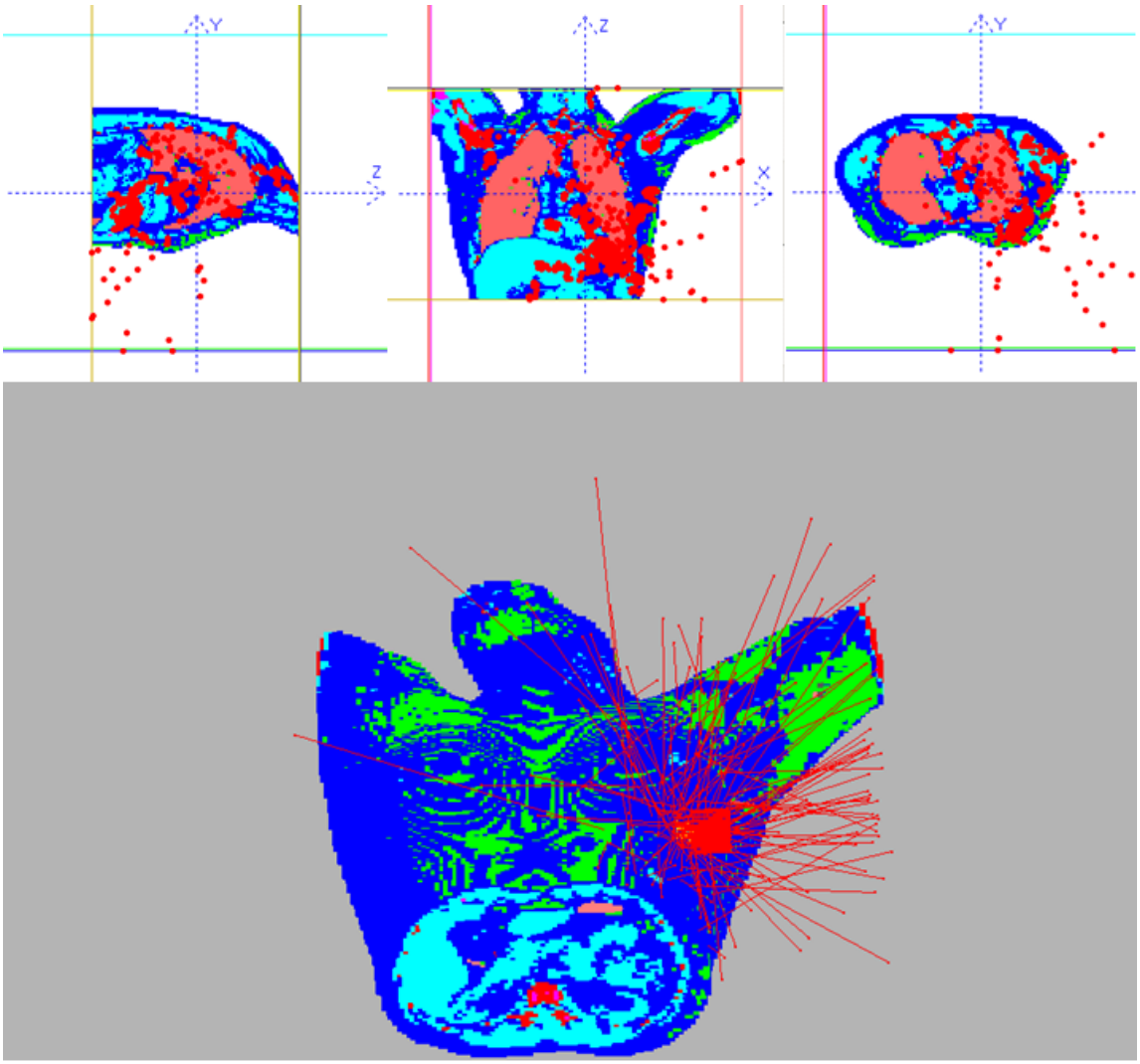

Figure 3-7. Mortiz planning screen with patient geometry and MCNP source and interaction particle tracks shown. In order to ensure proper tumor volume irradiation and to evaluate best beam angulations, several different iterations were run.

CHAPTER 4

RESULTS AND FINDINGS OF CALCULATIONS

Kerma Coefficient

The Kerma coefficients were first calculated for each element found in the tissues of interest. The tissues of interest were those tissues that are found in the female thorax: skin, mammary gland, heart, lung, adipose, muscle, ribs, and thyroid. These tissues were primarily made up of hydrogen, carbon, nitrogen oxygen, sodium, phosphorus, sulfur, chlorine, potassium, calcium, iron, and iodine. The elemental Kerma coefficient for boron was also calculated. The Kerma coefficient was first calculated at 1,000 energy point covering the range 10^{-10} to 20 MeV. Figure 4-1 shows the results of these calculations.

The relative importance of each element is clearly seen in Figure 4-1. For tissue compositions that include boron, the total Kerma coefficient below about 0.02 MeV will be dominated by the boron effect. The other elements in this energy range have a lower, almost negligible, contribution relative to the total Kerma coefficient. In borated tissues, the energy range above 0.02 MeV will be dominated by hydrogen. However, the contribution of hydrogen is less of a dominating factor in the overall Kerma coefficient than boron is below this energy level. The elemental Kerma coefficients for boron and hydrogen are approximately equal at 0.02 MeV, with a value of 1.7×10^{-11} Gy-cm^2. Also note that in absence of boron, the most important element below 1.2×10^{-4} MeV is nitrogen and above this value is hydrogen. However,

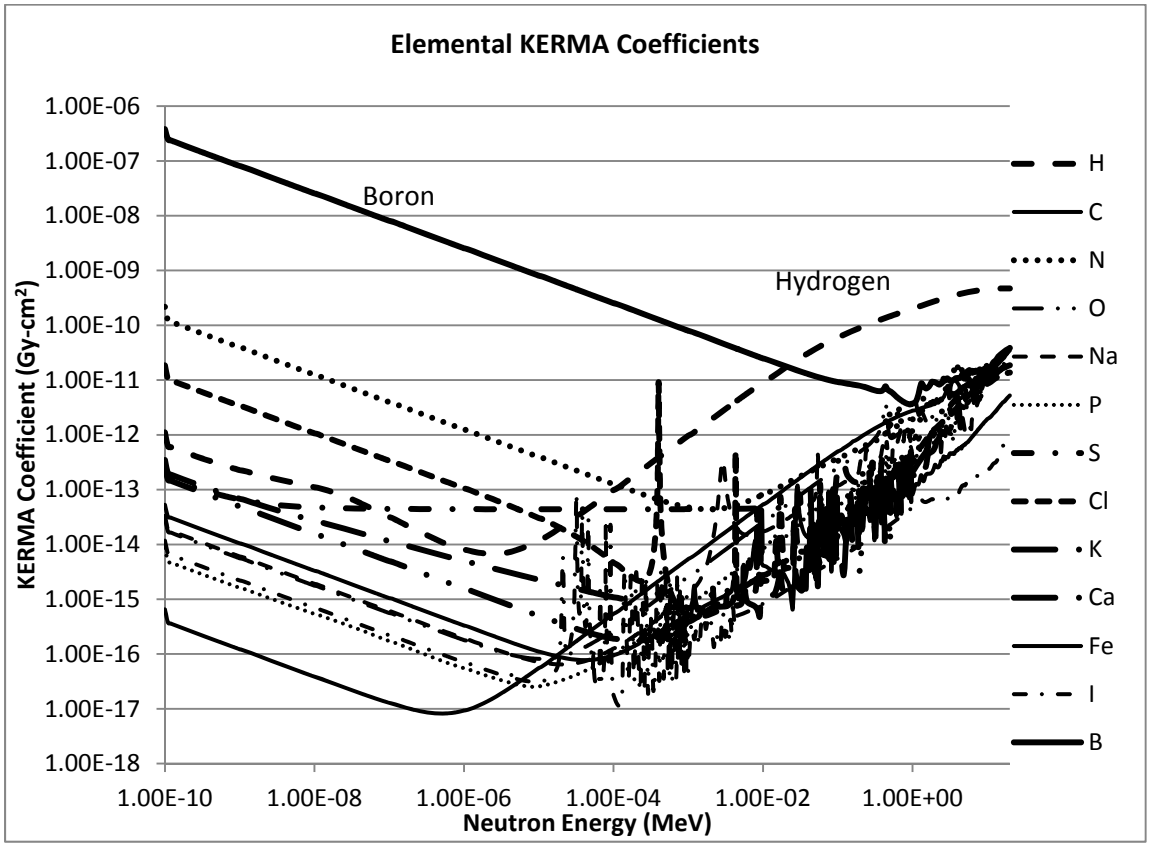

Figure 4-1. Elemental Kerma coefficients (Gy-cm2/MeV). Note the relative importance of boron at neutron energies below 0.02 MeV and the importance of hydrogen above 0.02 MeV. $K_B=K_H$ at 0.02 MeV K=1.7 x 10^{-11} Gy-cm^2. In the absence of boron the most important element below 1.2 x 10^{-4} MeV is nitrogen and above this value is hydrogen. Note the chlorine "spike" at 4 x 10^{-4} MeV, which can be observed in other tissue compositions.

also note the chlorine "spike" at 4 x 10^{-4} MeV, which can be observed in nonborated tissue compositions.

Tissue compositions were discussed and summarized in Chapter 3. Using these tissue compositions, and based on the elemental Kerma coefficients calculated and summarized above, the total tissue Kerma coefficient can be calculated. These tissue Kerma coefficients are based on the contribution of all the elements listed above and indicated boron concentrations, as applicable. Figure 4-2 shows the results of the Kerma tissue coefficients for the indicated tissues.

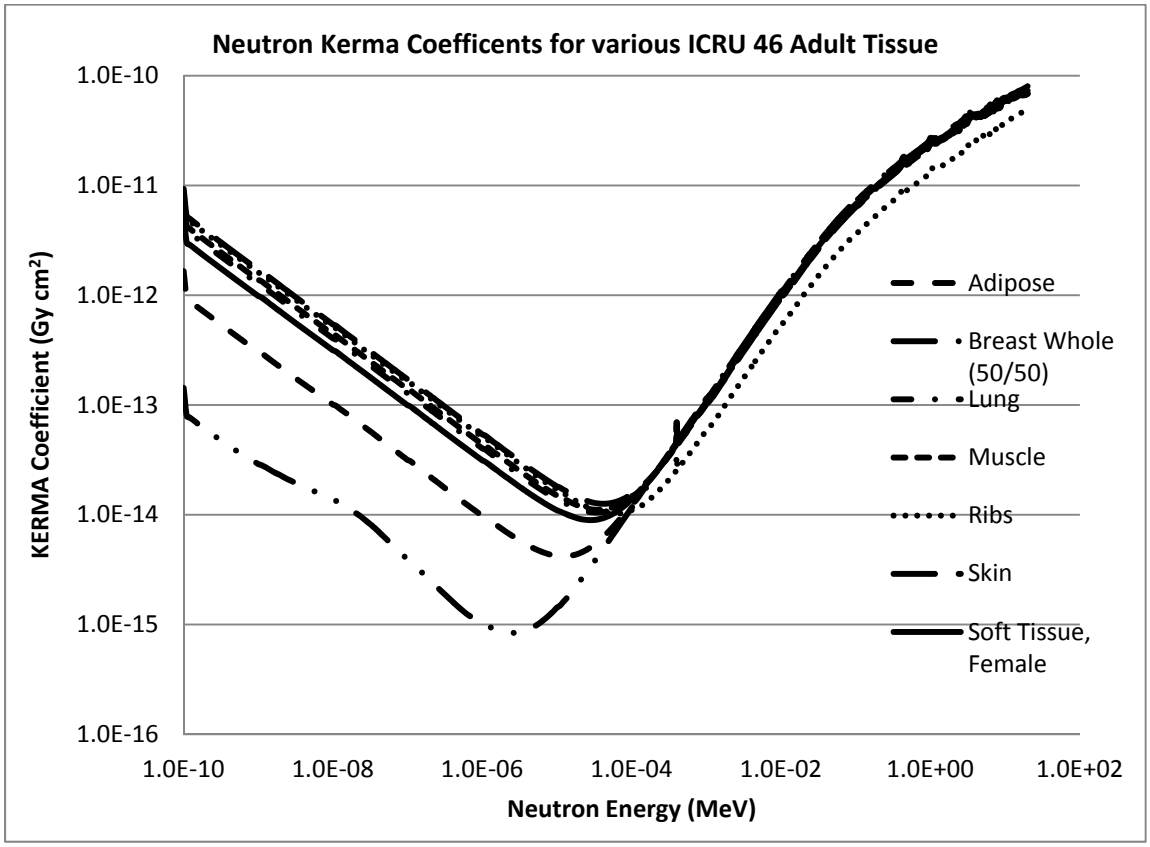

Figure 4-2. Tissue Kerma coefficients for neutrons calculated for various ICRU 46[30] tissues.

The Kerma coefficients used in the MCNP dose calculations for the patient-specific geometry, outside the tumor volume and skin, are based on female soft tissue; no other tissue compositions are used. One difficulty encountered during the current proof of concept study was how to best calculate the weighted dose in a complex geometry, such as the patient-specific geometry, in a meaningful manner but still be able to account for the varying changes in Kerma and neutron interactions due to changes in elemental composition, density, etc. As can be seen in Figure 4-2, many of the tissue Kerma factors are essentially equal above about 1×10^{-4} MeV in nonborated tissues. And below this energy, the Kerma coefficient is dominated by the boron concentration. In order to simplify the dose calculations, female soft tissue was assumed for all dose calculations outside the tumor volume and the skin dose calculation. The density and

composition of female soft tissue most readily represents the entire group than any on single tissue. In other words, the sole use of female soft tissue in borated tissue compositions has little to no effect on the overall dose estimation. In nonborated tissues, the effect would be to slightly underestimate the dose to those tissues that have actual Kerma coefficients greater than female soft tissue. This difference in dose estimation due to the use of soft tissue for all Kerma approximations is less than 30% in muscle and up to a factor of 2 greater than areas high in fat at low energies.

Borated tissue neutron Kerma coefficients are shown in Figure 4-3. The effects of the different boron concentration in the tissue are noted with ease, but the relative differences for

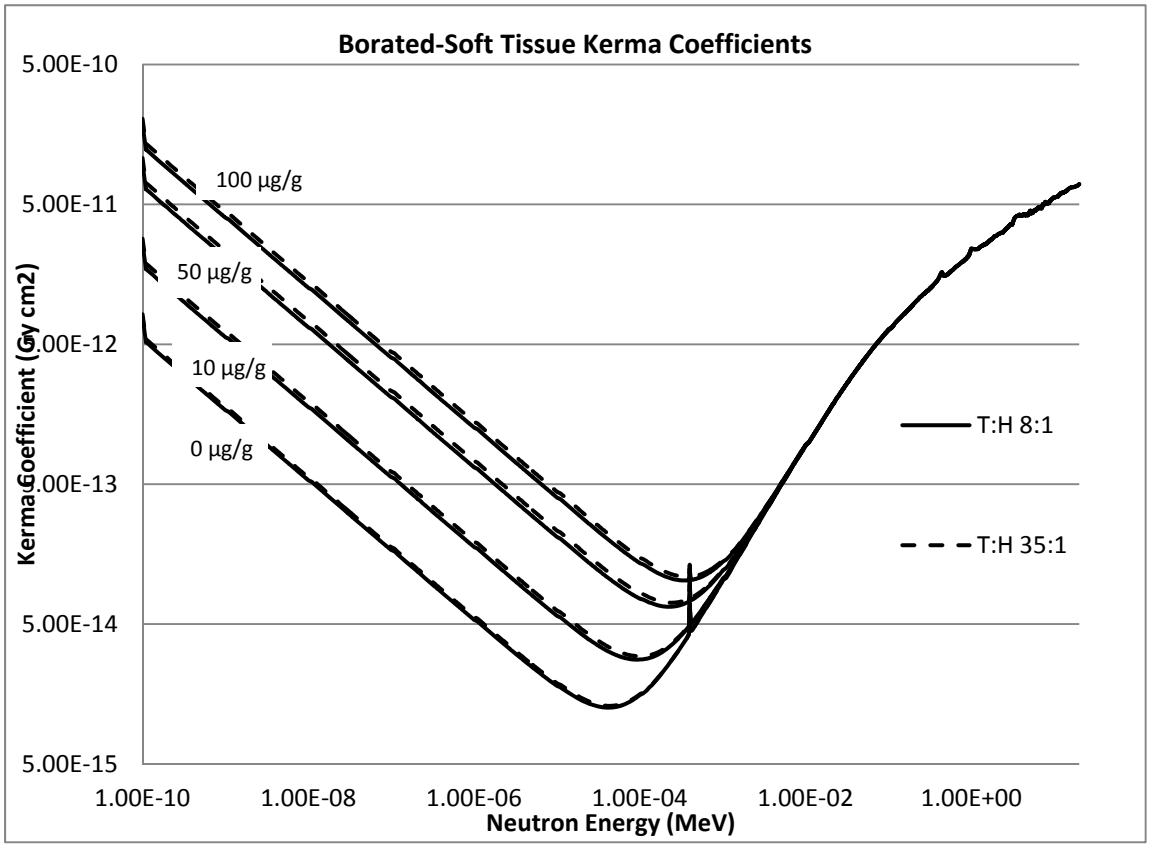

Figure 4-3. Total tissue Kerma coefficient for borated tissues. Note chlorine "spike" near 4 x 10^{-4} MeV.

the same concentration caused by the different T:H ratios are not as great. The relative effect on overall Kerma coefficient is illustrated here, demonstrating that the greatest impact on Kerma coefficient, and thus dose, is the boron concentration. The smaller, but observable, difference in Kerma coefficients observed is due to the different elemental composition and density of the tumor volume due to these composition changes. Also note the convergence in Kerma coefficients between 10^{-3} and 10^{-2} MeV. As was observed above, the relative contribution of boron below this energy range and hydrogen above this energy range is evident here. Photon Kerma coefficients were also calculated using the same techniques as applied to the neutron Kerma coefficients. Calculations were performed for the same elements and tissue compositions. The results of these calculations for the nonborated tissue compounds are shown in Figure 4-4. Figure 4-5 shows the calculated photon Kerma coefficients for borated soft

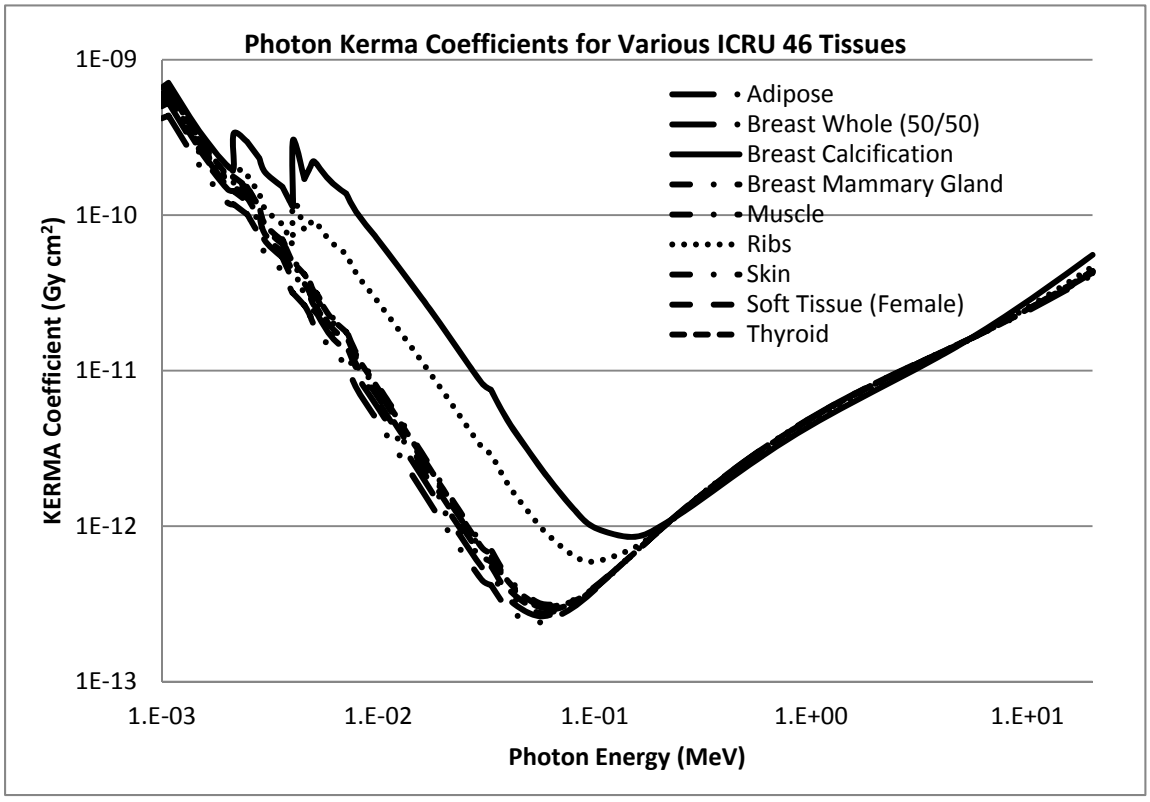

Figure 4-4. Photon Kerma coefficients for nonborated tissues

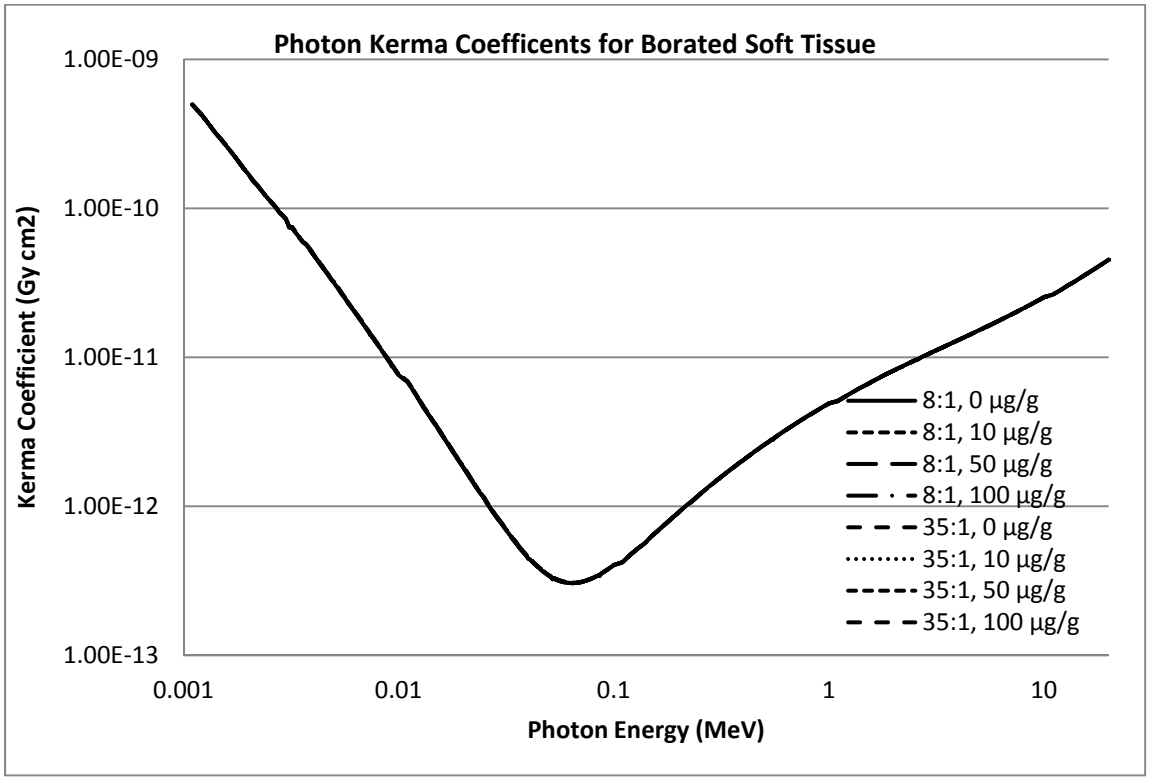

Figure 4-5. Photon Kerma coefficients for borated soft tissue. All T:H ratios and boron concentrations listed in the legend are shown in the Figure. All datasets shown in the legend are present in the graph.

tissues at the varying T:H ratios and boron concentration levels. Note that for the majority of elements and all the borated compounds, the photon Kerma coefficients are essentially equal. Figure 4-5 shows all the coefficients for the tissues listed in the legend. For these data it can be determined that the boron concentration has little effect on the total Kerma coefficient and that the tissue composition is the most significant factor for photons Kerma determination.

Also observed in Figures 4-1, 4-2, and 4-3 is a prominent “spike” that is not typically observed in other published Kerma values. This spike is associated with the elemental Kerma coefficient of chlorine. In other published data, coefficients are often extrapolated over large energy ranges or do not include the contribution from all the elements to the total Kerma coefficient. Consequently, this spike is not observed. The question of how much of a

contribution to the overall Kerma coefficient this spike and other portions of the spectrum are to the overall total Kerma coefficient is justly asked. Figure 4-6 shows the total tissue Kerma coefficients for borated and nonborated soft tissue superimposed over the neutron source energy spectrum. The most likely neutron source energy occurs in the most minimal regions of the Kerma curves. This information may be useful for beam optimization in future studies. But in the current study it tends to suggest that more information is needed in order to determine the actual contribution to the total Kerma coefficient.

In order to more closely examine this question, the total tissue Kerma coefficient was multiplied by the relative neutron source abundance. This gives a clearer picture of the relative

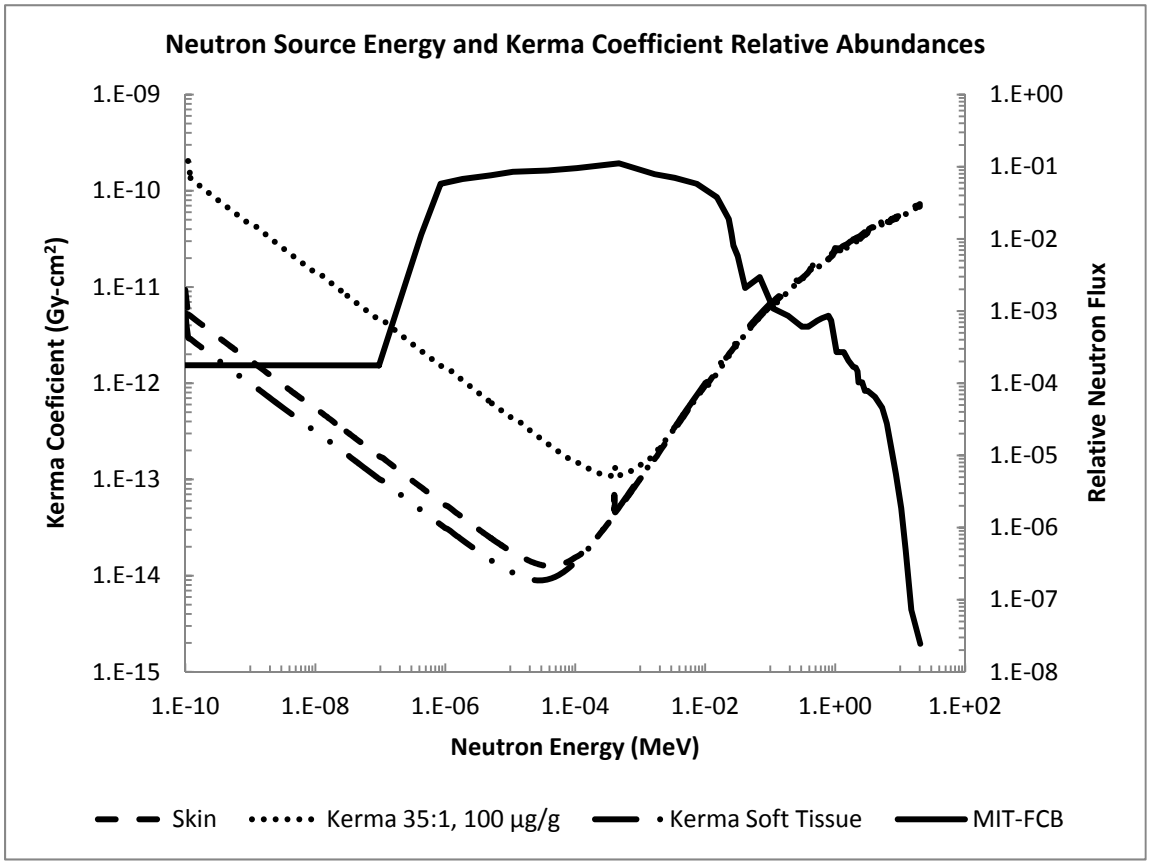

Figure 4-6. Neutron source energy relative abundance and Kerma coefficients for nonborated soft tissue, skin, and borated (35:1, 100 µg/g) soft tissue

Kerma contribution to total dose per neutron energy range. Figure 4-7 displays the results for normal soft tissue. Note the majority of contribution to the total Kerma coefficient falls in the range of about 1.5 x 10^{-3} to 4 x 10^{-2} MeV. This is the region of the elemental Kerma curve that was dominated by hydrogen in the absence of boron. This demonstrates the importance of neutron interactions with hydrogen in the overall contribution to dose. Figure 4-8 shows the relative contribution to the total tissue Kerma coefficient for borated soft tissue. The contribution of lower energy neutrons is apparent in the curve.

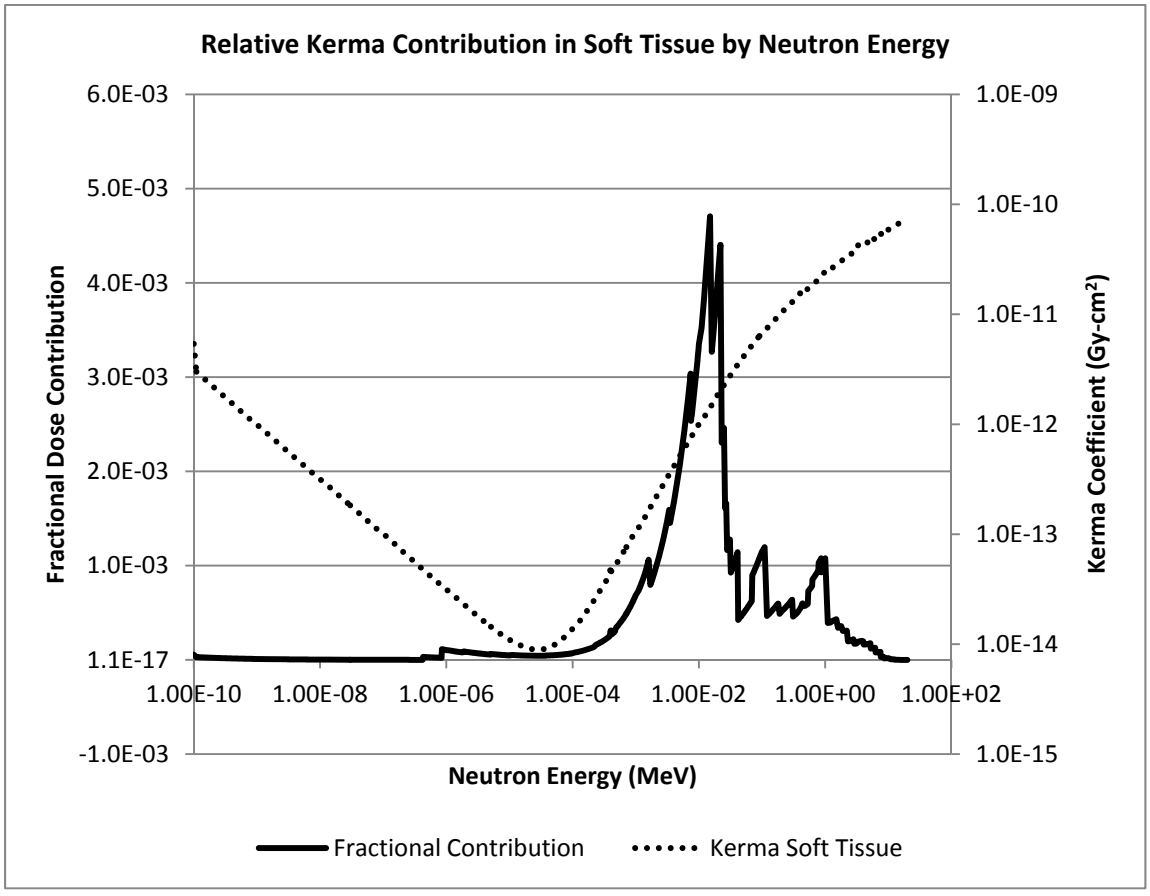

Figure 4-7. Relative Kerma contribution in soft tissue per neutron energy associated with beam source, unmoderated by tissue

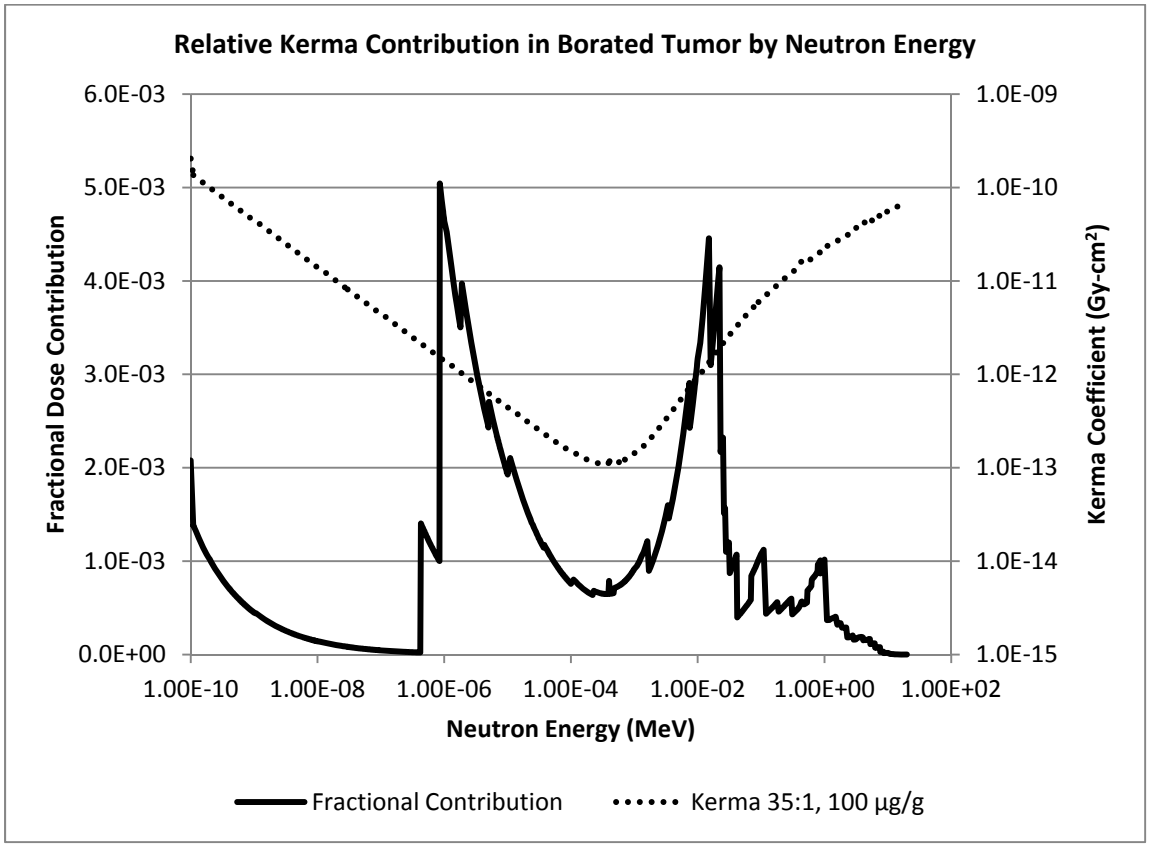

Figure 4-8. Relative Kerma contribution in borated tissue per neutron energy associated with beam source unmoderated by tissue

Clearly this preceding example examines only the relative contributions of neutron energies observed in the source beam and does not account for any slowing that will occur as the beam penetrates into tissue. As the neutrons slow, the contribution of the low energy Kerma coefficient is expected to have a greater and greater impact on the total Kerma coefficient, which will lead to higher boron-effect efficiency in the target volume. Of course as the beam penetrates deeper in tissue, the fluence will also decrease, eventually reducing to a point where it is no longer useful from the therapy perspective. This is discussed below in the context of the T/S ratios.

With respect to the chlorine spike mentioned above, it is clear that while the contribution can be calculated, the effect to the overall Kerma coefficient is very small.

Considering the presence of many of these spikes associated with other elements, it is worthwhile to consider the cumulative effect of all the elements combined. In other words, taken individually the contribution may be insignificant to the effect of boron or hydrogen, but taken collectively these small contributions effectively increase the overall Kerma coefficient and should not be rejected too hastily. The ability to easily calculate relevant Kerma coefficients for source and target tissues leads to more realistic dose estimates. The process and results of Kerma calculations present in this study include a more complete set of elements in the Kerma coefficients than what has been previously provided.

Kerma Coefficient Comparison

In order to demonstrate the validity of the results of the calculation of Kerma coefficients, the results were compared to available published data. It was expected that the calculated data would be able to accurately reproduce the elemental Kerma coefficients for more common elements such as hydrogen, etc. In fact this was the case. Figure 4-9 shows the calculated Kerma coefficient for hydrogen compared to the data published in ICRU 63.[28] There is very good agreement (average less than 2% difference between calculated data and published data) for all areas of the curves except for the low energy area around about 10^{-8} MeV. In this region, the published data were extrapolated between calculated values.

The same calculations and comparisons were performed for the ICRU 63 published values of carbon, oxygen, and nitrogen. Throughout the majority of the comparison curves, there remains an average +/- 2% maximum Kerma coefficient difference over the 1,000 energy points at which Kerma was calculated. The only exception is through energy ranges in which extrapolation of published values is clear. The graphs for these elements are not provided here. As with the comparison of hydrogen, no deviation from between the datasets is apparent so no

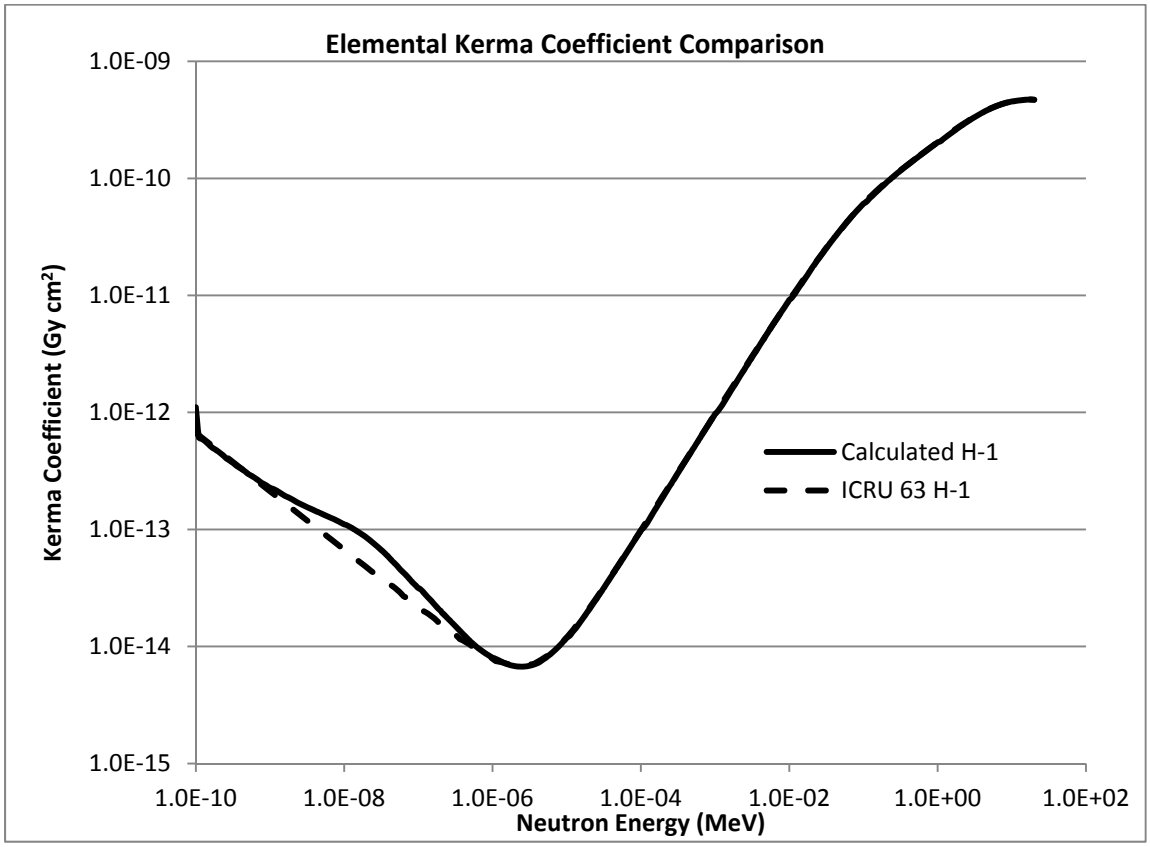

Figure 4-9. Elemental Kerma coefficient for hydrogen. A comparison of the calculated Kerma coefficient per neutron energy and published data in ICRU 63[28] is shown. Note extrapolated area of published data.

additional value is added by providing the graphs. Tables of calculated values for all elemental and tissue Kerma factors are provided in Appendix A.

As was noted in Chapter 3, not all elements were available in published sources for use in the calculation of tissue Kerma coefficients for the tissues of interest in this study. The primary reason stated in Chapter 2 for the effort of calculating Kerma coefficients was to fill in the gaps in the values that are available in published locations. As was noted above, the additional contribution of the total Kerma value is small for most of these additional elements, compared to the significant contributions from hydrogen and boron. However the cumulative effect of the other elements results in a significant contribution that should not be overlooked.

These calculation efforts demonstrate a simple procedure to obtain Kerma coefficients for use in any potential combination yet to be studied.

Skin Dose

Dose to the skin was calculated using the Kerma coefficients for the skin from neutrons originating from the MIT-FCB neutron source described in Chapter 3. Dose was calculated at the center of the incident beam for both neutrons and photons over an MCNP mesh tally with depth increments of 0.25 mm. Figure 4-10 shows the results of these calculations for the skin for the first 3 mm depth. The increase of total weighted dose with depth is expected based on the types of neutron interactions with matter. The neutron and photon dose increases slightly over the thickness of the skin. Further analysis of the data was performed to determine the depth at

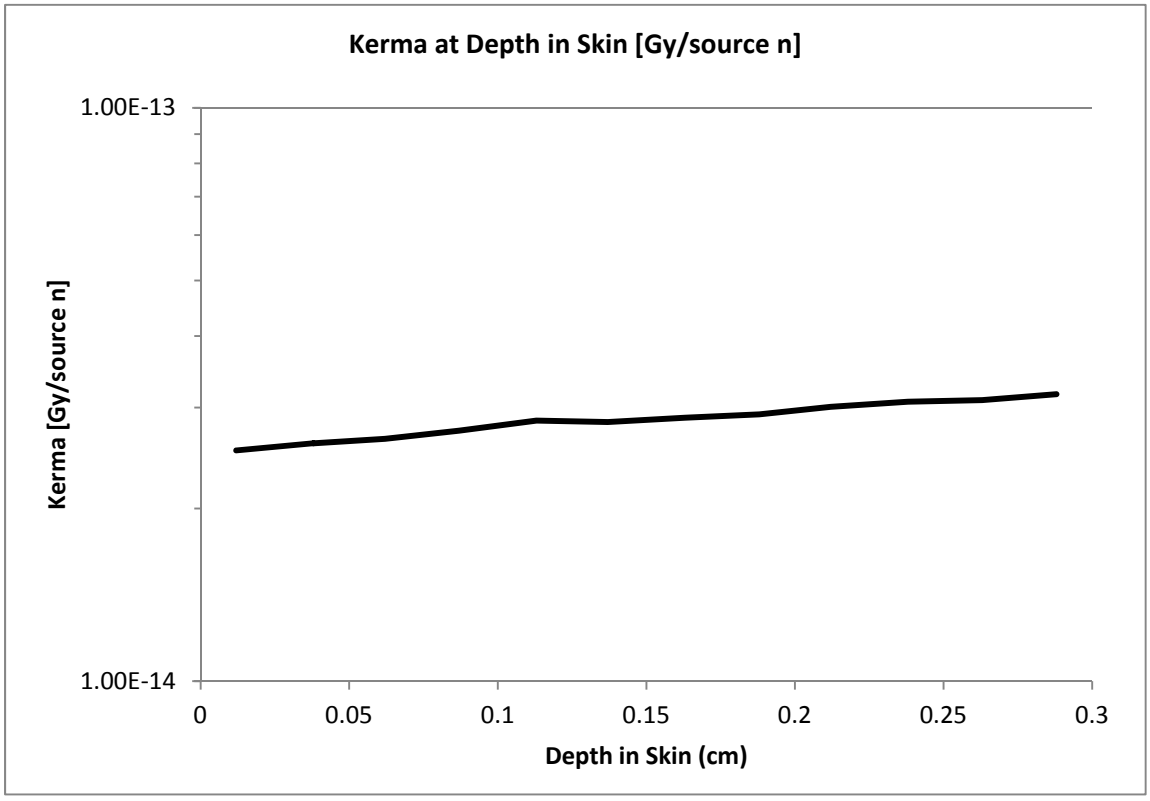

Figure 4-10. Kerma rate (Gy per source neutron) at varying depth in skin (ρ=1.09g/cm^3)

which the maximum dose occurs. As observed in Figure 4-11, this maximum neutron and photon dose depth is about 2 cm for soft tissue, which is assumed to make up the subcutaneous layer as well as the other underlying layers as described in Chapter 3 for the description of Kerma coefficients. Because the maximum dose is at a depth much greater than the thickness of the skin, the most conservative estimate of skin dose is to assume dose is measured at the maximum depth of the skin. For this study, the maximum skin thickness was assumed to be 3 mm. This is greater than the average skin thickness for the breast, but still provides a reasonable estimate for the skin without being too conservative. Because the skin dose to tissue dose is one key evaluation parameter in this study, using a value that was overly conservative would provide unwarranted bias to the evaluation.

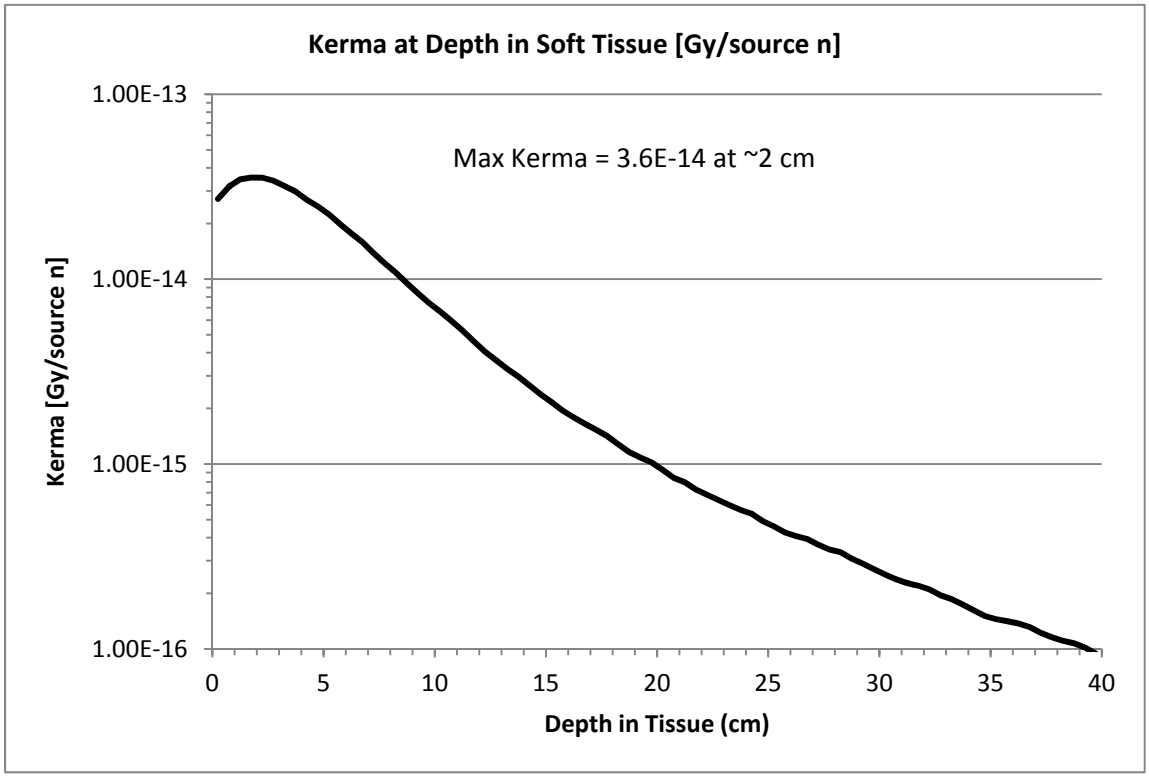

Figure 4-11. Kerma rate (Gy per source neutron) at varying depths in Soft Tissue (ρ=1.02 g/cm^3)

The total weighted skin dose rate was calculated to be 2.98 x 10^{-14} Gy/n. This value accounts for the total Kerma coefficients for both neutrons and photons for the atomic makeup and density of skin assumed for this study. No boron was assumed to be present in the skin. For the assumed neutron source fluence rate of 5 x 10^{9} n/s-cm^2 and a beam diameter of 8 cm, the total neutron source flux was assumed to be 2.5 x 10^{11} n/s. At the skin depth of 3 mm, and an assumed RBE_n of 3 for the skin, the average total weighted skin dose of 2.25 x 10^{-2} Gy/s was assumed.

Tumor-to-Skin Dose Ratio

For the estimation of T/S ratio at varying depths in tissue, a 1 cm diameter spherical tumor of the varying T:H ratios and boron concentrations was modeled at varying depths. The indicated T:H and boron concentrations are assumed to exist only in the tumor volume. No boron is assumed to exist outside the volume of interest.

The resulting tumor dose rates to the above stated skin dose rates were used to estimate T/S dose ratios. For both T:H of 8:1 and 35:1, the only boron concentrations that produced high enough T/S ratios were 50 and 100 μg/g. Any boron concentration level less than these values, regardless of the tumor depth, resulted in T/S ratios less than 2.3, with most combinations resulting in T/S ratios less than 2. The results of the spherical tumor depth-dose simulation are shown in Figure 4-12 for T:H of 8:1 and Figure 4-13 for T:H of 35:1. These Figures show the almost exponential decrease in T/S ratio and tumor depth decreases.

As can be expected, there is exists a maximum depth at which the T/S ratio no longer is high enough in order to meet the basic treatment requirement of a T/S ratio of at least 2.7. The maximum depth for T:H 8:1 for which this condition is met is approximately 4.7 cm. The maximum depth for T:H 35:1 is approximately 4.9 cm. From these results, it can be shown that

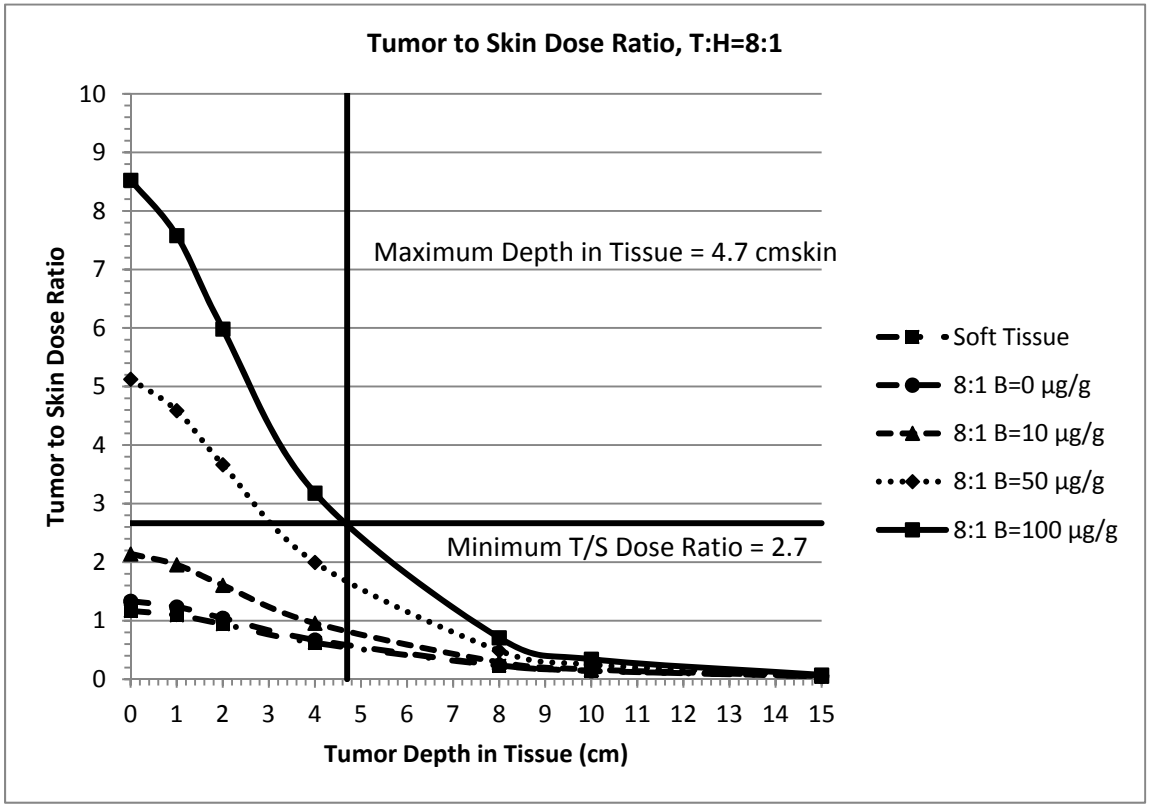

Figure 4-12. Tumor to skin weighted dose ratio (RBE_n=3) for tumor-to-healthy tissue ratio of 8:1. Maximum depth in tissue such that T/S ≥ 2.7 is 4.7 cm in Soft Tissue.

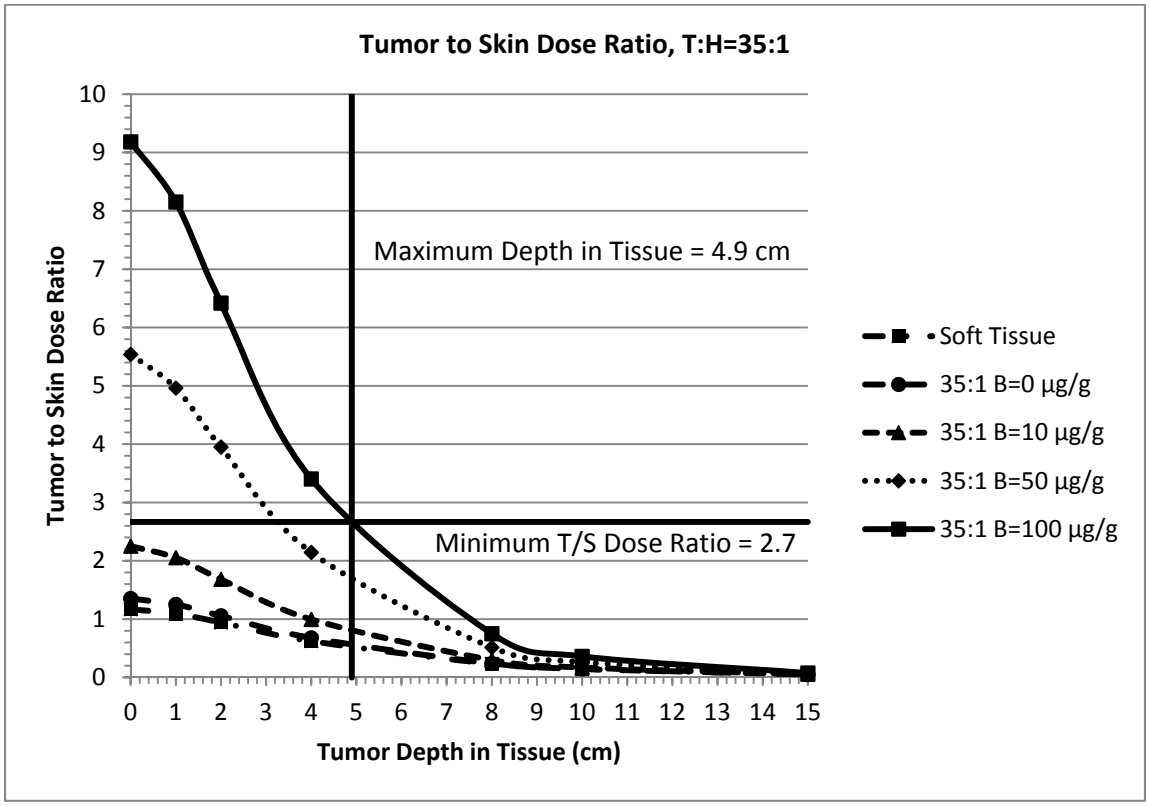

Figure 4-13. Tumor to skin weighted dose ratio (RBE_n=3) for tumor-to-healthy tissue ratio of 35:1. Maximum depth in tissue such that T/S ≥ 2.7 is 4.9 cm in Soft Tissue.

the most important factor in T/S ratio is the overall boron concentration found in the treatment volume. While the T:H ratio is important in order to have enough cancer receptor cell to capture the boron, the overall boron concentration is a more sensitive indication of dose efficiency in the context of T/S ratios.

Fluence to Tumor

As a result of the dose-depth calculations, an estimate of the approximate neutron fluence can be made. It was determined that the maximum depth for a spherical tumor volume with a T:H of 35:1 and boron concentration of 100 μg/g was 4.9 cm. Using the MCNP mesh tally for neutron fluence over the volume of the soft tissue used for the dose depth calculation, the neutron fluence at the maximum depths can be determined. During the dose depth calculation the F4 tally was used for a mesh that consisted of $1cm^3$ tally volumes. The results are shown in Figure 4-14 as the neutron fluence as a function of depth in soft tissue (nonborated). It is observed that the minimum fluence at a depth of 4.9 cm is 1.6×10^{-2} n/cm2. Similar observations for the remaining T:H and boron concentrations are given in Table 4-1.

Table 4-1. Table of minimum Neutron Fluence for T/S greater than 2.7.

	Neutron Fluence (n/cm^2)
Soft Tissue	T/S < 2.7, NA
8:1 B=0 μg/g	T/S < 2.7, NA
8:1 B=10 μg/g	T/S < 2.7, NA
8:1 B=50 μg/g	3.20E-02
8:1 B=100 μg/g	1.70E-02
35:1 B=0 μg/g	T/S < 2.7, NA
35:1 B=10 μg/g	T/S < 2.7, NA
35:1 B=50 μg/g	3.00E-02
35:1 B=100 μg/g	1.60E-02

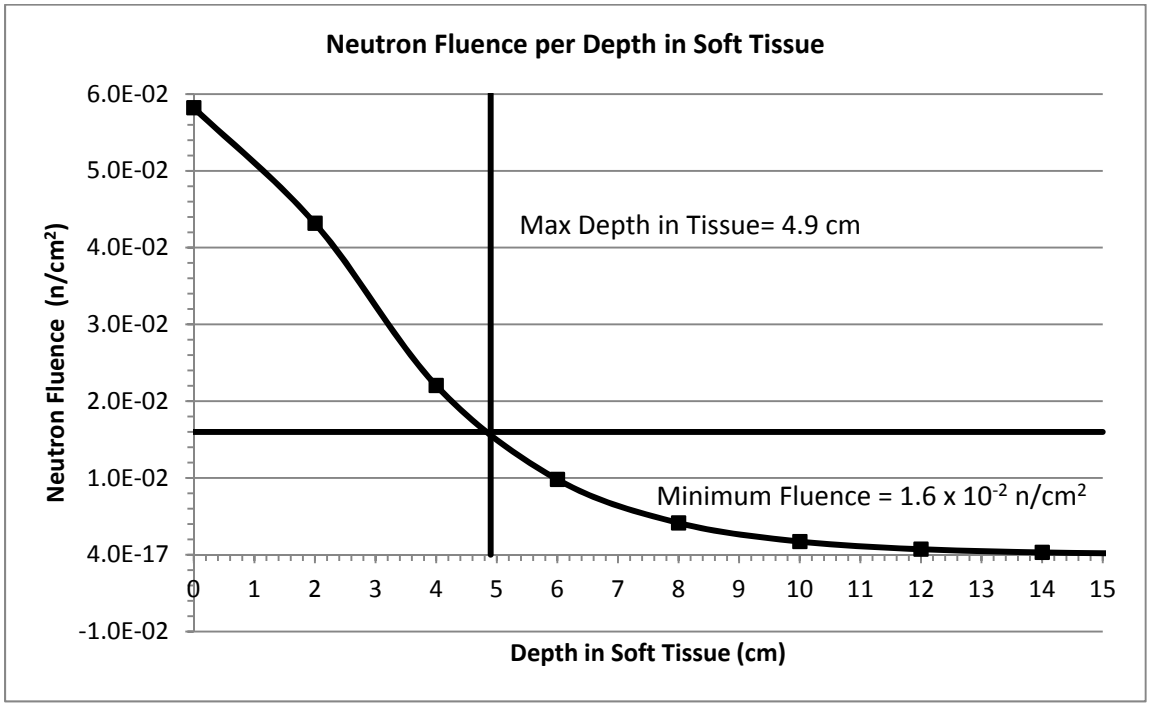

Figure 4-14. Neutron fluence per depth in soft tissue. Maximum depth of 4.9 cm correlated to tumor T:H ratio of 35:1 and a boron concentration of 100 μg/g such that T/S > 2.7.

Patient-Specific Dose Estimation

The main effort in this proof of concept study was to establish a model that could be used to compare the dose that a patient would receive during a conventional photon radiation therapy postsurgery. As was described in Chapter 2 and 3, the model that was selected to compare dose was for a patient who received whole breast irradiation following lumpectomy. The average dose to the tumor volume was 53 Gy. Imaging and therapy data was obtained for this patient. A simulation using a process of a series of steps was undertaken to calculate radiation dose to the patient and individual organs for comparison of dose and other pertinent parameters. The steps to calculate dose to the patient for the proposed BNCT therapy included:

1. Process patient CT images using Scan2MCNP to generate lattice geometry for MCNP input geometry definition

2. Use Moritz for visualization of tumor volume placement, beam positioning definition, and general visualization
3. Create MCNP input files that includes geometry, source, and tissue definitions
4. Create and run MATLAB script and functions to process MCNP mesh tallies into 3-D dose array (scripts and functions in Appendix B)
5. Load 3-D dose date into CERR for dose metric evaluation

The results of these steps are described below. The results of many of the MCNP were output in files containing close to 4.5 million lines of data. It is impractical to report all the data obtained during this effort. The results described below are a summary representation of the data obtained.

The results of the MCNP mesh tallies provided dose per source neutron at each point throughout the patient. Simple multiplication by source fluence rate and irradiation time resulted in the total dose at any given point in the patient. For areas within the tumor volume, mesh tallies based on the borated Kerma coefficients were used. All areas outside the tumor volume were derived from mesh tallies that were based on nonborated Kerma coefficients. The organ contours that were defined in the original patient file were used for the BNCT DHV and average dose determinations. This greatly simplified the comparison process and ensured the same body regions were being compared during the evaluation.

Irradiation times were chosen so that the average dose to the tumor volume in each T:H and boron-concentration scenario would be equivalent to the mean dose from the photon-based therapy. By using the same mean dose to the tumor volume in each scenario, T/S ratios and DVH comparisons were simplified. The results of these dose calculations are shown in Table 4-2. The organs and regions of interest are the same as those that were originally defined clinically for the patient during actual clinical therapy. The total skin dose from the photon

Table 4-2. Summary tissue and skin dose results for patient-specific hypothetical treatment scenario

	Irradiation Time (s)	Lump Cavity (Gy)	Heart (Gy)	LT Lung (Gy)	Total Lung (Gy)	Body (Gy)	Total Skin (Gy)	T/S
Photon Dose	na	51.4 (46 53.3)	2.4 (0.3 50.1)	7.1 (0.1 51.1)	3.3 (0.1 51.1)	4.6 (0.1 54.7)	17.8	2.9
Soft Tissue	6465	51.4 (40.7 60.9)	5.2 (0.9 25.7)	4.6 (1.3 31.1)	2.4 (0.1 31.1)	2.0 (0.1 51.9)	145.4	0.4
8:1, 0µg/g	5207	51.2 (36.7 58.3)	4.1 (0.9 19.9)	3.7 (1.1 24.5)	1.9 (0.1 24.5)	1.6 (0.1 40.5)	117.1	0.4
35:1, 0µg/g	5120	51.4 (36.5 58.9)	4.0 (0.7 19.5)	3.6 (1.1 24.3)	1.9 (0.1 24.3)	1.6 (0.1 40.1)	115.1	0.4
8:1, 10µg/g	2450	51.5 (31.1 59.7)	1.9 (0.3 9.5)	1.7 (0.5 11.5)	0.9 (0.1 11.5)	0.8 (0.1 18.9)	55.1	0.9
35:1, 10µg/g	2288	51.4 (30.5 59.9)	1.8 (0.3 8.7)	1.6 (0.5 10.9)	0.9 (0.1 10.9)	0.7 (0.1 17.7)	51.5	1.0
8:1, 50µg/g	815	51.5 (27.9 60.1)	0.6 (0.1 3.1)	0.6 (0.1 3.9)	0.3 (0.1 3.9)	0.3 (0.1 6.3)	18.3	2.8
35:1, 50µg/g	743	51.4 (27.7 60.1)	0.6 (0.1 2.9)	0.5 (0.1 3.5)	0.3 (0.1 3.5)	0.3 (0.1 5.7)	16.7	3.1
8:1, 100µg/g	454	51.4 (27.5 59.7)	0.3 (0.1 1.7)	0.3 (0.1 2.1)	0.2 (0.1 2.1)	0.2 (0.1 3.5)	10.2	5.0
35:1, 100µg/g	417	51.4 (27.5 59.3)	0.3 (0.1 1.5)	0.3 (0.1 1.9)	0.2 (0.1 1.9)	0.2 (0.1 3.3)	9.4	5.5

therapy is the sum of the entrance regions of interest defied in the patient plan. The skin doses for the BNCT therapy scenarios were calculated using the skin dose rate discussed earlier. The mean, max, and min dose for each region of interest is given to better illustrate the different DVH's observed in the various organs between the T:H and boron concentrations.

From the information in the table for the treatment scenario described for this study, it is evident that only those scenarios in which at least 50 μg/g of boron were present in the treatment volume met the minimum T/S ratios required by the proposed BNCT therapy design parameters. The T:H ratios modeled for this study (8:1 and 35:1) showed only a slight change in the effect on the therapeutic ratios.

The dose distribution through the treatment volume for the photon-based therapy is clearly more uniform than that modeled for the BNCT therapy (Figure 4-15). The first and most obvious reason for this is the fact that the treatment volume modeled for the BNCT based therapy did not exactly overlap the photon treatment volume. Because the BNCT therapy relied on the boron concentration in this volume in order to provide the treatment dose, and because it was not entirely contained in the same volume as the photon volume, there was an immediate difference in the uniformity in the treatment volumes. The photon therapy dose was delivered in several fractions through multiple beam entrance angles, one medial and one lateral. The effect on the dose distribution through the tumor region is much more uniform for the photon therapy (Figure 4-16). The dose in the BNCT scenario was from a single fractionation from a single entrance angle (Figure 4-17). The placement of the neutron beam will greatly impact the overall uniformity of the dose distribution due to the limited range of the neutrons as they travel through the tissue.

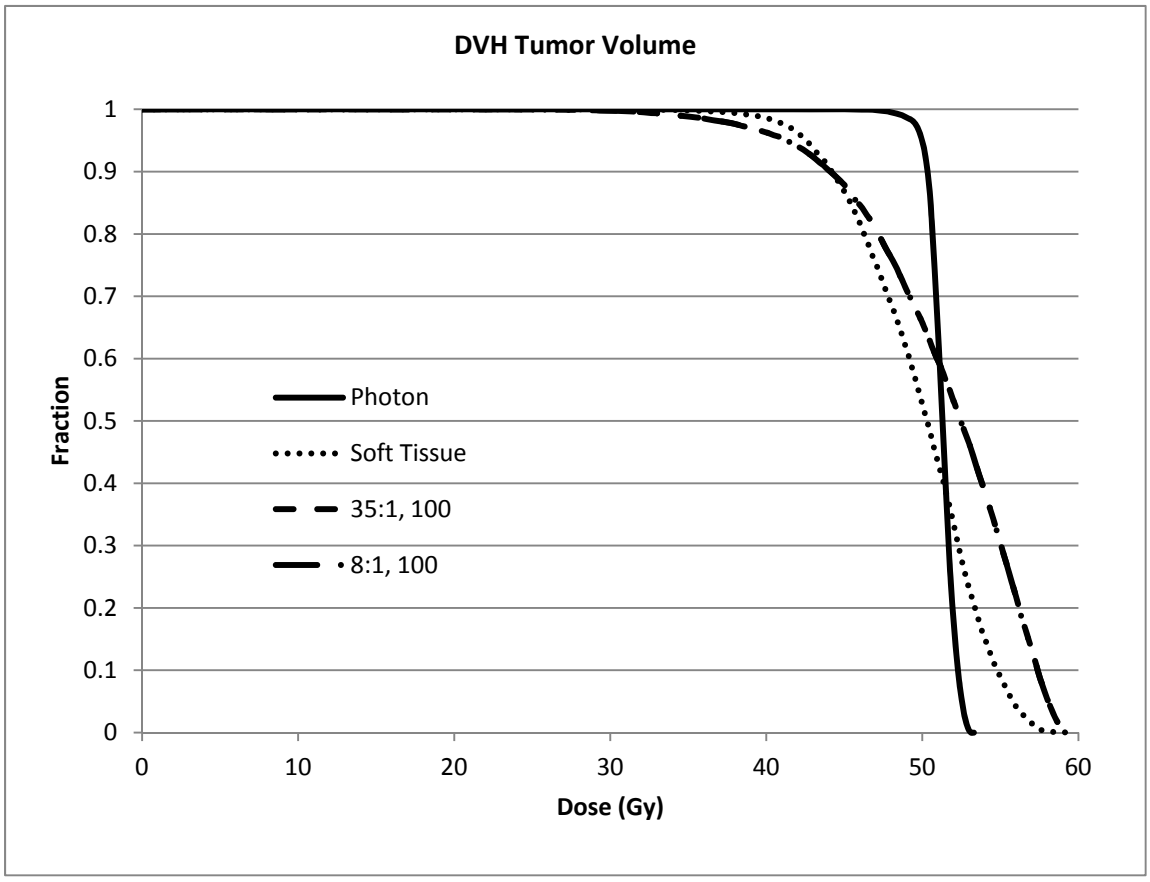

Figure 4-15. Dose volume histogram from the tumor volume. All four DVHs shown have the same mean dose

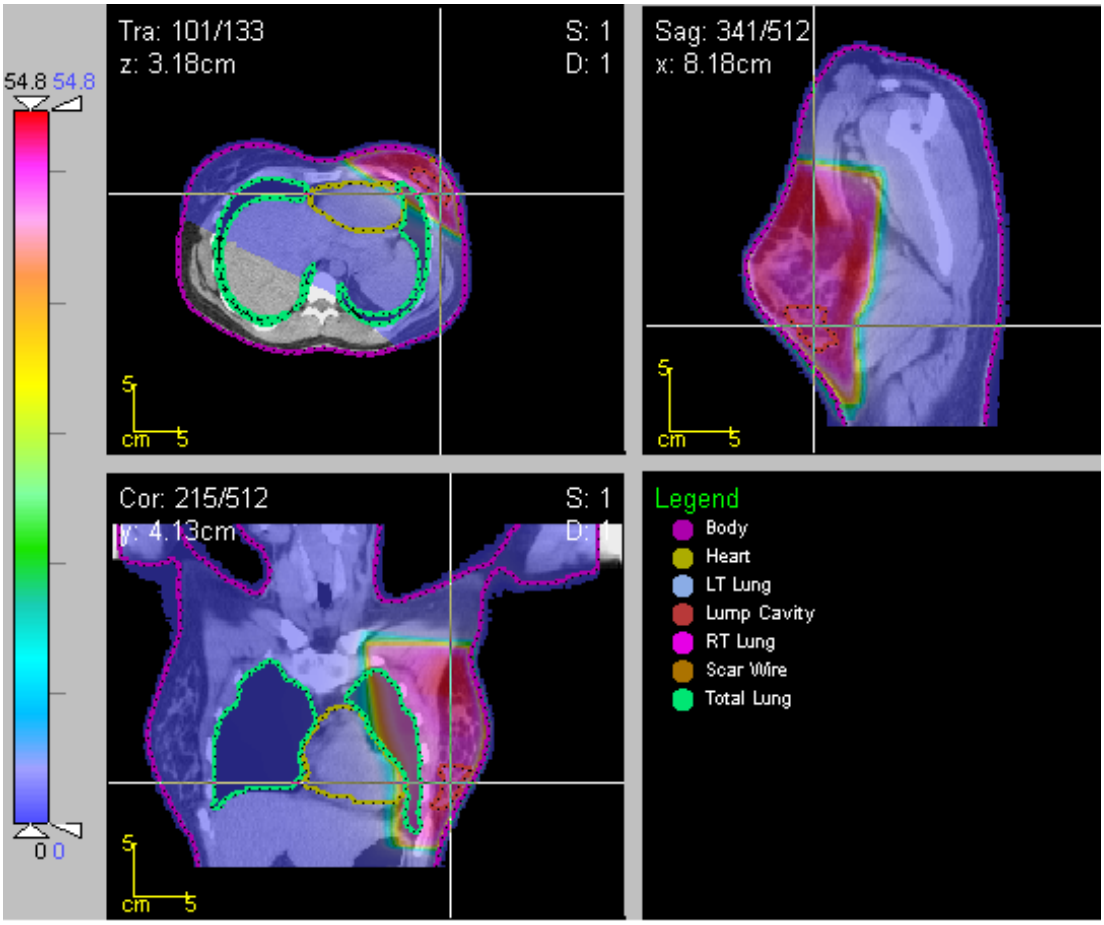

Figure 4-16. Screen shot from CERR of clinical patient and photon dose distribution through the breast. The tumor region is centered in the image at the "Crosshairs." Mean dose to the tumor region was 51.4 Gy. The pink region represents that portion that received dose above approximately 45 Gy.

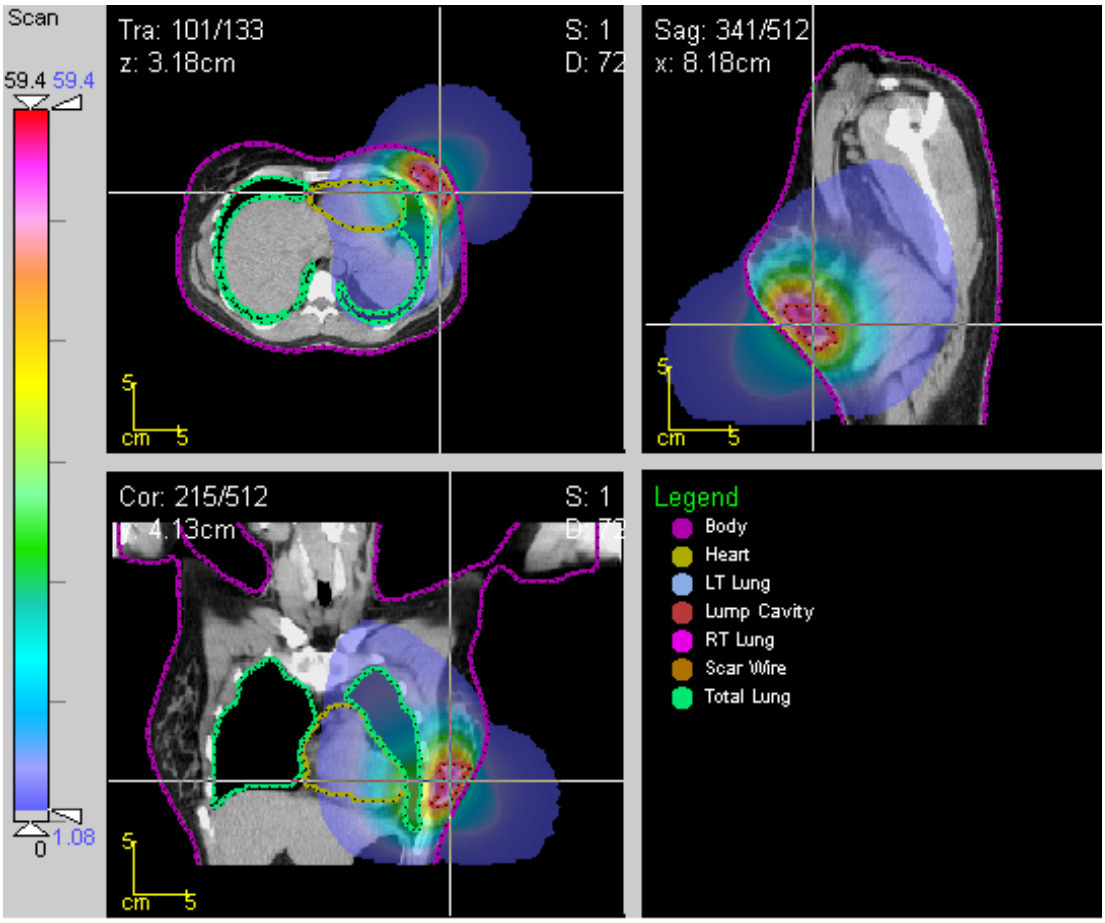

Figure 4-17. Screen shot from CERR for hypothetical BNCT treatment with T:H = 35:1 and boron concentration of 100 µg/g. The tumor region is centered in the image at the "Crosshairs." Mean dose to the tumor region was 51.4 Gy. The pink region represents that portion that received dose above approximately 50 Gy.

Another reason for the difference in the uniformity through the treatment volume is due to changes in neutron fluence to the deeper portions of the tumor volume and relative intensity of the boron effect toward the center of the tumor volume due to radiation summation. Note the dose distribution through the treatment volumes shown in Figures 4-18 and 4-19. The image in Figure 4-19 shows a close-up view of one axial slice of the tumor volume. The color-coded region in pink represents dose to tissue at or above about 45 Gy. The dose at or above this level clearly extends well beyond the defined edge of the treatment volume. Contrast this image with the image in Figure 4-19, which represents the dose distribution due to the boron effect in the treatment volume. Both the varying intensity within the treatment volume as well the relative thickness of the dose contours on the leading and trailing edges of the volume are observed in this image. This image also illustrates the misalignment between the clinically defined treatment volume and the volume defined for the BNCT calculation. Further analyses of the differences between these distributions and any potential benefit or drawback of the respective treatment process are reserved for Chapter 5.

Another result shown in Table 4-2 is the T/S ratios for this specific case. The T/S ratios for boron concentrations above 50 μg/g all exceed the design parameter of 2.7. The T/S ratio is as high as 5.5 for the greatest boron concentration of 100 μg/g. The skin doses for these 100 μg/g scenarios approach the secondary goal of this study of examining lower skin doses. The fact that the same average dose to the treatment volume is obtainable while reducing the effect to the skin is encouraging and improves the viability of the proposed therapy regimen. This issue is further explored in Chapter 5.

Finally, Table 4-2 lists the doses to organs outside the treatment volume. Because of the limited range of the neutron beam in tissue, lower doses to regions outside the treatment

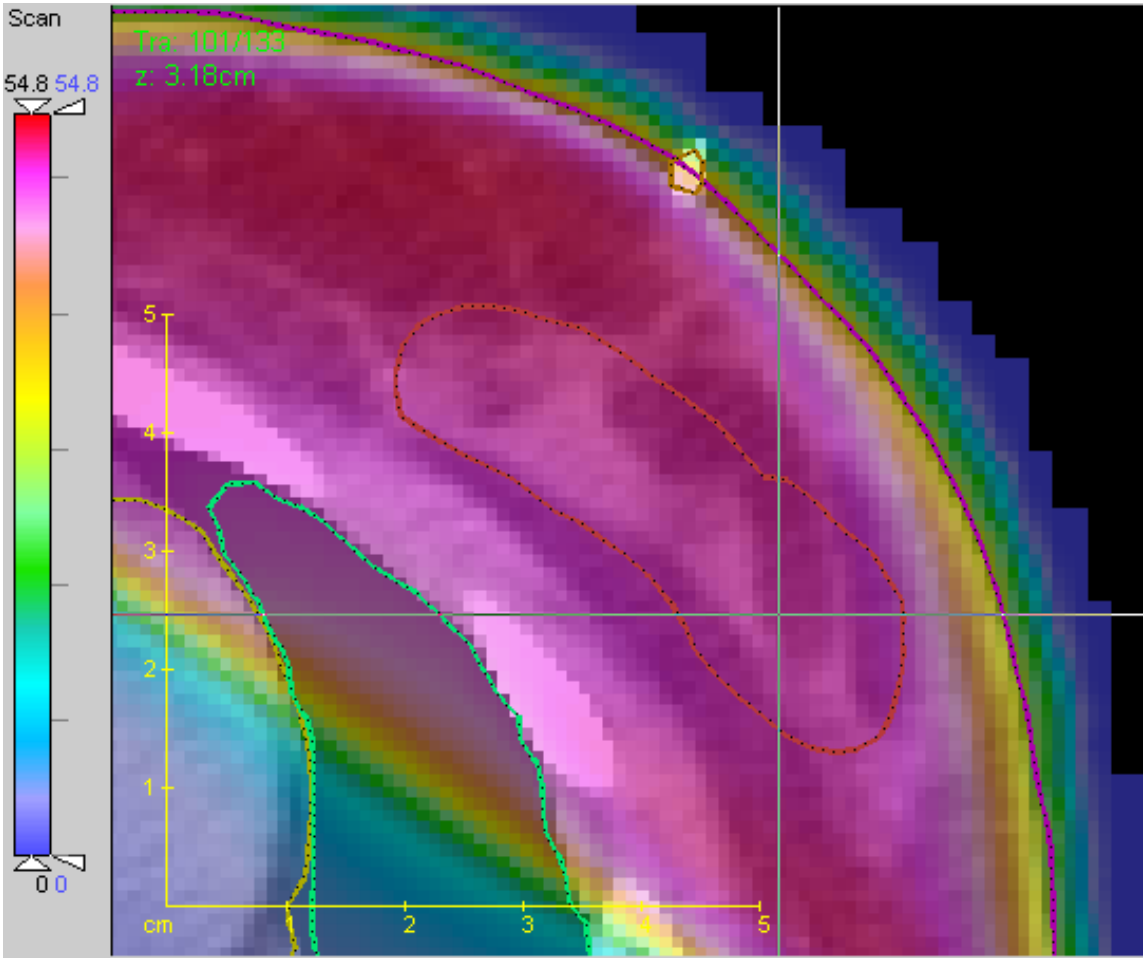

Figure 4-18. Close-up of single axial slice of tumor volume with color-contour of dose from photons overlaid. Note the dose contour represented in pink (corresponding to 45 Gy or above) extends well outside the tumor volume.

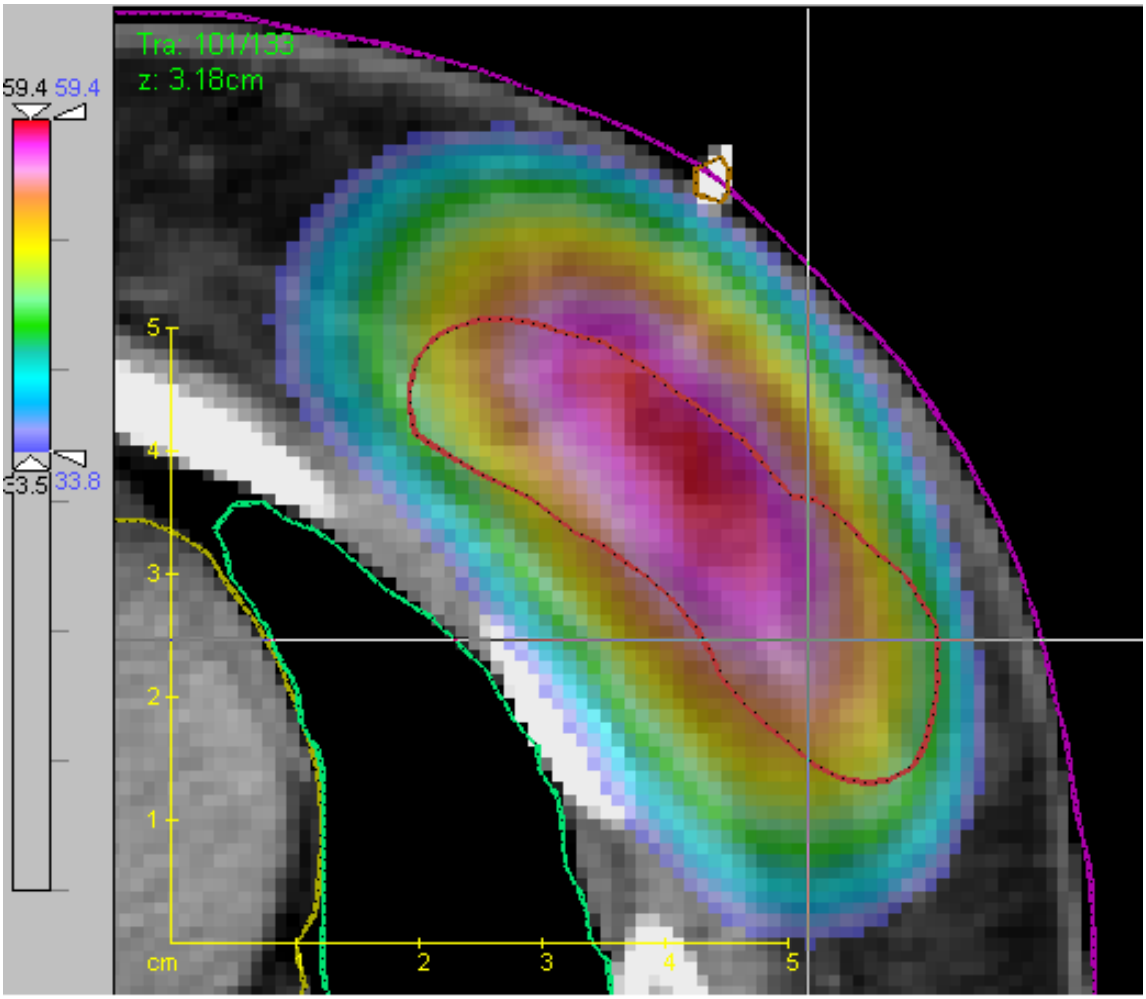

Figure 4-19. Close-up of single axial slice of the tumor volume with color-contour of dose from BNCT overlaid. Note the dose contour represented in pink (corresponding to 50 Gy and above) is limited in range well within the tumor region. The relative thickness of the dose contours on the leading and trailing edges represents the change in neutron fluence and the change in subsequent boron effect. This image also illustrates the misalignment between the tumor volume defined in the clinical record and that defined for the BNCT scenario.

volume are expected. Also, the photon based treatment satisfies the criteria for current whole breast irradiation techniques with the goal to irradiate much of the breast tissue outside the lump cavity as described in Chapter 2. Thus, higher doses outside the treatment volume in the photon based therapy are to be expected. The goal of these higher doses to the whole breast, as described previously, is to treat any cancer cell that may remain following surgery. One potential advantage of the proposed BNCT treatment regimen is the possibility of replacing whole breast irradiation with partial breast irradiation using BNCT. Because the boron delivery agent will target specific cancer cells, the possibility of successful targeted beam therapy is more likely using BNCT than using photons. While this is an exciting possibility, additional exploration is needed in order to evaluate the efficacy of BNCT in patients without clear tumor delineation. However, even with the whole breast irradiation techniques the dose to the lung is always minimized due to its proximity to the treatment volume and because of its relative sensitivity to the effects of radiation. Thus, the comparison of dose to the left lung is of particular interest as a point of comparison for the current proof of concept study. As reported in Table 4-2, the dose to the left lung in every BNCT-based scenario is less than the dose from the photon based therapy. In fact the dose to the lung in the scenarios with boron concentrations greater than 50 μg/g are less than 10% of the dose from the photon based therapy. The DVH for the left lung is shown in Figure 4-20. This is partially due to the treatment beam angulation between the two therapy regimens but nevertheless is important because of the reduced risk of radiation-induced injuries. Additional DVHs are shown for the total lung (Figure 4-21) and the heart (Figure 4-22). Each of these also shows the dose savings to the organ in question for the BNCT proposed regimen.

It should be pointed out that the mean dose to the heart in the BNCT treatment scenarios that did not have any boron did exceed the mean dose to the heart from photons.

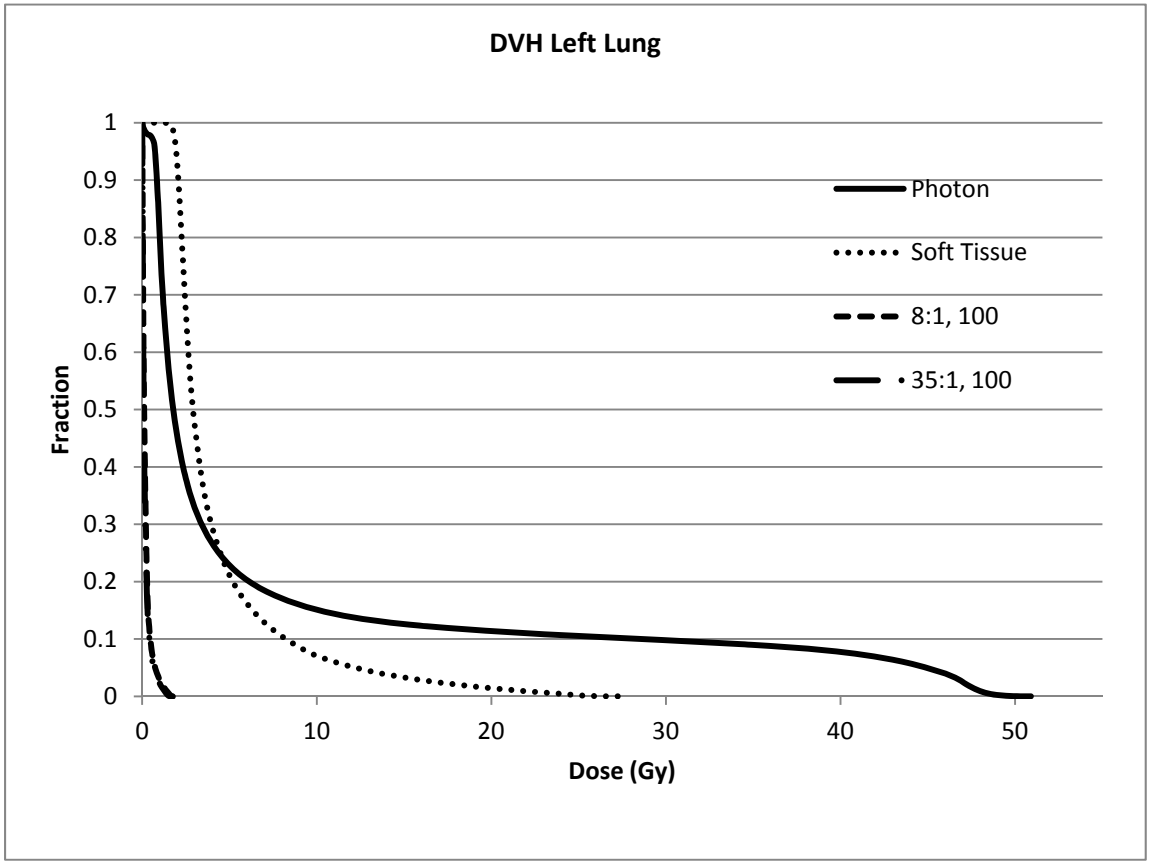

Figure 4-20. DVH for the left lung.

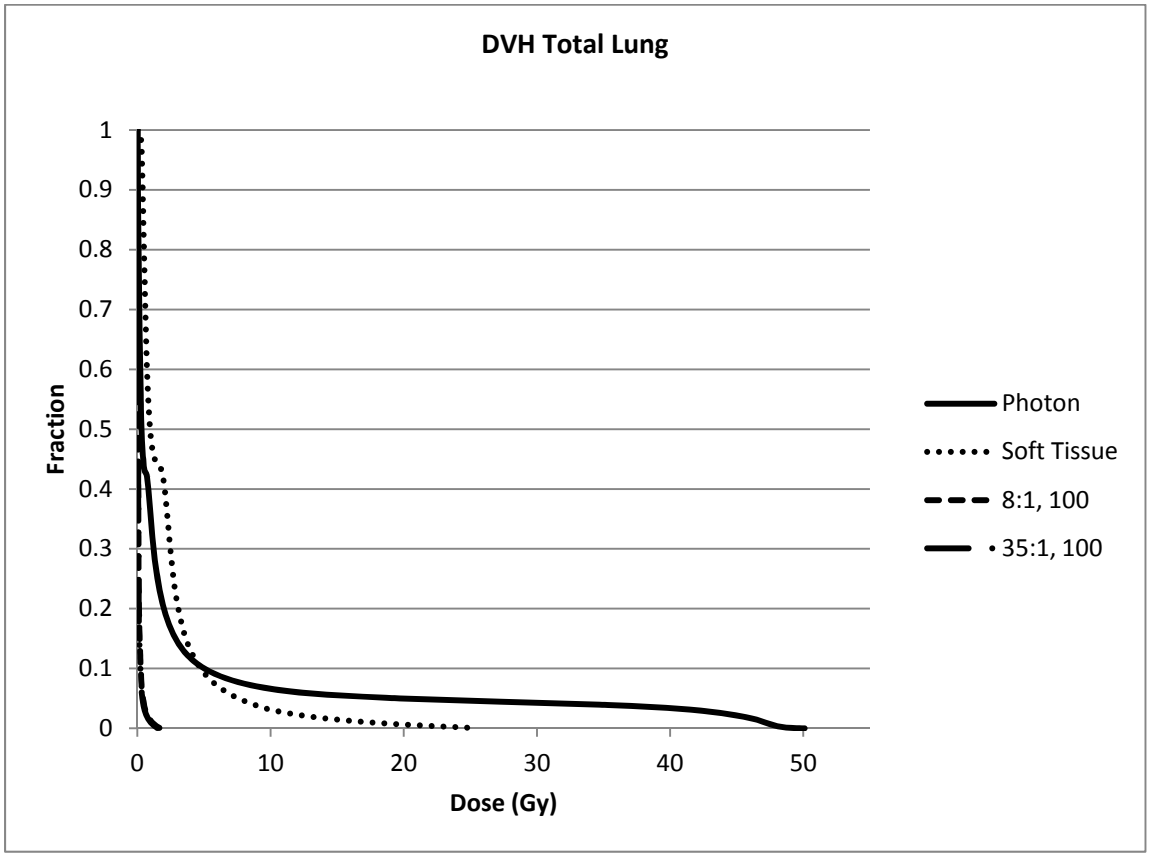

Figure 4-21. DVH for the total lung

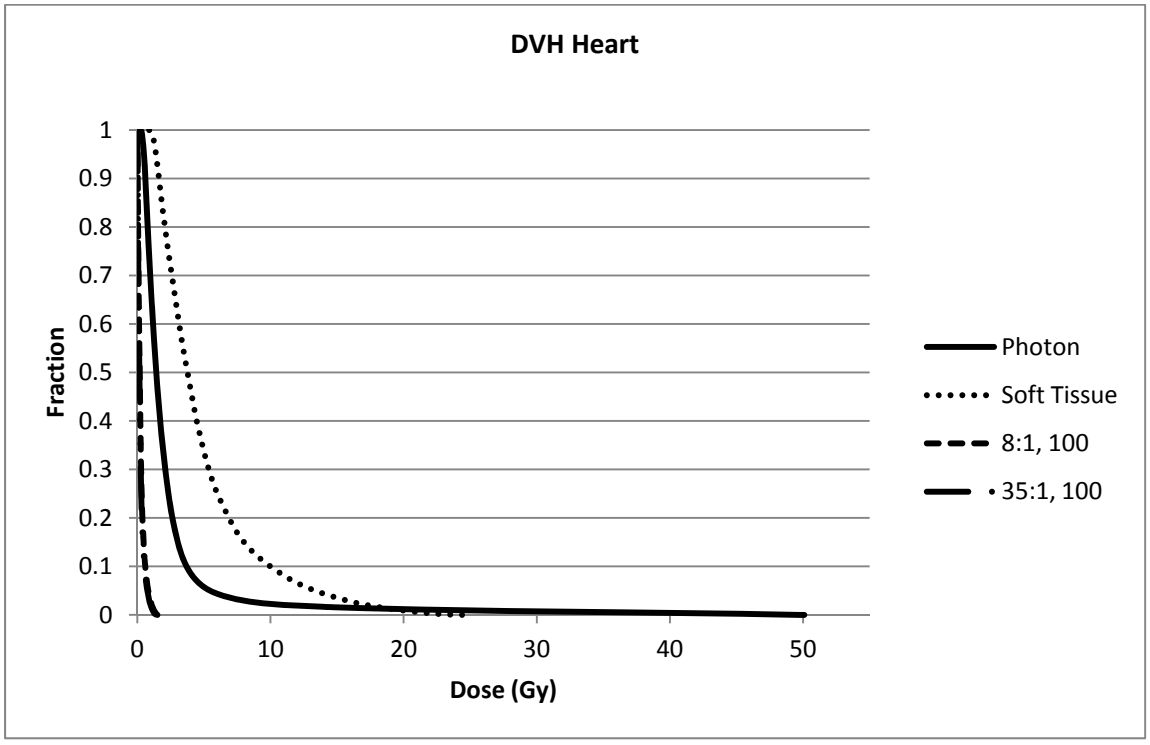

Figure 4-22. DVH for the heart

These scenarios are not likely because they involved nonborated tumor sites. However, it is interesting to point out that the maximum dose to the heart from photons was more than twice the max dose from the nonborated scenarios. Also, it was observed that the heart dose in the BNCT scenarios was largely caused by the tumor placement and the proximity to the heart. These observations lead to the thought that caution should be used when drawing absolute conclusions from these scenarios as beam placement, relative location of the tumor volume and other organs, and other patient specific parameters will determine the absolute therapeutic ratios, dose distributions, and overall effectiveness of any radiation therapy.

As can be seen from Table 4-2 and in Figures 4-20 through 4-22, in all of the treatment scenarios, including the photon dose, dose/volumes below the recommended limits were met. However, for the cases in which boron was present in the tumor volume, the dose/volumes were much less than photon dose. As was pointed out for the dose limits to the lung, there is a significant interest in achieving doses to the organs as low as practicable. In this regard, the BNCT regimen appears as if lower peripheral organ doses are achievable, even when the beam direction is always ideal for low doses to these organs.

The results described here have shown that, with a reasonable amount of certainty, that the treatment design parameters for the proposed BNCT therapy regime results are achievable under the given assumptions described in the previous chapters. Additionally, from a dose standpoint, similar results as compared to photon therapy are also achievable. The discussion that follows in Chapter 5 will further examine these results.

Treatment Time

The required treatment times for the BNCT based regimen varied from 41 minutes for T:H of 8:1 with 10 μg/g boron down to 7 minutes for T:H of 35:1 with 100 μg/g boron. This is a

vast improvement over treatment times required to deliver the same dose in photon therapy. Photon therapy for WBI is typically delivered in 2 Gy fractions over the course of several weeks. The obvious conclusion that can be drawn from this is the idea that the same therapeutic doses would be able to be delivered in a fraction of the time. Not only does the improvement exist for the convenience of not having to return to the treatment center for several weeks, but also issues such as patient motion and geometric reproducibility between fractions are greatly reduced or eliminated.

The effect of fractionation is not studied here. Thus, the comparison between the effects of fractionated doses from photons and a single dose from neutrons cannot be made directly. However, one purpose of dose fractionation is to allow healthy tissues an opportunity to heal and allow for tumor cells to change in to a more radiosensitive phase of their cell cycle. The cellular toxicity to even relatively radiosensitive cells is higher with BNCT based therapy because of the uptake into the cellular nucleus of boron. Whereas the effect on cellular toxicity from photons is much less because of the relative LET of the photon and the likelihood of photon interaction with the cell's nucleus. So, in order to better evaluate the effect of a single fraction on the tumor cells, more information is needed. However, if the CBE is in the range of the assumed value of 3.8, the effect of sensitivity is already several factors higher than for photons.

Finally, the effect of total irradiation time on the peripheral organs should not be understated. As has been shown, the higher the boron concentration in the tumor volume, the less irradiation time and, consequently, the lower the dose to peripheral organs. As irradiation time in photon therapy increases, the dose to the surrounding tissues and organs also increases. In the proposed BNCT regimen, this is also true, but at a much lower rate. First, the neutron beam is limited in a much greater fashion than the photon beam by simple attenuation. But,

because the BNCT regimen accounts for the boron effect, greater therapeutic ratios between the tumor volume and the surrounding tissues can be achieved through greater amounts of boron. However, this is only true to a point; it was shown that above 316 μg/g boron that self-shielding because significant enough the additional boron did not increase dose to the target volume.

CHAPTER 5

CONCLUSIONS AND FUTURE WORK

The preceding proof of concept study was performed in order to test the assumptions made in previous works regarding the feasibility of proposed BNCT for HER2+ breast cancers. The current study was able to test these parameters by developing a treatment specific procedure for calculating dose to the patient using the treatment parameters defined in the previous efforts as a framework for a hypothetical treatment to a patient. The results of these dose calculations demonstrated that the proposed BNCT regimen is likely able to deliver the desired dose to the tumor region, if the initial conditions of the study assumptions are met. A large assumption was made regarding the boron concentration levels within tumor cells. At the time of this study, this capability had not been positively demonstrated. Therefore, the overall conclusion of this study is that the proposed BNCT treatment for HER2+ is feasible if boron can be delivered to the tumor cells in concentrations greater than 50 μg/g boron.

The feasibility of the proposed BNCT treatment was evaluated by several key factors which are described below. By demonstrating the feasibility in each of these areas, it was assumed that the proof of concept study was successful. However, the concept is established based only on the initial treatment assumptions, many of which remain to be demonstrated. The key feasibility evaluations are discussed below and were based on tumor dose, skin dose, and dose to peripheral organs.

Feasibility Based on Tumor Dose

The feasibility of the study can be based on the ability of the proposed treatment to deliver the desired dose to the tumor volume, without over exposing the skin. It was demonstrated that this is possible if the tumor depth was not too great and the boron concentration levels were high enough. As was mentioned in Chapter 2, the goal of radiation therapy in breast conservation is local control of the tumor. That is, that the radiation will be effective in killing the cancerous cells without excessive harm to the healthy cells and surrounding tissues. To this end, the dose level of 50 Gy has been shown to be effective in this regard. Here, the assumption is made that if the same dose to the tumor volume can be delivered as is accomplished in conventional photon therapy, that similar control would be achieved. Thus, because the tumor dose from the BNCT regimen was successfully delivered to the tumor volume in the patient specific scenario, while meeting all other treatment design parameters, this portion of the study was considered to meet the primary objective of the BNCT regimen.

In the patient-specific example, the photon based dose to the tumor volume was 51.4 Gy. In all cases examined for the BNCT regimen that included at least 50 μg/g boron, this same equivalent dose was able to be delivered to the tumor volume and still meet the other initial treatment conditions. The tumor equivalent dose from the boron reaction was calculated assuming a CBE of 3.8. This value appears to be a reasonable estimate of the actual CBE for the treatment regimen based on other similar CBE for BNCT therapies; however, it has not been shown to be specifically applicable in this situation for these tumors and neutron source. A large part of the assumption of the CBE comes from how the boron will ultimately be delivered into the cell. On the one hand, the CBE could be lower than the assumed value and still be able to meet the design goals of the proposed treatment regimen. A lower CBE would result in

higher skin doses, shallower maximum treatment depths, and less overall efficiency. On the other hand, if future work shows that the CBE of 3.8 is an underestimate, as is implied in previous work,[6] the overall effectiveness of the proposed regimen would be improved.

Uniformity of the dose throughout the treatment volume varied between the photon-based therapy and the BNCT regimen. This is illustrated in Figure 4-15. As was mentioned in the results, part of this was due to geometric difference between the photon-based tumor volume and the MCNP generated, borated tumor volume. However, this does not account for all the nonuniformity observed. The question is then rightly asked of what effect this would have on the local control of the cancer cells. It is first noted that, as described in Chapter 2, a dose of 50 Gy may not be necessary if the efficiency to the tumor cells was greater. Keep in mind that one reason the whole breast is irradiated in photon-based therapy is to ensure that all cancer cells are treated. If the delivery of boron using the proposed delivery agent performs as is anticipated, the question of the necessity of such a large, whole-breast uniform dose may be rightly questions and a new target dose may need to be established. Also consider that the DVH in Figure 4-15 is based on a mean dose that would be equivalent to the photon mean dose. It is feasible that the mean dose could increase, ensuring that the entire volume had the same mean dose of 50 Gy, and still meet the other treatment criteria.

So, from the initial results of the dose calculations, the treatment protocol appears feasible based on dose alone. However, there remain questions regarding the proposed delivery agent's performance capabilities and the biological effectiveness that such performance will ultimately result in. Unfortunately, these performance characteristics could not be modeled in this study. The calculated results were given in a form that will allow easy modification of boron concentration and CBE values once better data are obtained. But, given

the assumptions of this study and the characteristics of the proposed delivery agent, the proposed BNCT treatment regimen for HER2+ breast cancers seems entirely feasible.

Feasibility Based on Skin Dose

The dose to the skin is an important factor in determining the feasibility of the treatment protocol. If it is not possible to deliver dose to the tumor without causing excessive harm to the patient's skin, then there would be no reason to pursue the treatment regimen further because it would serve as no improvement over the current radiation therapy techniques. Skin dose is important not only because of the possibility of severe damage, but also from the standpoint of general skin function and patient satisfaction with the overall breast conservation therapy. For this study, the goal to maintain skin dose to less than 18 Gy was achieved for all scenarios, which modeled at least a 50 μg/g boron concentration in the tumor. However, at boron concentration of 100 μg/g, skin dose of about 10 Gy were calculated. This is an important indication and reminder that although the max dose to the skin design goal is achievable, a lower skin dose is certainly possible. The lower the skin dose, the lower the unwanted side effects to the patient, and the likelihood the patient's comfort and satisfaction will increase as a result.

For this study, the neutron RBE in the skin was assumed to be 3. This is a reasonable estimate based on studies performed on the effect of neutrons in the skin. However, with the considerations of the skin of the breast (e.g., skin thicknesses, cell types, etc.) this value may need to be reevaluated for future work.

Another factor that will determine not only skin dose, but also tumor dose, is the depth of the tumor to be treated. Figures 4-12 and 4-13 show the maximum tumor depth as a function of boron concentration. The higher the concentration, the deeper the tumor may be

and still be able to meet the minimum T/S ratios. For the scenarios run in this study, the absolute maximum tumor depth that was deemed feasible, given the highest boron concentration, was 4.9 cm in soft tissue. This is an important observation because it helps to set a limit on which patients may be candidates for the proposed BNCT regimen. The depth of the tumor, relative to the outer surface of the skin, can vary somewhat depending on the beam angle. In this study, only the beam angle that would result in the shallowest tumor depth was examined, but other treatment configurations could easily be added. Typically, patients are treated in the supine position; however, for patients with sufficient breast size and composition, the prone position may allow more treatment options.

These results have shown that the proposed BNCT treatment regimen is feasible given the treatment parameters with respect to skin dose. As with the determination made for the tumor volume, the biological effectiveness of the neutrons in the skin cells should be reevaluated to ensure that the appropriate RBE is being used. The results of this study have been generated in such a form to allow for easy adjustment of these values for future changes.

Feasibility Based on Dose to Peripheral Organs

The dose to the organs outside the treatment volume is of concern to reduce unintended effects or unnecessary harm to the patient. As was summarized in Chapter 2, the radiation effects to the lung are of particular concern. In every case, except one, the dose to the periphery organs from BNCT based therapy was less than the dose to the same organs from photon therapy. In the case of no boron in the tumor tissue, the results of the neutron beam resulted in a higher mean dose to the heart than the photon therapy dose. But because this is not really a likely treatment scenario, this result could be ignored.

In the case of the lung, the dose to the left lung from the photon therapy was 3.3 Gy. In the BNCT based therapy, the dose to the left lung was about 0.6 Gy for the 50 μg/g borated tissues and about 0.3 Gy for the 100 μg/g borated tissues. The dose to the lung is up to 10% of the dose from the photon therapy. This is a significant improvement, even considering that the beam position was not selected to minimize dose to peripheral organs, but rather to minimize tumor depth. Because of the limited range of the neutron beam, the dose in the peripheral organs would be expected to have a lower overall dose, unless they had some concentration of boron that would significantly increase the dose.

Based on the observations made in this study, the dose to the peripheral organs, when the tumor cavity has some level of boron, will be less than the dose to the organ from photon therapy. A certain fluctuation in this conclusion is expected based upon tumor depth and location relative to the peripheral organs. In all cases doses lower than the organ tolerance levels for single and multiple fractions were observed. This is especially important in the lung where no threshold for injury is present, but is beneficial to the overall quality of treatment and care for the patient.

Limits of Current Study

This study was limited in scope to examining the treatment parameters that have been previously proposed for the BNCT for HER2+ breast cancers. As such, an exhaustive evaluation of treatment optimization parameters was not performed. Issues such as beam angles, larger selections of boron concentrations, treatment sites, etc. were not examined. Calculations and scenarios were established to demonstrate different key concepts of the proposed therapy. However, only the proposed treatment limits and performance characteristics were evaluated. Thus, the limit of the current study applies only to the assumptions describes in Chapter 1 from

previous work. The results of this study are valid within the scope of these assumptions. If any of the assumptions are changed the validity of these results must be reexamined.

Comparisons have been made of tumor volume target values. In the case of the photon based therapy, the dose was delivered in 2 Gy fractions, whereas the BNCT dose was assumed to have been delivered in a single fraction. No attempt was made to try and compare the real biological effect of these two dose rates. It is likely that the BNCT dose, delivered in the single fraction, will have a greater biological effect,[41] but this should be verified for the neutron source, boron concentration, and the specific tissue type.

Other Results

The primary focus of the current study was to demonstrate the proof of concept of the proposed BNCT treatment for HER2+ breast cancer. In order to calculate dose in this study, an expanded set of Kerma coefficients was required. A calculation method for easily determining these factors was described and demonstrated to provide reliable results. The total set of elemental Kerma coefficients and tissue Kerma coefficients cover the majority of elements and organs that are expected in the average anatomy of the female thorax. These results represent a set of data not published in other locations.

Recommendations for Future Work

As has been commented in numerous places throughout this work, there are several key areas in which additional work is vital to demonstrating future potential of the proposed BNCT treatment regimen. The following recommendations are listed:

- Development of boron delivery agent. Key to every calculation performed in this study was the assumption that a delivery agent was feasible that could deliver boron to the cancer cells at the described concentrations. As was pointed out in several of the

results, the conclusions drawn from the calculations hinge on the concentration of boron being available in the tumor cell. Without positive confirmation of this boron delivery, additional calculations based on these assumptions serve little benefit to the potential of future calculations.

- Determination of CBE specific for delivery agent in HER2+ breast cancer cells. The CBE used in this study assumes a biological effect based on uptake of the cancer cells both into the cell membrane and into the nucleus. As was described in previous work, if the boron is not available inside the nucleus for neutron capture, the biological effect will be vastly different. The uptake into the nucleus will be highly dependent upon the performance characteristics of the delivery agent. Thus, once the delivery agent is synthesized, the CBE values can be updated.
- Determination of RBE specific for breast tissue. The RBE used in this study was the RBE established for skin in other mammals and applied to humans. However, the neutron effect on health breast tissue was not specifically established. This would be an important factor to consider when performing future feasibility studies. In short, a definitive answer should be given to the question of healthy breast tissue's sensitivity to neutrons.
- Establishment of tumor target dose, given per performance characteristics of boron delivery agent. The tumor target dose of 50 Gy was established for photon therapy. Because a certain amount of boron is expected to be taken up in the nucleus of the cell, it is anticipated that a lower dose may be possible to create the same biological effectiveness as the photon dose goal. Additionally, the effect of the dose fractions should also be addressed. The tumor dose should account for both biological effect for both the dose and fractionation.

APPENDIX A

KERMA COEFFICIENT TABLES

The results of the Kerma coefficient calculations are summarized in the following tables. Only a portion of the data is given in this appendix. The original calculations were performed at 1,000 energy points. The included tables are:

1. Neutron Elemental Kerma Coefficient (Gy-cm^2)
2. Neutron Tissue Kerma Coefficient (Gy-cm^2)
3. Photon Tissue Kerma Coefficient (Gy-cm^2)

Table A-1. Neutron elemental Kerma coefficients (Gy-cm^2)

Neutron Energy (MeV)	H	N	B	C	O	Na	P	S	Cl	K	Ca	Fe	I
1.00E-10	1.11E-12	2.18E-10	3.82E-07	6.52E-16	3.07E-14	3.33E-14	8.73E-15	2.77E-13	1.85E-11	3.48E-13	2.71E-13	5.29E-14	1.17E-14
2.00E-10	4.65E-13	8.96E-11	1.83E-07	2.75E-16	1.26E-14	1.37E-14	3.60E-15	1.20E-13	7.62E-12	1.45E-13	1.12E-13	2.37E-14	4.97E-15
3.00E-10	3.80E-13	7.26E-11	1.48E-07	2.23E-16	1.02E-14	1.11E-14	2.93E-15	1.01E-13	6.18E-12	1.19E-13	9.06E-14	1.92E-14	4.04E-15
4.00E-10	3.34E-13	6.29E-11	1.28E-07	1.93E-16	8.86E-15	9.60E-15	2.54E-15	8.99E-14	5.35E-12	1.04E-13	7.84E-14	1.66E-14	3.49E-15
5.00E-10	3.00E-13	5.61E-11	1.14E-07	1.72E-16	7.90E-15	8.57E-15	2.27E-15	8.27E-14	4.77E-12	9.32E-14	7.00E-14	1.48E-14	3.12E-15
6.00E-10	2.80E-13	5.12E-11	1.04E-07	1.57E-16	7.21E-15	7.81E-15	2.07E-15	7.75E-14	4.35E-12	8.56E-14	6.38E-14	1.35E-14	2.84E-15
7.00E-10	2.62E-13	4.74E-11	9.64E-08	1.46E-16	6.67E-15	7.23E-15	1.92E-15	7.37E-14	4.03E-12	7.98E-14	5.91E-14	1.25E-14	2.63E-15
8.00E-10	2.48E-13	4.43E-11	9.02E-08	1.36E-16	6.24E-15	6.76E-15	1.80E-15	7.06E-14	3.77E-12	7.52E-14	5.53E-14	1.17E-14	2.46E-15
9.00E-10	2.37E-13	4.18E-11	8.50E-08	1.28E-16	5.88E-15	6.38E-15	1.70E-15	6.82E-14	3.55E-12	7.13E-14	5.21E-14	1.10E-14	2.32E-15
1.00E-09	2.26E-13	3.96E-11	8.06E-08	1.22E-16	5.58E-15	6.05E-15	1.62E-15	6.62E-14	3.37E-12	6.80E-14	4.94E-14	1.05E-14	2.20E-15
2.00E-09	1.81E-13	2.83E-11	5.75E-08	8.71E-17	3.99E-15	4.33E-15	1.17E-15	5.67E-14	2.41E-12	5.11E-14	3.54E-14	7.49E-15	1.57E-15
3.00E-09	1.57E-13	2.30E-11	4.68E-08	7.06E-17	3.24E-15	3.51E-15	9.60E-16	5.29E-14	1.96E-12	4.31E-14	2.87E-14	6.08E-15	1.28E-15
4.00E-09	1.45E-13	1.99E-11	4.05E-08	6.10E-17	2.80E-15	3.03E-15	8.36E-16	5.10E-14	1.69E-12	3.84E-14	2.48E-14	5.25E-15	1.10E-15
5.00E-09	1.36E-13	1.78E-11	3.61E-08	5.44E-17	2.50E-15	2.71E-15	7.52E-16	4.98E-14	1.51E-12	3.52E-14	2.22E-14	4.69E-15	9.86E-16
6.00E-09	1.29E-13	1.62E-11	3.30E-08	4.96E-17	2.28E-15	2.47E-15	6.89E-16	4.90E-14	1.38E-12	3.28E-14	2.02E-14	4.28E-15	9.00E-16
7.00E-09	1.24E-13	1.50E-11	3.05E-08	4.59E-17	2.11E-15	2.29E-15	6.40E-16	4.84E-14	1.27E-12	3.09E-14	1.87E-14	3.96E-15	8.32E-16
8.00E-09	1.19E-13	1.40E-11	2.85E-08	4.29E-17	1.97E-15	2.14E-15	6.01E-16	4.80E-14	1.19E-12	2.93E-14	1.75E-14	3.70E-15	7.78E-16
9.00E-09	1.14E-13	1.32E-11	2.69E-08	4.04E-17	1.86E-15	2.02E-15	5.68E-16	4.76E-14	1.12E-12	2.81E-14	1.65E-14	3.49E-15	7.33E-16
1.00E-08	1.11E-13	1.25E-11	2.55E-08	3.83E-17	1.76E-15	1.91E-15	5.40E-16	4.73E-14	1.07E-12	2.70E-14	1.56E-14	3.31E-15	6.96E-16
2.00E-08	8.50E-14	8.93E-12	1.82E-08	2.74E-17	1.26E-15	1.36E-15	3.93E-16	4.60E-14	7.59E-13	2.11E-14	1.11E-14	2.36E-15	4.96E-16
3.00E-08	6.87E-14	7.26E-12	1.48E-08	2.24E-17	1.02E-15	1.11E-15	3.23E-16	4.54E-14	6.18E-13	1.81E-14	9.06E-15	1.92E-15	4.04E-16
4.00E-08	5.78E-14	6.28E-12	1.28E-08	1.95E-17	8.86E-16	9.60E-16	2.81E-16	4.52E-14	5.35E-13	1.62E-14	7.84E-15	1.66E-15	3.49E-16
5.00E-08	5.00E-14	5.61E-12	1.14E-08	1.75E-17	7.91E-16	8.57E-16	2.50E-16	4.50E-14	4.78E-13	1.49E-14	7.00E-15	1.48E-15	3.12E-16
6.00E-08	4.41E-14	5.12E-12	1.04E-08	1.61E-17	7.21E-16	7.82E-16	2.26E-16	4.49E-14	4.35E-13	1.39E-14	6.38E-15	1.35E-15	2.85E-16

Table A-1. (continued)

Neutron Energy (MeV)	H	N	B	C	O	Na	P	S	Cl	K	Ca	Fe	I
7.00E-08	4.00E-14	4.74E-12	9.65E-09	1.50E-17	6.68E-16	7.24E-16	2.08E-16	4.48E-14	4.03E-13	1.31E-14	5.91E-15	1.25E-15	2.63E-16
8.00E-08	3.64E-14	4.43E-12	9.01E-09	1.41E-17	6.24E-16	6.76E-16	1.94E-16	4.47E-14	3.77E-13	1.25E-14	5.53E-15	1.17E-15	2.46E-16
9.00E-08	3.37E-14	4.17E-12	8.49E-09	1.34E-17	5.88E-16	6.37E-16	1.82E-16	4.46E-14	3.55E-13	1.19E-14	5.21E-15	1.10E-15	2.32E-16
1.00E-07	3.17E-14	3.98E-12	8.10E-09	1.28E-17	5.61E-16	6.08E-16	1.73E-16	4.46E-14	3.38E-13	1.15E-14	4.97E-15	1.05E-15	2.21E-16
2.00E-07	2.01E-14	2.84E-12	5.76E-09	9.82E-18	4.00E-16	4.34E-16	1.23E-16	4.43E-14	2.41E-13	8.99E-15	3.54E-15	7.50E-16	1.58E-16
3.00E-07	1.54E-14	2.30E-12	4.68E-09	8.71E-18	3.25E-16	3.52E-16	9.89E-17	4.42E-14	1.95E-13	7.72E-15	2.87E-15	6.09E-16	1.28E-16
4.00E-07	1.28E-14	1.98E-12	4.04E-09	8.29E-18	2.81E-16	3.04E-16	8.49E-17	4.42E-14	1.68E-13	6.93E-15	2.48E-15	5.25E-16	1.11E-16
5.00E-07	1.11E-14	1.78E-12	3.61E-09	8.18E-18	2.51E-16	2.72E-16	7.57E-17	4.42E-14	1.50E-13	6.39E-15	2.22E-15	4.69E-16	9.93E-17
6.00E-07	1.00E-14	1.62E-12	3.29E-09	8.24E-18	2.30E-16	2.48E-16	6.90E-17	4.41E-14	1.37E-13	5.98E-15	2.02E-15	4.28E-16	9.07E-17
7.00E-07	9.28E-15	1.50E-12	3.05E-09	8.41E-18	2.13E-16	2.30E-16	6.44E-17	4.41E-14	1.27E-13	5.65E-15	1.87E-15	3.97E-16	8.40E-17
8.00E-07	8.74E-15	1.40E-12	2.85E-09	8.65E-18	2.00E-16	2.15E-16	6.07E-17	4.41E-14	1.18E-13	5.38E-15	1.75E-15	3.71E-16	7.87E-17
9.00E-07	8.34E-15	1.32E-12	2.69E-09	8.95E-18	1.88E-16	2.03E-16	5.77E-17	4.41E-14	1.11E-13	5.15E-15	1.65E-15	3.49E-16	7.43E-17
1.00E-06	8.01E-15	1.25E-12	2.54E-09	9.29E-18	1.79E-16	1.92E-16	5.50E-17	4.41E-14	1.05E-13	4.95E-15	1.56E-15	3.31E-16	7.05E-17
2.00E-06	6.80E-15	8.94E-13	1.82E-09	1.34E-17	1.31E-16	1.39E-16	4.04E-17	4.40E-14	7.44E-14	3.93E-15	1.12E-15	2.37E-16	5.13E-17
3.00E-06	6.79E-15	7.28E-13	1.48E-09	1.83E-17	1.10E-16	1.15E-16	3.40E-17	4.40E-14	5.99E-14	3.42E-15	9.09E-16	1.94E-16	4.28E-17
4.00E-06	7.19E-15	6.28E-13	1.28E-09	2.35E-17	9.87E-17	1.01E-16	3.03E-17	4.40E-14	5.12E-14	3.09E-15	7.85E-16	1.68E-16	3.84E-17
5.00E-06	7.86E-15	5.61E-13	1.14E-09	2.87E-17	9.19E-17	9.15E-17	2.80E-17	4.39E-14	4.52E-14	2.87E-15	7.02E-16	1.51E-16	3.54E-17
6.00E-06	8.56E-15	5.12E-13	1.04E-09	3.39E-17	8.76E-17	8.51E-17	2.66E-17	4.39E-14	4.08E-14	2.70E-15	6.42E-16	1.39E-16	3.32E-17
7.00E-06	9.36E-15	4.73E-13	9.62E-10	3.94E-17	8.47E-17	8.02E-17	2.58E-17	4.39E-14	3.73E-14	2.56E-15	5.93E-16	1.29E-16	3.20E-17
8.00E-06	1.02E-14	4.43E-13	9.01E-10	4.47E-17	8.30E-17	7.66E-17	2.53E-17	4.39E-14	3.46E-14	2.45E-15	5.55E-16	1.22E-16	3.14E-17
9.00E-06	1.10E-14	4.18E-13	8.49E-10	5.00E-17	8.20E-17	7.37E-17	2.51E-17	4.39E-14	3.22E-14	2.35E-15	5.24E-16	1.16E-16	3.13E-17
1.00E-05	1.19E-14	3.96E-13	8.04E-10	5.54E-17	8.16E-17	7.15E-17	2.57E-17	4.39E-14	3.02E-14	2.27E-15	4.97E-16	1.11E-16	3.15E-17
2.00E-05	2.07E-14	2.83E-13	5.74E-10	1.07E-16	9.05E-17	6.47E-17	3.30E-17	4.39E-14	1.96E-14	1.82E-15	3.59E-16	8.69E-17	3.78E-16

Table A-1. (continued)

Neutron Energy (MeV)	H	N	B	C	O	Na	P	S	Cl	K	Ca	Fe	I
3.00E-05	3.01E-14	2.30E-13	4.67E-10	1.61E-16	1.09E-16	6.73E-17	4.05E-17	4.39E-14	1.45E-14	1.59E-15	2.97E-16	7.93E-17	1.12E-15
4.00E-05	3.98E-14	1.99E-13	4.03E-10	2.16E-16	1.30E-16	7.33E-17	4.81E-17	4.39E-14	1.15E-14	1.45E-15	2.62E-16	7.75E-17	9.01E-16
5.00E-05	4.94E-14	1.78E-13	3.60E-10	2.70E-16	1.53E-16	8.07E-17	5.57E-17	4.39E-14	9.40E-15	1.35E-15	2.39E-16	7.83E-17	1.29E-16
6.00E-05	5.91E-14	1.62E-13	3.28E-10	3.24E-16	1.77E-16	8.91E-17	6.33E-17	4.39E-14	7.91E-15	1.27E-15	2.23E-16	8.06E-17	2.50E-17
7.00E-05	6.89E-14	1.50E-13	3.03E-10	3.79E-16	2.01E-16	9.80E-17	7.10E-17	4.39E-14	6.79E-15	1.21E-15	2.11E-16	8.38E-17	3.04E-17
8.00E-05	7.87E-14	1.41E-13	2.84E-10	4.34E-16	2.26E-16	1.07E-16	7.87E-17	4.39E-14	5.90E-15	1.16E-15	2.02E-16	8.76E-17	1.56E-15
9.00E-05	8.84E-14	1.33E-13	2.67E-10	4.88E-16	2.51E-16	1.17E-16	8.64E-17	4.39E-14	5.20E-15	1.12E-15	1.96E-16	9.17E-17	1.98E-15
1.00E-04	9.82E-14	1.26E-13	2.53E-10	5.43E-16	2.76E-16	1.26E-16	9.42E-17	4.39E-14	4.63E-15	1.09E-15	1.91E-16	9.62E-17	1.79E-17
2.00E-04	1.92E-13	9.06E-14	1.80E-10	1.06E-15	5.19E-16	2.25E-16	1.68E-16	4.39E-14	2.27E-15	9.00E-16	1.79E-16	1.45E-16	2.85E-15
3.00E-04	2.88E-13	7.48E-14	1.47E-10	1.60E-15	7.75E-16	3.32E-16	2.46E-16	4.39E-14	2.90E-15	8.15E-16	1.93E-16	1.98E-16	3.82E-16
4.00E-04	3.85E-13	6.58E-14	1.27E-10	2.14E-15	1.03E-15	4.42E-16	3.23E-16	4.39E-14	8.93E-12	7.68E-16	2.14E-16	2.50E-16	9.54E-17
5.00E-04	4.85E-13	5.98E-14	1.13E-10	2.71E-15	1.30E-15	5.60E-16	4.03E-16	4.40E-14	3.12E-15	7.38E-16	2.41E-16	3.02E-16	2.45E-15
6.00E-04	5.81E-13	5.57E-14	1.03E-10	3.24E-15	1.55E-15	6.77E-16	4.80E-16	4.40E-14	1.19E-15	7.21E-16	2.68E-16	3.49E-16	3.40E-17
7.00E-04	6.77E-13	5.28E-14	9.52E-11	3.78E-15	1.81E-15	8.01E-16	5.57E-16	4.40E-14	7.79E-16	7.10E-16	2.96E-16	3.95E-16	8.49E-17
8.00E-04	7.74E-13	5.06E-14	8.89E-11	4.32E-15	2.06E-15	9.39E-16	6.35E-16	4.40E-14	6.19E-16	7.02E-16	3.26E-16	4.40E-16	3.39E-16
9.00E-04	8.72E-13	4.88E-14	8.37E-11	4.87E-15	2.33E-15	1.09E-15	7.13E-16	4.40E-14	5.43E-16	6.98E-16	3.56E-16	4.83E-16	3.28E-16
1.00E-03	9.70E-13	4.75E-14	7.93E-11	5.42E-15	2.59E-15	1.26E-15	7.92E-16	4.40E-14	5.04E-16	6.95E-16	3.87E-16	5.26E-16	5.06E-17
2.00E-03	1.88E-12	4.37E-14	5.64E-11	1.06E-14	5.06E-15	8.07E-15	1.54E-15	4.42E-14	5.38E-16	7.13E-16	6.82E-16	8.63E-16	4.08E-16
3.00E-03	2.82E-12	4.59E-14	4.58E-11	1.60E-14	7.63E-15	2.61E-13	2.31E-15	4.44E-14	6.96E-16	7.38E-16	9.77E-16	1.14E-15	4.28E-16
4.00E-03	3.76E-12	5.00E-14	3.95E-11	2.14E-14	1.02E-14	2.70E-14	3.09E-15	4.46E-14	9.75E-16	7.59E-16	1.26E-15	2.17E-15	6.52E-16
5.00E-03	4.70E-12	5.50E-14	3.52E-11	2.68E-14	1.28E-14	1.67E-14	3.88E-15	4.48E-14	1.04E-15	8.01E-16	1.54E-15	1.71E-15	5.27E-16
6.00E-03	5.60E-12	6.01E-14	3.21E-11	3.22E-14	1.54E-14	1.50E-14	4.66E-15	4.50E-14	1.17E-15	9.72E-16	1.80E-15	2.90E-15	5.82E-16
7.00E-03	6.50E-12	6.54E-14	2.96E-11	3.76E-14	1.80E-14	1.50E-14	6.07E-15	4.52E-14	1.28E-15	8.00E-16	2.08E-15	4.36E-15	6.42E-16

Table A-1. (continued)

Neutron Energy (MeV)	H	N	B	C	O	Na	P	S	Cl	K	Ca	Fe	I
8.00E-03	7.38E-12	7.07E-14	2.77E-11	4.29E-14	2.05E-14	1.55E-14	8.67E-15	4.53E-14	1.50E-15	7.12E-16	2.28E-15	1.17E-14	7.03E-16
9.00E-03	8.29E-12	7.61E-14	2.61E-11	4.84E-14	2.32E-14	1.63E-14	9.27E-15	4.55E-14	2.44E-15	4.76E-16	2.62E-15	5.66E-15	7.67E-16
1.00E-02	9.16E-12	8.13E-14	2.48E-11	5.37E-14	2.58E-14	1.73E-14	8.55E-15	4.57E-14	2.14E-15	2.05E-15	2.73E-15	4.12E-15	8.31E-16
2.00E-02	1.70E-11	1.27E-13	1.78E-11	1.05E-13	5.04E-14	2.81E-14	1.41E-14	4.71E-14	3.64E-15	1.29E-15	4.16E-15	2.52E-15	1.43E-15
3.00E-02	2.44E-11	1.71E-13	1.47E-11	1.57E-13	7.62E-14	4.08E-14	2.30E-14	4.93E-14	7.71E-15	1.60E-15	5.60E-15	5.00E-14	2.04E-15
4.00E-02	3.10E-11	2.04E-13	1.29E-11	2.08E-13	1.01E-13	5.39E-14	3.52E-14	4.87E-14	7.80E-15	3.80E-15	6.27E-15	1.32E-14	2.61E-15
5.00E-02	3.70E-11	2.38E-13	1.17E-11	2.58E-13	1.27E-13	7.45E-14	4.30E-14	4.86E-14	1.09E-14	3.04E-15	7.11E-15	1.25E-14	3.17E-15
6.00E-02	4.25E-11	2.67E-13	1.09E-11	3.08E-13	1.52E-13	8.14E-14	5.00E-14	4.80E-14	1.22E-14	3.74E-14	6.74E-15	1.29E-14	3.70E-15
7.00E-02	4.76E-11	2.97E-13	1.03E-11	3.56E-13	1.77E-13	8.78E-14	5.74E-14	4.68E-14	1.79E-14	6.07E-15	6.21E-15	7.18E-15	4.16E-15
8.00E-02	5.23E-11	3.23E-13	9.85E-12	4.04E-13	2.02E-13	9.80E-14	6.46E-14	4.81E-14	1.47E-14	1.11E-14	5.34E-15	1.08E-14	4.64E-15
9.00E-02	5.68E-11	3.50E-13	9.48E-12	4.52E-13	2.27E-13	1.09E-13	7.17E-14	7.45E-14	1.48E-14	6.94E-15	4.03E-14	2.98E-14	5.11E-15
1.00E-01	6.09E-11	3.74E-13	9.19E-12	4.98E-13	2.52E-13	1.18E-13	5.80E-14	3.21E-13	1.97E-14	3.24E-14	6.86E-15	2.63E-14	5.55E-15
2.00E-01	9.14E-11	5.82E-13	7.80E-12	9.05E-13	4.95E-13	3.18E-13	8.14E-14	1.61E-13	5.78E-14	2.51E-14	3.00E-15	8.32E-14	9.83E-15
3.00E-01	1.14E-10	7.53E-13	6.57E-12	1.27E-12	8.04E-13	2.73E-13	1.34E-13	1.53E-13	9.11E-14	6.38E-14	1.06E-13	2.26E-14	1.43E-14
4.00E-01	1.31E-10	8.92E-13	6.58E-12	1.58E-12	1.97E-12	6.26E-13	1.43E-13	2.57E-13	1.11E-13	7.92E-14	5.66E-14	1.20E-13	1.85E-14
5.00E-01	1.46E-10	2.41E-12	6.23E-12	1.85E-12	9.09E-13	3.51E-13	2.01E-13	1.96E-13	1.34E-13	9.59E-14	1.08E-14	6.29E-14	2.30E-14
6.00E-01	1.60E-10	1.02E-12	5.05E-12	2.08E-12	9.64E-13	7.80E-13	2.43E-13	2.11E-13	2.15E-13	1.14E-13	2.35E-13	5.42E-14	2.76E-14
7.00E-01	1.72E-10	1.78E-12	4.27E-12	2.29E-12	1.13E-12	1.34E-12	2.50E-13	2.64E-13	2.07E-13	1.35E-13	1.29E-13	7.50E-14	3.25E-14
8.00E-01	1.83E-10	1.32E-12	3.83E-12	2.46E-12	1.33E-12	1.00E-12	2.48E-13	2.96E-13	2.90E-13	1.58E-13	1.54E-13	1.32E-13	3.74E-14
9.00E-01	1.94E-10	1.13E-12	3.61E-12	2.62E-12	1.85E-12	9.70E-13	3.14E-13	2.80E-13	3.29E-13	1.83E-13	3.16E-13	6.99E-14	4.24E-14
1.00E+00	2.04E-10	1.91E-12	3.71E-12	2.76E-12	5.35E-12	7.16E-13	3.63E-13	3.72E-13	3.96E-13	2.10E-13	1.66E-13	8.24E-14	4.73E-14
2.00E+00	2.77E-10	3.26E-12	9.12E-12	3.71E-12	1.92E-12	1.09E-12	7.40E-13	1.54E-12	1.29E-12	1.06E-12	6.05E-13	2.85E-13	6.41E-14
3.00E+00	3.28E-10	8.84E-12	1.04E-11	7.79E-12	2.02E-12	1.44E-12	2.06E-12	3.63E-12	2.15E-12	2.91E-12	2.48E-12	3.92E-13	6.85E-14

Table A-1. (continued)

Neutron Energy (MeV)	H	N	B	C	O	Na	P	S	Cl	K	Ca	Fe	I
4.00E+00	3.65E-10	1.69E-11	1.09E-11	8.81E-12	3.71E-12	2.36E-12	1.74E-12	5.84E-12	3.23E-12	4.86E-12	5.94E-12	5.27E-13	7.65E-14
5.00E+00	3.91E-10	1.21E-11	1.26E-11	5.34E-12	4.23E-12	1.16E-12	6.70E-12	7.63E-12	4.37E-12	6.11E-12	8.02E-12	6.60E-13	1.19E-13
6.00E+00	4.12E-10	1.16E-11	1.42E-11	5.81E-12	5.42E-12	1.34E-12	7.71E-12	8.42E-12	5.67E-12	8.29E-12	9.79E-12	8.60E-13	1.42E-13
7.00E+00	4.27E-10	1.05E-11	1.48E-11	4.67E-12	5.04E-12	2.84E-12	8.74E-12	8.83E-12	6.56E-12	9.50E-12	1.10E-11	1.10E-12	1.68E-13
8.00E+00	4.39E-10	1.45E-11	1.53E-11	1.15E-11	6.35E-12	4.48E-12	9.56E-12	9.64E-12	7.06E-12	9.76E-12	1.21E-11	1.38E-12	1.77E-13
9.00E+00	4.48E-10	1.18E-11	1.55E-11	1.12E-11	8.62E-12	6.60E-12	1.20E-11	1.03E-11	7.63E-12	1.01E-11	1.29E-11	1.68E-12	1.89E-13
1.00E+01	4.55E-10	1.65E-11	1.68E-11	1.14E-11	1.19E-11	8.37E-12	1.36E-11	1.10E-11	8.57E-12	1.08E-11	1.32E-11	1.95E-12	2.21E-13
2.00E+01	4.70E-10	3.33E-11	3.87E-11	3.48E-11	2.01E-11	3.92E-11	2.05E-11	1.49E-11	1.37E-11	2.05E-11	1.87E-11	5.24E-12	9.54E-13

Table A-2. Neutron tissue Kerma coefficients (Gy-cm^2)

Neutron Energy (MeV)	Adipose	Brain	Breast Whole (50/50)	Breast Calcification	Breast Mammary Gland	Heart	Lung	Muscle	Ribs	Skin	Soft Tissue, Female	Thyroid
1.00E-10	1.66E-12	4.99E-12	1.43E-13	1.21E-12	6.69E-12	7.16E-12	6.95E-12	7.56E-12	8.85E-12	9.33E-12	5.38E-12	5.38E-12
2.00E-10	6.84E-13	2.05E-12	5.99E-14	4.98E-13	2.75E-12	2.95E-12	2.86E-12	3.11E-12	3.64E-12	3.84E-12	2.21E-12	2.21E-12
3.00E-10	5.55E-13	1.66E-12	4.89E-14	4.04E-13	2.23E-12	2.39E-12	2.32E-12	2.52E-12	2.95E-12	3.11E-12	1.80E-12	1.80E-12
4.00E-10	4.81E-13	1.44E-12	4.29E-14	3.49E-13	1.93E-12	2.07E-12	2.01E-12	2.18E-12	2.56E-12	2.70E-12	1.55E-12	1.55E-12
5.00E-10	4.29E-13	1.29E-12	3.86E-14	3.12E-13	1.72E-12	1.85E-12	1.79E-12	1.95E-12	2.28E-12	2.41E-12	1.39E-12	1.39E-12
6.00E-10	3.92E-13	1.17E-12	3.59E-14	2.84E-13	1.57E-12	1.68E-12	1.63E-12	1.78E-12	2.08E-12	2.19E-12	1.27E-12	1.27E-12
7.00E-10	3.63E-13	1.09E-12	3.35E-14	2.63E-13	1.46E-12	1.56E-12	1.51E-12	1.65E-12	1.93E-12	2.03E-12	1.17E-12	1.17E-12
8.00E-10	3.40E-13	1.02E-12	3.16E-14	2.46E-13	1.36E-12	1.46E-12	1.41E-12	1.54E-12	1.80E-12	1.90E-12	1.10E-12	1.10E-12
9.00E-10	3.21E-13	9.59E-13	3.02E-14	2.32E-13	1.28E-12	1.38E-12	1.33E-12	1.45E-12	1.70E-12	1.79E-12	1.03E-12	1.03E-12
1.00E-09	3.05E-13	9.10E-13	2.89E-14	2.20E-13	1.22E-12	1.30E-12	1.27E-12	1.38E-12	1.61E-12	1.70E-12	9.81E-13	9.81E-13
2.00E-09	2.20E-13	6.53E-13	2.28E-14	1.58E-13	8.74E-13	9.36E-13	9.08E-13	9.88E-13	1.15E-12	1.22E-12	7.04E-13	7.04E-13
3.00E-09	1.80E-13	5.31E-13	1.98E-14	1.28E-13	7.10E-13	7.60E-13	7.37E-13	8.02E-13	9.37E-13	9.89E-13	5.72E-13	5.72E-13
4.00E-09	1.57E-13	4.60E-13	1.81E-14	1.11E-13	6.15E-13	6.58E-13	6.38E-13	6.94E-13	8.10E-13	8.56E-13	4.96E-13	4.96E-13
5.00E-09	1.41E-13	4.12E-13	1.69E-14	9.88E-14	5.50E-13	5.89E-13	5.71E-13	6.21E-13	7.24E-13	7.65E-13	4.44E-13	4.44E-13
6.00E-09	1.29E-13	3.76E-13	1.60E-14	9.01E-14	5.02E-13	5.37E-13	5.21E-13	5.67E-13	6.61E-13	6.99E-13	4.05E-13	4.05E-13
7.00E-09	1.20E-13	3.48E-13	1.53E-14	8.34E-14	4.65E-13	4.98E-13	4.83E-13	5.25E-13	6.11E-13	6.47E-13	3.75E-13	3.75E-13
8.00E-09	1.12E-13	3.26E-13	1.47E-14	7.80E-14	4.35E-13	4.65E-13	4.52E-13	4.91E-13	5.72E-13	6.05E-13	3.51E-13	3.51E-13
9.00E-09	1.06E-13	3.07E-13	1.41E-14	7.35E-14	4.10E-13	4.39E-13	4.26E-13	4.63E-13	5.39E-13	5.70E-13	3.31E-13	3.31E-13
1.00E-08	1.01E-13	2.92E-13	1.36E-14	6.97E-14	3.89E-13	4.17E-13	4.04E-13	4.39E-13	5.11E-13	5.41E-13	3.14E-13	3.14E-13
2.00E-08	7.26E-14	2.09E-13	1.04E-14	4.97E-14	2.78E-13	2.98E-13	2.89E-13	3.14E-13	3.65E-13	3.87E-13	2.25E-13	2.25E-13
3.00E-08	5.90E-14	1.70E-13	8.42E-15	4.05E-14	2.26E-13	2.42E-13	2.35E-13	2.56E-13	2.97E-13	3.15E-13	1.83E-13	1.83E-13

Table A-2. (continued)

Neutron Energy (MeV)	Adipose	Brain	Breast Whole (50/50)	Breast Calcification	Breast Mammary Gland	Heart	Lung	Muscle	Ribs	Skin	Soft Tissue, Female	Thyroid
4.00E-08	5.09E-14	1.47E-13	7.10E-15	3.50E-14	1.96E-13	2.09E-13	2.03E-13	2.21E-13	2.57E-13	2.72E-13	1.58E-13	1.58E-13
5.00E-08	4.53E-14	1.31E-13	6.15E-15	3.13E-14	1.75E-13	1.87E-13	1.81E-13	1.97E-13	2.30E-13	2.43E-13	1.41E-13	1.41E-13
6.00E-08	4.11E-14	1.19E-13	5.43E-15	2.85E-14	1.59E-13	1.70E-13	1.65E-13	1.80E-13	2.09E-13	2.21E-13	1.28E-13	1.28E-13
7.00E-08	3.80E-14	1.10E-13	4.94E-15	2.64E-14	1.47E-13	1.58E-13	1.53E-13	1.66E-13	1.94E-13	2.05E-13	1.19E-13	1.19E-13
8.00E-08	3.54E-14	1.03E-13	4.50E-15	2.47E-14	1.38E-13	1.47E-13	1.43E-13	1.55E-13	1.81E-13	1.91E-13	1.11E-13	1.11E-13
9.00E-08	3.33E-14	9.70E-14	4.17E-15	2.32E-14	1.30E-13	1.39E-13	1.34E-13	1.46E-13	1.70E-13	1.80E-13	1.05E-13	1.05E-13
1.00E-07	3.17E-14	9.25E-14	3.93E-15	2.22E-14	1.23E-13	1.32E-13	1.28E-13	1.39E-13	1.63E-13	1.72E-13	9.96E-14	9.96E-14
2.00E-07	2.23E-14	6.57E-14	2.52E-15	1.58E-14	8.78E-14	9.40E-14	9.12E-14	9.92E-14	1.16E-13	1.22E-13	7.08E-14	7.08E-14
3.00E-07	1.80E-14	5.32E-14	1.94E-15	1.28E-14	7.12E-14	7.62E-14	7.39E-14	8.04E-14	9.39E-14	9.91E-14	5.74E-14	5.74E-14
4.00E-07	1.55E-14	4.58E-14	1.61E-15	1.10E-14	6.13E-14	6.56E-14	6.37E-14	6.93E-14	8.10E-14	8.54E-14	4.94E-14	4.94E-14
5.00E-07	1.38E-14	4.10E-14	1.40E-15	9.87E-15	5.48E-14	5.87E-14	5.70E-14	6.20E-14	7.24E-14	7.64E-14	4.42E-14	4.42E-14
6.00E-07	1.26E-14	3.74E-14	1.27E-15	9.00E-15	5.00E-14	5.35E-14	5.20E-14	5.65E-14	6.61E-14	6.97E-14	4.03E-14	4.03E-14
7.00E-07	1.17E-14	3.46E-14	1.18E-15	8.33E-15	4.63E-14	4.95E-14	4.81E-14	5.23E-14	6.12E-14	6.45E-14	3.73E-14	3.73E-14
8.00E-07	1.09E-14	3.24E-14	1.11E-15	7.80E-15	4.33E-14	4.64E-14	4.50E-14	4.90E-14	5.72E-14	6.03E-14	3.49E-14	3.49E-14
9.00E-07	1.03E-14	3.05E-14	1.06E-15	7.34E-15	4.08E-14	4.37E-14	4.24E-14	4.61E-14	5.39E-14	5.68E-14	3.29E-14	3.29E-14
1.00E-06	9.77E-15	2.89E-14	1.01E-15	6.96E-15	3.87E-14	4.14E-14	4.02E-14	4.37E-14	5.11E-14	5.39E-14	3.12E-14	3.12E-14
2.00E-06	7.12E-15	2.08E-14	8.52E-16	4.98E-15	2.78E-14	2.97E-14	2.89E-14	3.14E-14	3.66E-14	3.86E-14	2.24E-14	2.24E-14
3.00E-06	5.96E-15	1.71E-14	8.43E-16	4.06E-15	2.28E-14	2.44E-14	2.37E-14	2.57E-14	2.99E-14	3.16E-14	1.84E-14	1.84E-14
4.00E-06	5.30E-15	1.49E-14	8.85E-16	3.51E-15	1.98E-14	2.12E-14	2.06E-14	2.24E-14	2.59E-14	2.74E-14	1.60E-14	1.60E-14
5.00E-06	4.91E-15	1.35E-14	9.60E-16	3.14E-15	1.79E-14	1.91E-14	1.86E-14	2.01E-14	2.33E-14	2.46E-14	1.45E-14	1.45E-14
6.00E-06	4.65E-15	1.25E-14	1.04E-15	2.87E-15	1.65E-14	1.76E-14	1.71E-14	1.85E-14	2.13E-14	2.27E-14	1.34E-14	1.34E-14

Table A-2. (continued)

Neutron Energy (MeV)	Adipose	Brain	Breast Whole (50/50)	Breast Calcification	Breast Mammary Gland	Heart	Lung	Muscle	Ribs	Skin	Soft Tissue, Female	Thyroid
7.00E-06	4.47E-15	1.17E-14	1.13E-15	2.66E-15	1.54E-14	1.64E-14	1.60E-14	1.73E-14	1.98E-14	2.11E-14	1.25E-14	1.25E-14
8.00E-06	4.35E-15	1.11E-14	1.23E-15	2.50E-15	1.45E-14	1.55E-14	1.51E-14	1.63E-14	1.86E-14	1.99E-14	1.19E-14	1.19E-14
9.00E-06	4.27E-15	1.06E-14	1.33E-15	2.36E-15	1.39E-14	1.48E-14	1.44E-14	1.56E-14	1.77E-14	1.89E-14	1.14E-14	1.14E-14
1.00E-05	4.22E-15	1.02E-14	1.43E-15	2.24E-15	1.33E-14	1.41E-14	1.38E-14	1.49E-14	1.68E-14	1.81E-14	1.09E-14	1.09E-14
2.00E-05	4.47E-15	8.66E-15	2.46E-15	1.66E-15	1.09E-14	1.14E-14	1.12E-14	1.20E-14	1.28E-14	1.42E-14	9.17E-15	9.17E-15
3.00E-05	5.21E-15	8.52E-15	3.58E-15	1.41E-15	1.03E-14	1.07E-14	1.05E-14	1.12E-14	1.12E-14	1.29E-14	8.93E-15	8.93E-15
4.00E-05	6.14E-15	8.88E-15	4.72E-15	1.28E-15	1.04E-14	1.07E-14	1.06E-14	1.11E-14	1.05E-14	1.26E-14	9.23E-15	9.23E-15
5.00E-05	7.13E-15	9.47E-15	5.87E-15	1.21E-15	1.08E-14	1.10E-14	1.09E-14	1.14E-14	1.02E-14	1.27E-14	9.78E-15	9.78E-15
6.00E-05	8.17E-15	1.02E-14	7.02E-15	1.16E-15	1.14E-14	1.16E-14	1.14E-14	1.19E-14	1.02E-14	1.30E-14	1.05E-14	1.05E-14
7.00E-05	9.23E-15	1.10E-14	8.17E-15	1.14E-15	1.21E-14	1.22E-14	1.21E-14	1.25E-14	1.03E-14	1.35E-14	1.12E-14	1.12E-14
8.00E-05	1.03E-14	1.18E-14	9.33E-15	1.13E-15	1.29E-14	1.29E-14	1.28E-14	1.32E-14	1.04E-14	1.41E-14	1.21E-14	1.21E-14
9.00E-05	1.14E-14	1.27E-14	1.05E-14	1.13E-15	1.37E-14	1.37E-14	1.36E-14	1.39E-14	1.07E-14	1.48E-14	1.29E-14	1.29E-14
1.00E-04	1.25E-14	1.37E-14	1.16E-14	1.14E-15	1.46E-14	1.45E-14	1.44E-14	1.47E-14	1.10E-14	1.55E-14	1.38E-14	1.38E-14
2.00E-04	2.33E-14	2.31E-14	2.27E-14	1.36E-15	2.37E-14	2.32E-14	2.32E-14	2.33E-14	1.50E-14	2.36E-14	2.32E-14	2.32E-14
3.00E-04	3.46E-14	3.34E-14	3.42E-14	1.70E-15	3.38E-14	3.30E-14	3.29E-14	3.29E-14	2.01E-14	3.29E-14	3.34E-14	3.34E-14
4.00E-04	4.59E-14	7.05E-14	4.56E-14	2.08E-15	5.30E-14	6.96E-14	6.96E-14	5.16E-14	3.43E-14	6.92E-14	5.26E-14	5.26E-14
5.00E-04	5.77E-14	5.46E-14	5.75E-14	2.49E-15	5.49E-14	5.33E-14	5.32E-14	5.30E-14	3.10E-14	5.25E-14	5.45E-14	5.45E-14
6.00E-04	6.90E-14	6.50E-14	6.88E-14	2.90E-15	6.52E-14	6.32E-14	6.32E-14	6.28E-14	3.64E-14	6.22E-14	6.49E-14	6.49E-14
7.00E-04	8.03E-14	7.55E-14	8.02E-14	3.31E-15	7.56E-14	7.33E-14	7.32E-14	7.28E-14	4.19E-14	7.19E-14	7.53E-14	7.53E-14
8.00E-04	9.18E-14	8.61E-14	9.17E-14	3.73E-15	8.62E-14	8.35E-14	8.34E-14	8.29E-14	4.75E-14	8.18E-14	8.58E-14	8.58E-14
9.00E-04	1.03E-13	9.68E-14	1.03E-13	4.15E-15	9.68E-14	9.37E-14	9.37E-14	9.31E-14	5.32E-14	9.18E-14	9.65E-14	9.65E-14

Table A-2. (continued)

Neutron Energy (MeV)	Adipose	Brain	Breast Whole (50/50)	Breast Calcification	Breast Mammary Gland	Heart	Lung	Muscle	Ribs	Skin	Soft Tissue, Female	Thyroid
1.00E-03	1.15E-13	1.08E-13	1.15E-13	4.58E-15	1.07E-13	1.04E-13	1.04E-13	1.03E-13	5.89E-14	1.02E-13	1.07E-13	1.07E-13
2.00E-03	2.22E-13	2.07E-13	2.23E-13	8.63E-15	2.07E-13	2.00E-13	2.00E-13	1.98E-13	1.12E-13	1.95E-13	2.07E-13	2.07E-13
3.00E-03	3.33E-13	3.11E-13	3.34E-13	1.28E-14	3.10E-13	3.00E-13	3.00E-13	2.97E-13	1.67E-13	2.92E-13	3.09E-13	3.09E-13
4.00E-03	4.44E-13	4.14E-13	4.45E-13	1.71E-14	4.12E-13	3.99E-13	3.99E-13	3.95E-13	2.22E-13	3.89E-13	4.12E-13	4.12E-13
5.00E-03	5.56E-13	5.17E-13	5.57E-13	2.13E-14	5.16E-13	4.99E-13	4.98E-13	4.94E-13	2.78E-13	4.86E-13	5.15E-13	5.15E-13
6.00E-03	6.62E-13	6.16E-13	6.64E-13	2.54E-14	6.14E-13	5.94E-13	5.93E-13	5.89E-13	3.31E-13	5.79E-13	6.13E-13	6.13E-13
7.00E-03	7.69E-13	7.15E-13	7.71E-13	2.97E-14	7.13E-13	6.89E-13	6.89E-13	6.83E-13	3.84E-13	6.72E-13	7.12E-13	7.12E-13
8.00E-03	8.73E-13	8.12E-13	8.76E-13	3.40E-14	8.10E-13	7.83E-13	7.83E-13	7.76E-13	4.36E-13	7.63E-13	8.09E-13	8.09E-13
9.00E-03	9.81E-13	9.12E-13	9.83E-13	3.82E-14	9.09E-13	8.79E-13	8.79E-13	8.71E-13	4.90E-13	8.57E-13	9.08E-13	9.08E-13
1.00E-02	1.08E-12	1.01E-12	1.09E-12	4.19E-14	1.01E-12	9.72E-13	9.72E-13	9.64E-13	5.41E-13	9.48E-13	1.00E-12	1.00E-12
2.00E-02	2.01E-12	1.87E-12	2.02E-12	7.80E-14	1.87E-12	1.80E-12	1.80E-12	1.79E-12	1.00E-12	1.76E-12	1.86E-12	1.86E-12
3.00E-02	2.90E-12	2.69E-12	2.90E-12	1.14E-13	2.68E-12	2.59E-12	2.59E-12	2.57E-12	1.45E-12	2.53E-12	2.68E-12	2.68E-12
4.00E-02	3.68E-12	3.42E-12	3.69E-12	1.47E-13	3.41E-12	3.29E-12	3.29E-12	3.27E-12	1.84E-12	3.21E-12	3.41E-12	3.41E-12
5.00E-02	4.41E-12	4.09E-12	4.42E-12	1.79E-13	4.08E-12	3.94E-12	3.94E-12	3.91E-12	2.20E-12	3.84E-12	4.08E-12	4.08E-12
6.00E-02	5.08E-12	4.71E-12	5.09E-12	2.08E-13	4.70E-12	4.54E-12	4.54E-12	4.50E-12	2.54E-12	4.43E-12	4.70E-12	4.70E-12
7.00E-02	5.69E-12	5.28E-12	5.70E-12	2.35E-13	5.27E-12	5.09E-12	5.08E-12	5.04E-12	2.84E-12	4.96E-12	5.26E-12	5.26E-12
8.00E-02	6.27E-12	5.81E-12	6.27E-12	2.61E-13	5.80E-12	5.60E-12	5.59E-12	5.55E-12	3.13E-12	5.46E-12	5.79E-12	5.79E-12
9.00E-02	6.81E-12	6.31E-12	6.82E-12	3.01E-13	6.30E-12	6.08E-12	6.08E-12	6.03E-12	3.41E-12	5.93E-12	6.29E-12	6.29E-12
1.00E-01	7.31E-12	6.78E-12	7.32E-12	3.09E-13	6.76E-12	6.53E-12	6.53E-12	6.47E-12	3.66E-12	6.37E-12	6.76E-12	6.76E-12
2.00E-01	1.11E-11	1.03E-11	1.11E-11	5.10E-13	1.03E-11	9.91E-12	9.90E-12	9.82E-12	5.58E-12	9.67E-12	1.03E-11	1.03E-11
3.00E-01	1.39E-11	1.29E-11	1.40E-11	7.58E-13	1.29E-11	1.25E-11	1.25E-11	1.24E-11	7.07E-12	1.22E-11	1.29E-11	1.29E-11

Table A-2. (continued)

Neutron Energy (MeV)	Adipose	Brain	Breast Whole (50/50)	Breast Calcification	Breast Mammary Gland	Heart	Lung	Muscle	Ribs	Skin	Soft Tissue, Female	Thyroid
4.00E-01	1.65E-11	1.57E-11	1.67E-11	1.27E-12	1.55E-11	1.52E-11	1.52E-11	1.51E-11	8.64E-12	1.48E-11	1.55E-11	1.55E-11
5.00E-01	1.81E-11	1.66E-11	1.80E-11	8.93E-13	1.67E-11	1.60E-11	1.60E-11	1.59E-11	9.14E-12	1.57E-11	1.67E-11	1.67E-11
6.00E-01	1.97E-11	1.81E-11	1.97E-11	1.05E-12	1.82E-11	1.74E-11	1.74E-11	1.73E-11	9.95E-12	1.71E-11	1.81E-11	1.81E-11
7.00E-01	2.13E-11	1.96E-11	2.12E-11	1.12E-12	1.96E-11	1.89E-11	1.89E-11	1.87E-11	1.08E-11	1.85E-11	1.96E-11	1.96E-11
8.00E-01	2.27E-11	2.09E-11	2.27E-11	1.24E-12	2.10E-11	2.02E-11	2.02E-11	2.00E-11	1.15E-11	1.97E-11	2.10E-11	2.10E-11
9.00E-01	2.42E-11	2.24E-11	2.42E-11	1.56E-12	2.24E-11	2.17E-11	2.16E-11	2.15E-11	1.24E-11	2.11E-11	2.24E-11	2.24E-11
1.00E+00	2.64E-11	2.60E-11	2.71E-11	2.97E-12	2.54E-11	2.53E-11	2.53E-11	2.50E-11	1.45E-11	2.45E-11	2.54E-11	2.54E-11
2.00E+00	3.43E-11	3.16E-11	3.42E-11	2.06E-12	3.17E-11	3.05E-11	3.05E-11	3.03E-11	1.75E-11	2.98E-11	3.17E-11	3.17E-11
3.00E+00	4.27E-11	3.79E-11	4.18E-11	3.31E-12	3.87E-11	3.65E-11	3.64E-11	3.63E-11	2.20E-11	3.61E-11	3.86E-11	3.86E-11
4.00E+00	4.80E-11	4.33E-11	4.72E-11	5.42E-12	4.40E-11	4.19E-11	4.18E-11	4.17E-11	2.59E-11	4.14E-11	4.39E-11	4.39E-11
5.00E+00	4.91E-11	4.60E-11	4.92E-11	7.36E-12	4.59E-11	4.45E-11	4.45E-11	4.42E-11	2.73E-11	4.35E-11	4.58E-11	4.58E-11
6.00E+00	5.20E-11	4.91E-11	5.23E-11	8.77E-12	4.88E-11	4.75E-11	4.75E-11	4.71E-11	2.94E-11	4.64E-11	4.88E-11	4.88E-11
7.00E+00	5.29E-11	5.03E-11	5.34E-11	9.29E-12	4.98E-11	4.86E-11	4.86E-11	4.82E-11	3.00E-11	4.74E-11	4.98E-11	4.98E-11
8.00E+00	5.88E-11	5.36E-11	5.81E-11	1.06E-11	5.41E-11	5.18E-11	5.17E-11	5.15E-11	3.32E-11	5.10E-11	5.40E-11	5.40E-11
9.00E+00	6.02E-11	5.61E-11	6.01E-11	1.23E-11	5.61E-11	5.42E-11	5.42E-11	5.39E-11	3.48E-11	5.32E-11	5.60E-11	5.60E-11
1.00E+01	6.21E-11	5.93E-11	6.26E-11	1.41E-11	5.88E-11	5.76E-11	5.76E-11	5.71E-11	3.71E-11	5.63E-11	5.88E-11	5.88E-11
2.00E+01	8.03E-11	7.07E-11	7.75E-11	2.13E-11	7.31E-11	6.86E-11	6.84E-11	6.86E-11	4.91E-11	6.87E-11	7.28E-11	7.28E-11

Table A-3. Photon tissue Kerma coefficients (Gy-cm^2)

Photon Energy (MeV)	Adipose	Brain	Breast Whole (50/50)	Breast Calcification	Breast Mammary Gland	Heart	Lung	Muscle	Ribs	Skin	Soft Tissue (Female)	Thyroid
1.00E-03	4.20E-10	5.91E-10	5.02E-10	6.61E-10	5.22E-10	5.95E-10	6.07E-10	5.94E-10	5.56E-10	5.71E-10	5.29E-10	6.04E-10
1.04E-03	4.28E-10	6.10E-10	5.16E-10	6.85E-10	5.36E-10	6.15E-10	6.28E-10	6.14E-10	5.73E-10	5.89E-10	5.44E-10	6.24E-10
1.07E-03	4.36E-10	6.30E-10	5.29E-10	7.09E-10	5.51E-10	6.35E-10	6.49E-10	6.34E-10	5.90E-10	6.07E-10	5.59E-10	6.44E-10
1.07E-03	4.37E-10	6.32E-10	5.29E-10	7.09E-10	5.52E-10	6.36E-10	6.51E-10	6.35E-10	5.91E-10	6.09E-10	5.60E-10	6.46E-10
1.50E-03	2.07E-10	2.99E-10	2.50E-10	3.41E-10	2.61E-10	3.00E-10	3.08E-10	3.00E-10	2.81E-10	2.88E-10	2.65E-10	3.06E-10
2.00E-03	1.21E-10	1.78E-10	1.48E-10	2.08E-10	1.55E-10	1.79E-10	1.84E-10	1.79E-10	1.69E-10	1.71E-10	1.57E-10	1.82E-10
2.15E-03	1.17E-10	1.72E-10	1.43E-10	2.00E-10	1.49E-10	1.73E-10	1.77E-10	1.72E-10	1.62E-10	1.65E-10	1.51E-10	1.76E-10
2.15E-03	1.18E-10	1.75E-10	1.43E-10	3.34E-10	1.50E-10	1.74E-10	1.79E-10	1.74E-10	2.05E-10	1.66E-10	1.53E-10	1.77E-10
2.47E-03	1.01E-10	1.51E-10	1.23E-10	2.97E-10	1.29E-10	1.51E-10	1.54E-10	1.50E-10	1.80E-10	1.43E-10	1.32E-10	1.53E-10
2.47E-03	1.02E-10	1.52E-10	1.23E-10	2.97E-10	1.31E-10	1.52E-10	1.56E-10	1.52E-10	1.82E-10	1.45E-10	1.33E-10	1.53E-10
2.82E-03	7.43E-11	1.12E-10	9.00E-11	2.32E-10	9.55E-11	1.11E-10	1.15E-10	1.11E-10	1.38E-10	1.06E-10	9.75E-11	1.12E-10
2.82E-03	7.43E-11	1.14E-10	9.00E-11	2.32E-10	9.61E-11	1.13E-10	1.16E-10	1.12E-10	1.38E-10	1.08E-10	9.81E-11	1.14E-10
3.00E-03	5.65E-11	8.77E-11	6.83E-11	1.88E-10	7.37E-11	8.66E-11	8.99E-11	8.63E-11	1.10E-10	8.29E-11	7.53E-11	8.71E-11
3.61E-03	4.41E-11	6.89E-11	5.34E-11	1.52E-10	5.77E-11	6.80E-11	7.06E-11	6.78E-11	8.74E-11	6.51E-11	5.91E-11	6.83E-11
3.61E-03	4.41E-11	7.05E-11	5.34E-11	1.52E-10	5.77E-11	6.96E-11	7.17E-11	6.99E-11	8.79E-11	6.56E-11	6.01E-11	6.89E-11
4.00E-03	3.18E-11	5.16E-11	3.87E-11	1.15E-10	4.19E-11	5.09E-11	5.24E-11	5.12E-11	6.54E-11	4.78E-11	4.38E-11	5.02E-11
4.04E-03	3.15E-11	5.12E-11	3.83E-11	1.14E-10	4.15E-11	5.04E-11	5.19E-11	5.07E-11	6.48E-11	4.74E-11	4.34E-11	4.97E-11
4.04E-03	3.15E-11	5.12E-11	3.83E-11	3.04E-10	4.15E-11	5.04E-11	5.19E-11	5.07E-11	1.30E-10	4.74E-11	4.34E-11	4.97E-11
4.56E-03	2.63E-11	4.29E-11	3.20E-11	1.71E-10	3.47E-11	4.23E-11	4.36E-11	4.26E-11	8.01E-11	3.97E-11	3.64E-11	4.17E-11
4.56E-03	2.63E-11	4.29E-11	3.20E-11	1.71E-10	3.47E-11	4.23E-11	4.36E-11	4.26E-11	8.01E-11	3.97E-11	3.64E-11	4.17E-11
4.70E-03	2.45E-11	4.00E-11	2.98E-11	1.87E-10	3.23E-11	3.94E-11	4.06E-11	3.97E-11	8.41E-11	3.70E-11	3.39E-11	3.88E-11
4.85E-03	2.24E-11	3.68E-11	2.73E-11	2.04E-10	2.97E-11	3.62E-11	3.73E-11	3.64E-11	8.84E-11	3.39E-11	3.11E-11	3.56E-11

Table A-3. (continued)

Photon Energy (MeV)	Adipose	Brain	Breast Whole (50/50)	Breast Calcification	Breast Mammary Gland	Heart	Lung	Muscle	Ribs	Skin	Soft Tissue (Female)	Thyroid
4.85E-03	2.24E-11	3.68E-11	2.73E-11	2.04E-10	2.97E-11	3.62E-11	3.73E-11	3.64E-11	8.84E-11	3.39E-11	3.11E-11	3.56E-11
5.00E-03	2.02E-11	3.33E-11	2.46E-11	2.22E-10	2.68E-11	3.27E-11	3.37E-11	3.30E-11	9.27E-11	3.07E-11	2.81E-11	3.22E-11
5.19E-03	1.93E-11	3.18E-11	2.35E-11	2.14E-10	2.55E-11	3.13E-11	3.22E-11	3.15E-11	8.92E-11	2.93E-11	2.68E-11	3.07E-11
5.19E-03	1.93E-11	3.18E-11	2.35E-11	2.14E-10	2.55E-11	3.13E-11	3.22E-11	3.15E-11	8.92E-11	2.93E-11	2.68E-11	3.07E-11
6.00E-03	1.38E-11	2.31E-11	1.69E-11	1.65E-10	1.84E-11	2.27E-11	2.34E-11	2.29E-11	6.82E-11	2.12E-11	1.94E-11	2.22E-11
7.11E-03	1.10E-11	1.85E-11	1.35E-11	1.38E-10	1.47E-11	1.81E-11	1.87E-11	1.83E-11	5.63E-11	1.69E-11	1.55E-11	1.78E-11
7.11E-03	1.10E-11	1.85E-11	1.34E-11	1.38E-10	1.47E-11	1.81E-11	1.87E-11	1.83E-11	5.63E-11	1.69E-11	1.55E-11	1.78E-11
8.00E-03	7.54E-12	1.28E-11	9.23E-12	1.02E-10	1.01E-11	1.26E-11	1.29E-11	1.27E-11	4.13E-11	1.17E-11	1.07E-11	1.23E-11
1.00E-02	4.68E-12	8.04E-12	5.73E-12	6.89E-11	6.31E-12	7.87E-12	8.12E-12	7.95E-12	2.76E-11	7.32E-12	6.70E-12	7.66E-12
1.50E-02	1.93E-12	3.39E-12	2.38E-12	3.26E-11	2.63E-12	3.32E-12	3.42E-12	3.35E-12	1.28E-11	3.07E-12	2.81E-12	3.21E-12
2.00E-02	1.03E-12	1.83E-12	1.27E-12	1.87E-11	1.41E-12	1.78E-12	1.84E-12	1.81E-12	7.30E-12	1.65E-12	1.51E-12	1.72E-12
3.00E-02	4.53E-13	7.83E-13	5.47E-13	8.35E-12	6.06E-13	7.63E-13	7.86E-13	7.73E-13	3.24E-12	7.06E-13	6.50E-13	7.34E-13
3.32E-02	4.19E-13	7.14E-13	5.03E-13	7.54E-12	5.55E-13	6.96E-13	7.16E-13	7.05E-13	2.93E-12	6.45E-13	5.95E-13	6.70E-13
3.32E-02	4.19E-13	7.14E-13	5.03E-13	7.54E-12	5.55E-13	6.96E-13	7.16E-13	7.05E-13	2.93E-12	6.45E-13	5.95E-13	6.70E-13
4.00E-02	2.91E-13	4.66E-13	3.40E-13	4.67E-12	3.71E-13	4.55E-13	4.67E-13	4.61E-13	1.83E-12	4.24E-13	3.95E-13	4.39E-13
5.00E-02	2.46E-13	3.52E-13	2.75E-13	2.99E-12	2.94E-13	3.45E-13	3.52E-13	3.48E-13	1.21E-12	3.26E-13	3.09E-13	3.34E-13
6.00E-02	2.46E-13	3.16E-13	2.65E-13	2.10E-12	2.77E-13	3.11E-13	3.15E-13	3.13E-13	8.98E-13	2.98E-13	2.87E-13	3.04E-13
8.00E-02	3.02E-13	3.37E-13	3.12E-13	1.29E-12	3.17E-13	3.34E-13	3.36E-13	3.35E-13	6.46E-13	3.27E-13	3.22E-13	3.30E-13
1.00E-01	3.90E-13	4.10E-13	3.96E-13	9.79E-13	3.97E-13	4.07E-13	4.09E-13	4.08E-13	5.93E-13	4.02E-13	4.00E-13	4.05E-13
1.50E-01	6.58E-13	6.63E-13	6.61E-13	8.52E-13	6.57E-13	6.60E-13	6.60E-13	6.60E-13	7.19E-13	6.57E-13	6.59E-13	6.59E-13
2.00E-01	9.48E-13	9.47E-13	9.50E-13	9.91E-13	9.44E-13	9.44E-13	9.44E-13	9.43E-13	9.53E-13	9.40E-13	9.44E-13	9.43E-13
3.00E-01	1.54E-12	1.53E-12	1.54E-12	1.44E-12	1.53E-12	1.52E-12	1.52E-12	1.52E-12	1.48E-12	1.52E-12	1.53E-12	1.52E-12

Table A-3. (continued)

Photon Energy (MeV)	Adipose	Brain	Breast Whole (50/50)	Breast Calcification	Breast Mammary Gland	Heart	Lung	Muscle	Ribs	Skin	Soft Tissue (Female)	Thyroid
4.00E-01	2.10E-12	2.09E-12	2.11E-12	1.92E-12	2.09E-12	2.09E-12	2.08E-12	2.08E-12	2.02E-12	2.08E-12	2.09E-12	2.08E-12
5.00E-01	2.65E-12	2.63E-12	2.65E-12	2.39E-12	2.63E-12	2.62E-12	2.62E-12	2.62E-12	2.53E-12	2.61E-12	2.63E-12	2.62E-12
6.00E-01	3.16E-12	3.14E-12	3.16E-12	2.84E-12	3.14E-12	3.13E-12	3.13E-12	3.13E-12	3.02E-12	3.12E-12	3.14E-12	3.13E-12
8.00E-01	4.12E-12	4.09E-12	4.12E-12	3.69E-12	4.09E-12	4.08E-12	4.08E-12	4.07E-12	3.92E-12	4.06E-12	4.09E-12	4.08E-12
1.00E+00	4.98E-12	4.95E-12	4.98E-12	4.45E-12	4.94E-12	4.93E-12	4.93E-12	4.93E-12	4.74E-12	4.92E-12	4.94E-12	4.93E-12
1.25E+00	5.95E-12	5.91E-12	5.95E-12	5.31E-12	5.91E-12	5.89E-12	5.89E-12	5.88E-12	5.66E-12	5.87E-12	5.90E-12	5.89E-12
1.50E+00	6.82E-12	6.78E-12	6.83E-12	6.09E-12	6.77E-12	6.76E-12	6.75E-12	6.75E-12	6.49E-12	6.74E-12	6.77E-12	6.75E-12
2.00E+00	8.36E-12	8.31E-12	8.37E-12	7.51E-12	8.31E-12	8.29E-12	8.29E-12	8.28E-12	7.98E-12	8.26E-12	8.30E-12	8.29E-12
3.00E+00	1.09E-11	1.09E-11	1.10E-11	1.01E-11	1.09E-11	1.09E-11	1.09E-11	1.09E-11	1.05E-11	1.08E-11	1.09E-11	1.09E-11
4.00E+00	1.31E-11	1.32E-11	1.32E-11	1.26E-11	1.31E-11	1.31E-11	1.31E-11	1.31E-11	1.28E-11	1.31E-11	1.31E-11	1.31E-11
5.00E+00	1.51E-11	1.52E-11	1.52E-11	1.50E-11	1.52E-11	1.52E-11	1.52E-11	1.52E-11	1.50E-11	1.51E-11	1.52E-11	1.52E-11
6.00E+00	1.70E-11	1.72E-11	1.72E-11	1.75E-11	1.71E-11	1.72E-11	1.72E-11	1.72E-11	1.71E-11	1.71E-11	1.71E-11	1.72E-11
8.00E+00	2.07E-11	2.11E-11	2.09E-11	2.26E-11	2.08E-11	2.11E-11	2.11E-11	2.10E-11	2.13E-11	2.09E-11	2.09E-11	2.10E-11
1.00E+01	2.42E-11	2.49E-11	2.45E-11	2.79E-11	2.45E-11	2.48E-11	2.49E-11	2.48E-11	2.55E-11	2.47E-11	2.46E-11	2.48E-11
1.50E+01	3.28E-11	3.43E-11	3.35E-11	4.15E-11	3.36E-11	3.43E-11	3.44E-11	3.42E-11	3.60E-11	3.40E-11	3.37E-11	3.42E-11
2.00E+01	4.14E-11	4.38E-11	4.25E-11	5.55E-11	4.27E-11	4.38E-11	4.40E-11	4.37E-11	4.67E-11	4.33E-11	4.28E-11	4.38E-11

APPENDIX B

MATLAB SCRIPTS

The scripts and functions that were written for the handling of MCNP Mesh tallies are included here for reference. The scripts converted MCNP Mesh tallies to 3D dose array for input into CERR.

1. Script to call Mesh tally files and assign names, irradiation times, and biological weighting factors
2. Function mesh2CERR.m to create 3D dose matrix and pass data to load function
3. Function load2CERR.m passes data to CERR

MATLAB Script: runData.m

```
%Script for data handling
%Files for Mesh Tallies to load
file1=('c:\mcnp\BodyDose\b000.m');
file2=('c:\mcnp\BodyDose\b080.m');
file3=('c:\mcnp\BodyDose\b0810.m');
file4=('c:\mcnp\BodyDose\b0850.m');
file5=('c:\mcnp\BodyDose\b08100.m');
file6=('c:\mcnp\BodyDose\b350.m');
file7=('c:\mcnp\BodyDose\b3510.m');
file8=('c:\mcnp\BodyDose\b3550.m');
file9=('c:\mcnp\BodyDose\b35100.m');

%Set names for dose sets
setName1=('000');
setName2=('080');
setName3=('0810');
setName4=('0850');
setName5=('08100');
setName6=('350');
setName7=('3510');
setName8=('3550');
setName9=('35100');

%Irradiation times in seconds
time1=6465;
time2=5207;
time3=2450;
time4=815;
time5=454;
time6=5120;
time7=2288;
time8=743;
time9=417;

%Biological weighting factors RBE for neutrons and CBE for boron
nRBE=3.0;
bCBE=3.8;

%Call function to load data sets to CERR
mesh2CERR(file1,setName1,time1,nRBE,bCBE);
mesh2CERR(file2,setName2,time2,nRBE,bCBE);
mesh2CERR(file3,setName3,time3,nRBE,bCBE);
mesh2CERR(file4,setName4,time4,nRBE,bCBE);
mesh2CERR(file5,setName5,time5,nRBE,bCBE);
mesh2CERR(file6,setName6,time6,nRBE,bCBE);
mesh2CERR(file7,setName7,time7,nRBE,bCBE);
mesh2CERR(file8,setName8,time8,nRBE,bCBE);
mesh2CERR(file9,setName9,time9,nRBE,bCBE);
```

MATLAB Function: mesh2CERR.m

```
function mesh2CERR (fileSet,setName,timeIrr,RBE,CBE)
%Convert mesh tally files to 3D dose matrices
%

file=fileSet;
set=setName;

%irradiation parameters
radiusBeam=3; %Beam Radius used in scenario
areaBeam=pi*radiusBeam^2; %beam area cm^2
fluxDensity=5e9;  %n/sec/cm^2for MIT-FCB beam
time=timeIrr;  %irradiation time in seconds
sourceTerm=areaBeam*fluxDensity*time;  %total neutron source term

%setName defintions
setName1=[set '_n'];
setName2=[set '_p'];
setName3=[set '_nB'];
setName4=[set '_pB'];
setName5=[set '_n_RBE'];
setName6=[set '_nB_CBE'];
setName7=[set '_totalTumor'];
setName8=[set '_totalTissue'];

%import file
%
%tally54 is the absorbed neutron dose for Female Soft tissue
%tally64 is the absorbed photon dose for Female Soft tissue
%tally104 is the absorbed neutron dose for Borated tissue
%tally114 is the absorbed photon dose for Borated tissue
%all values are Gy per source neutron
fid = fopen(file);
tally54=textscan(fid,'%f %f %f %f
   %f','HeaderLines',15,'CollectOutput',1);
tally64=textscan(fid,'%f %f %f %f %f
   %f','HeaderLines',11,'CollectOutput',1);
tally104=textscan(fid,'%f %f %f %f
   %f','HeaderLines',11,'CollectOutput',1);
tally114=textscan(fid,'%f %f %f %f %f
   %f','HeaderLines',11,'CollectOutput',1);
fclose(fid);

%convert cell data to matrices
nAbsDose=cell2mat(tally54);
pAbsDose=cell2mat(tally64);
pAbsDose(:,1)=[]; %strip off extra column from photon data
nBDose=cell2mat(tally104);
pBDose=cell2mat(tally114);
pBDose(:,1)=[];

%prepare 3D Dose matrices
m=0;
```

```
n=zeros(100,100,67);
p=zeros(100,100,67);
nB=zeros(100,100,67);
pB=zeros(100,100,67);
n_RBE=zeros(100,100,67);
nB_CBE=zeros(100,100,67);

for i=1:100
    for j=100:-1:1
        for k=67:-1:1
            m=m+1;
            n(j,i,k) = nAbsDose(m,4)*sourceTerm;
            p(j,i,k) = pAbsDose(m,4)*sourceTerm;
            nB(j,i,k) = nBDose(m,4)*sourceTerm;
            pB(j,i,k) = pBDose(m,4)*sourceTerm;
            n_RBE(j,i,k) = nAbsDose(m,4)*sourceTerm*RBE;
            nB_CBE(j,i,k) = nBDose(m,4)*sourceTerm*CBE;
        end
    end
end

totalTumor=nB_CBE+pB;
totalTissue=n_RBE+p;

%define z index to pass to CERR
zdata=nAbsDose(1:67,3);
zdata=flipud(zdata);
zdata=zdata*(-1);

%script to load 3D dataset into open plan
%must have CERR open with Active Plan

loadScan(n,zdata,setName1);
loadScan(p,zdata,setName2);
loadScan(nB,zdata,setName3);
loadScan(pB,zdata,setName4);
loadScan(n_RBE,zdata,setName5);
loadScan(nB_CBE,zdata,setName6);
loadScan(totalTumor,zdata,setName7);
loadScan(totalTissue,zdata,setName8);
```

MATLAB Function: load2CERR.m

```
function loadScan(doseData,zdata,setName)

% Load Scan to CERR
global planC
indexS = planC{end};

size(doseData);

%regParamsS should contain geometric registration data including the
following fields:
regParamsS.horizontalGridInterval = 0.5; % (x voxel width)
regParamsS.verticalGridInterval   = 0.5; % (y voxel width)
regParamsS.coord1OFFirstPoint     = -24.75; % (x value of center of
upper left voxel on all slices)
regParamsS.coord2OFFirstPoint     = -24.75;  % (y value of center of
upper left voxel on all slices
regParamsS.zValues                = zdata;


assocScanNum=1;
assocScanUID=planC{indexS.scan}(assocScanNum).scanUID;
dose2CERR(doseData,[],setName,'test','test',[],regParamsS, 'no',...
    assocScanUID);
```

BIBLIOGRAPHY

1. Mundy, D. Monte Carlo Assessment of Boron Neutron Capture Therapy for the Treatment of Breast Cancer. M.S. Thesis, Purdue University, 2005.

2. Mundy, D.; Harb, W.; Jevremovic, T. Radiation binary targeted therapy for HER-2 positive breast cancers: assumptions, theoretical assessment and future directions. *Phys. Med. Biol.*, **2006**, *51*, 1377-1391.

3. Sztejnberg Gonçalves-Carralves, M.L.; Jevremovic, T. Numerical Assessment of Radiation Binary Targeted Therapy for Her-2 Positive Breast Cancers: Advanced Calculations and Radiation Dosimetry. *Phys. Med. Biol.*, **2007**, *52*, 4245-4264.

4. Sztejnberg Gonçalves-Carralves, M.L.; Jevremovic, T. MCNP5 Voxelized Dose Model for BNCT Applied to Breast Cancers. TRANSACTIONS: American Nuclear Society 2008 Annual Meeting, Vol. 98 (1), pp 757-758. American Nuclear Society. Anaheim, California, U.S.A., June 10th, 2008.

5. Sztejnberg, M.L.; Jevremovic, T. Advanced Applications of BNCT in Advanced Cancers. 17th International Conference on Nuclear Engineering, ICONE17, Brussels, Belgium, July 14th, 2009.

6. Sztejnberg, M.L. Boron Neutron Capture Therapy Applied to Advanced Breast Cancers: Engineering Simulation and Feasibility Study of the Radiation Treatment Protocol. Ph.D. Dissertation, Purdue, 2009.

7. Wu, X.; Liu, H.; et al. Immunofluorescent labeling of cancer marker Her2 and other cellular targets with semiconductor quantum dots. *Nature Biotechnology*, **2003**, *21*, 41-46.

8. Lee, M.W. Syndissertation and Biological Investigation of Boron-rich Oligomeric Phosphate Diesters. Ph.D. Dissertation, University of California, Los Angeles, 2005.

9. Cutuli, B.; de Lafontan, B.; et al. Breast-conserving surgery and radiotherapy: a possible treatment for lobular carcinoma in situ? *Eur. J. Cancer*, **2005**, *41*, 380-385.

10. Coderre, J.A.; Morris, G.M. The radiation biology of boron neutron capture therapy. *Radiat. Res.*, **1999**, *151*, 1-18.

11. Small, W.; Woloschak, G. Radiation Toxicity: a practical guide. Springer Science Business Media: New York, 2006.

12. Archambeau, J.O. ; Penzer, R.; Wasserman, T. Pathophysiology of irradiated skin and breast. *Int. J. Radiation Oncology Biol. Phys*, **1995**, *31*, 1171-1185.

13. Riley, K.J. ; Binns, P.J. ; Harling, O.K. A state-of-the-art epithermal neutron irradiation facility for neutron capture therapy. *Phys. Med. Biol.*, **2004**, *49*, 3725-3735.

14. Hunt, K.K.; Robb, G.L.; et al, Breast Cancer, 2nd Edition, Springer Science, 2008.

15. Marks , L.B.; Yorke, E.D.; et al. Use of normal tissue complication probability models in the clinic, *Int. J. Radiation Oncology Biol. Phys*., **2010**, *76*, S10-S19.

16. Bentzen, S.M.; Louis, D.S.; et al, Quantitative analyses of normal tissue effects in the clinic (QUANTEC): an introduction to the scientific issues. *Int. J. Radiation Oncology Biol. Phys*., **2010**, *76*, S3-S9.

17. Timmerman, R.D. An overview of hypofractionation and introduction to this issue of seminars in radiation oncology. *Semin. Radiat. Oncol.,* **2008,** *18,* 215–22.

18. Hoppe, B.S.; Laser, B.; Kowalski , A.V.; et al. Acute skin toxicity following stereotactic body radiation therapy for stage I non-small-cell lung cancer: who's at risk?, *Int. J. Radiat. Oncol. Biol. Phys*. **2008**, *72, 1*283–1286.

19. Grimm, J., Lacouture, T.; et al. Dose tolerance limits and dose volume histogram evaluation for stereotactic body radiotherapy. *Journal of Applied Clinical Medical Physics*[Online], **2011,** *12,* http://www.jacmp.org/index.php/jacmp/article/view/3368/2212 (accessed: 10/22/2012).

20. Gagliardi, G.; Constine, L.S.; et al. Radiation dose-volume effects in the heart, *Int. J. Radiation Oncology Biol. Phys*. **2010**, *76*, S77-S85.

21. Gomez, D.R.; Hunt, M.A.; et al. Low rate of thoracic toxicity in palliative paraspinal single-fraction stereotactic body radiation therapy, *Radiother. Oncol.,* **2009**, *93,* 414–418.

22. Chang, J.; Balter, P.; et al. Stereotactic body radiation therapy in centrally and superiorly located stage I or isolated recurrent non–small-cell lung cancer. *Int. J. Radiat. Oncol. Biol. Phys.* **2008**, *72*, 967–971.

23. Pope, T.L.; Read, M.E.; et al, Breast skin thickness: normal range and causes of thickening shown on film-screen mammography. *J. Can. Assoc. Radiol.* **1984**, *35,* 365-368.

24. US NRC, 10CFR20.1201, Federal Register, 72 FR68059, Dec. 4, 2007.

25. Goorley, J.T. ; Kiger III, W.S.; Zamenhof, R.G. Reference dosimetry calculations for neutron capture therapy with comparison of analytical and voxel models. *Med. Phys.*, **2002**, *29*, 145-156.

26. Los Alamos National Laboratory. Monte Carlo N-Particle Transport Code, MCNP5-1.60, May 2008.

27. Van Riper, K.A. Scan2MCNP User Manual, CT & MRI Scan Data to MCNP Input Format Conversion Software. White Rock Science, White Rock, New Mexico, USA. 2010.

28. Van Riper, K.A. Moritz User's Guide, Windows Version. White Rock Science, White Rock, New Mexico, USA. 2010.

29. Deasy, J.O.; Blanco, A.I. ; Clark, V.H. CERR (A computational environment for radiotherapy research). *Med. Phys.* **2003**, *30*, 979–985.

30. The 2007 Recommendations of the International Commission on Radiological Protection, Publication 103. Elsevier, 37(2-4), 2007.

31. Sun, X.; Qu, W. New calculation method of neutron Kerma coefficients for carbon and oxygen below 30 MeV. *Physical Review*, **2008**, *78*, 054610.

32. MacFarlane, R. E. The NJOY Nuclear Data Processing System, Version 91. Los Alamos National Laboratory, Los Alamos, NM, 1994.

33. Zhang, L.; Abdo, M. A. Kerma factor evaluation and its application in nuclear heating experiment analysis. *Fusion Eng. Des.,***1997***, 36,* 479-503.

34. Liu, Z. ; Chen, J. New calculations of neutron Kerma coefficients and dose equivalent. *J. Radiol. Prot,* **2008***, 28*, 185.

35. X-5 Monte Carlo Team. MCNP - A General Monte Carlo N-Particle Transport Code Version 5 Vol. 1-3, LA-UR-031987, LA-CP-03-0245, and LA-CP-03-0284, Los Alamos National Laboratory. 2003 (updated 2/1/2008).

36. Nuclear data for neutron and proton radiotherapy and for radiation protection, Report 63. Bethesda, MD: International Commission of Radiation Units and Measurements. 2000.

37. ENDF/B-VI Summary Documentation, BNL-NCS-17541, 4th Edition, Supplement 1, December 1996.

38. Photon, electron, proton, and neutron interaction data for body tissues, Report 46. Bethesda, MD: International Commission of Radiation Units and Measurements. 1991.

39. Maughan, R.L.; Chuba, P.J. ; et al. The elemental composition of tumors: kerma data for neutrons. *Med. Phys.*, **1997**, *24*, 1241-1444.

40. Chadwick, M.B.; Herman, M.; et al, ENDF/B-VII.0: Next generation evaluated nuclear data library for nuclear science and technology. *Nuclear Data Sheets,* **2006***, 107,* 2931-3060.

41. Park, C.; Papiez, L.; et al, Universal survival curve and single fraction equivalent dose: useful tools in understanding potency of ablative radiotherapy. *Int. J. Radiation Oncology Biol. Phys.,* **2008**, *70,* 847-852.